An Immune Gene Expression Signature Associated With Development of Human Hepatocellular Carcinoma Identifies Mice That Respond to Chemopreventive Agents

Short-title: Immune-mediated field cancerization as target for HCC prevention

Authors: Agrin Moeini[1], Sara Torrecilla[1], Victoria Tovar[1], Carla Montironi[1,2], Carmen Andreu-Oller[1], Judit Peix[1], Mónica Higuera[1,3], Dominik Pfister[4], Pierluigi Ramadori[4], Roser Pinyol[1], Manel Solé[1], Mathias Heikenwälder[4] ,Scott L. Friedman[2], Daniela Sia[2,*], Josep M. Llovet[1,2,5,*].

Affiliations:

1. Liver Cancer Translational Research Group, Institut d'Investigacions Biomèdiques August Pi i Sunyer (IDIBAPS)-Hospital Clínic, Liver Unit, Universitat de Barcelona, Barcelona, Catalonia, Spain.
2. Mount Sinai Liver Cancer Program, Department of Liver Diseases, Icahn School of Medicine at Mount Sinai, New York, USA.
3. Liver diseases, Vall d'Hebron Institut de Recerca (VHIR), Hospital Universitari Vall d'Hebron, Barcelona, Spain
4. Division of Chronic Inflammation and Cancer, German Cancer Research Center Heidelberg (DKFZ), Heidelberg, Germany
5. Institució Catalana de Recerca i Estudis Avançats (ICREA), Barcelona, Catalonia, Spain.

Grant Support:

JML is supported by the European Commission (EC)/Horizon 2020 Program (HEPCAR, Ref. 667273-2), U.S. Department of Defense (CA150272P3), an Accelerator Award *(CRUCK, AECC, AIRC)* (HUNTER, Ref. C9380/A26813), NCI Cancer Center Support Grant, National Cancer Institute, Tisch Cancer Institute (P30-CA196521), Samuel Waxman Cancer Research Foundation, Spanish National Health Institute (SAF2016-76390) and the Generalitat de Catalunya/AGAUR (SGR-1358). AM is supported by Spanish National Health Institute. ST and JP are funded by Centro de

Investigación Biomedica en Red de Enfermedades Hepáticas y Digestivas (Ciberehd-ISCIII). CM is a recipient of Josep Font grant. CAO is supported by “la Caixa” INPhINIT Fellowship Grant (LCF/BQ/IN17/11620024). RP is supported by HEPCAR and AECC. DS is supported by the Gilead Sciences Research Scholar Program in Liver Disease. SLF is supported by the National Institutes of Health Research project grant (R01, DK5662) and U.S. Department of Defense (CA150272P3). M.H. was supported by an ERC Consolidator grant (HepatoMetaboPath), the SFBTR 209, 1335 and SFBTR179. This project has received funding from the European Union’s Horizon 2020 research and innovation program under grant agreement No 667273 and the Helmholtz future topic (Zukunftsthema) Immunology and Inflammation.

Abbreviations: ALT: alanine aminotransferase; α-SMA: α-smooth muscle actin; AKT: protein kinase B; Asp: aspirin; AST: aspartate aminotransferase; CCl4: carbon tetrachloride; CD-HFD (choline-deficient high-fat diet); Clo: clopidogrel; DEN: diethylnitrosamine; EMT: epithelial-mesenchymal transition, ERK: extracellular signal-regulated kinase; FC: Fold change, FDR: false discovery rate; FFPE: formalin-fixed paraffin-embedded; FGFR: fibroblast growth factor receptor; GSEA: gene set enrichment analysis; HCC: hepatocellular carcinoma; HCV: hepatitis C virus; HSC: hepatic stellate cell; ICF: immune-mediated cancer field; IPA: ingenuity pathway analysis; mo: months; NTP: nearest template prediction; PDGFR: platelet-derived growth factor receptor; ssGSEA: single sample gene set enrichment analysis; TKIs: tyrosine kinase inhibitors; Treg: regulatory T cells; qRT-PCR: quantitative real-time polymerase chain reaction; VEGFR: vascular endothelial growth factor receptor.

***Correspondence:** Josep M. Llovet, MD, Liver Cancer Translational Research Laboratory, IDIBAPS-Hospital Clinic, Rosselló 153, 08039, Barcelona, Catalonia, Spain; Tel. 0034-932.279.155; Email address: jmllovet@clinic.cat; Daniela Sia, PhD, Mount Sinai Liver Cancer Program, Division of Liver Diseases, Tisch Cancer Institute, Icahn School of Medicine at Mount Sinai, Madison Ave 1425. 11F-70. Box 1123, New York, NY10029. USA. E-mail: daniela.sia@mssm.edu

Disclosures: Part of the study was supported with an investigator-initiated research grant by Boehringer Ingelheim. Prof. Josep M. Llovet has been a consultant, advisory board member and has received research funding from Boehringer Ingelheim; and is receiving research support from Bayer HealthCare Pharmaceuticals, Eisai Inc, Bristol-

Myers Squibb and Ipsen, and consulting fees from Bayer HealthCare Pharmaceuticals, Bristol-Myers Squibb, Eisai Inc, Celsion Corporation, Eli Lilly, Exelixis, Merck, Ipsen, Glycotest, Navigant, Leerink Swann LLC, Midatech Ltd, Fortress Biotech, Sprink Pharmaceuticals and Nucleix. Prof. Scott L Friedman has been a consultant for Abide Therapeutics, Allergan Pharmaceuticals, Angion Biomedica, Blade Therapeutics, Can-Fite Biopharma, Enanta Pharmaceuticals, Escient Therapeutics, Forbion, Galmed, Genfit, Glycotest, Glympse Bio, Metacrine Inc., Mistral Biosciences, Morphic Rock Therapeutics, North Sea Therapeutics, Novartis, Novo Nordisk, Pfizer Pharmaceuticals, Salix Pharmaceuticals, Scholar Rock, Seal Rock Therapeutics, Second Genome, Surrozen, Symic Bio, Viking Therapeutics and Kintai; has received research funding from Blade Therapeutics, Can-Fite Biopharma, Ferring Research Institute, Galmed; and has stock options from Intercept, Exalenz, Madrigal, Akarna Therapeutics, BirdRock Bio, Blade Therapeutics, Conatus, DeuteRx, Exalenz, Galectin, Galmed, Genfit, Glympse. The rest of the authors declare no conflict of interest relevant to the study reported.

Transcript profiling: Gene expression Omnibus accession number from previously deposited data from our group (GSE63898, GSE10143, GSE15654) and others (GSE84044). Newly profiled mice samples are in GEO under accession number (GSE125975 and GSE133969).

Author contribution: Study concept and design: AM, VT, DS, JML; acquisition of data: AM, ST, CM, JP, MH, MS; analysis and interpretation of data: AM, ST, VT, CM, CAO, MS; drafting of the manuscript: AM, DS, JML; critical revision of the manuscript for important intellectual content: RP, SF, DS, JML; obtained funding: JML; study supervision: JML, DS.

Acknowledgements: We thank Juan José Lozano for technical assistance in the normalization of transcriptomic array of the animal model. This study has been developed at the building of *Centre Esther Koplowitz* from IDIBAPS/CERCA Programme/Generalitat de Catalunya. We also acknowledge Angelo Sangiovanni and Massimo Colombo for providing the seminal cohort of cirrhotic patients in our previous studies[12,14].

ABSTRACT

Background & Aims: Cirrhosis and chronic inflammation precede development of hepatocellular carcinoma (HCC) in approximately 80% of cases. We investigated immune-related gene expression patterns in liver tissues surrounding early-stage HCCs and chemopreventive agents that might alter these patterns to prevent liver tumorigenesis.

Methods: We analyzed gene expression profiles of non-tumor liver tissues from 392 patients with early-stage HCC (training set, n=167 and validation set, n=225) and liver tissue from patients with cirrhosis without HCC (n=216, controls) to identify changes in expression of genes that regulate the immune response that could contribute to hepatocarcinogenesis. We defined 172 genes as markers for this deregulated immune response, which we called the immune-mediated cancer field (ICF). We analyzed the expression data of liver tissues from 216 patients with cirrhosis without HCC and investigated the association between this gene expression signature and development of HCC and outcomes of patients (median follow-up 10 years). Human liver tissues were also analyzed by histology. C57BL/6J mice were given a single injection of Diethylnitrosamine (DEN) followed by weekly doses of carbon tetrachloride to induce liver fibrosis and tumorigenesis. Mice were then given orally the multiple tyrosine inhibitor nintedanib or vehicle (controls); liver tissues were collected and histology, transcriptome, and protein analyses were performed. We also analyzed transcriptomes of liver tissues collected from mice on a choline-deficient high-fat diet, which developed chronic liver inflammation and tumors, given orally aspirin and clopidogrel or the anti-inflammatory agent sulindac vs mice on a chow (control) diet.

Results: We found the ICF gene expression pattern in 50% of liver tissues from patients with cirrhosis without HCC and in 60% of non-tumor liver tissues from patients with early-stage HCC. The liver tissues with the ICF gene expression pattern had 3 different features: increased numbers of effector T cells; increased expression of genes that suppress the immune response and activation of transforming growth factor beta signaling; or expression of genes that promote inflammation and activation of interferon gamma signaling. Patients with cirrhosis and liver tissues with the immunosuppressive profile (10% of cases) had a higher risk of HCC (hazard ratio, 2.41; 95% 1.21–4.80). Mice with chemically-induced fibrosis or diet-induced steatohepatitis given nintedanib or aspirin and clopidogrel downregulated the ICF gene expression pattern in liver and developed fewer and smaller tumors than mice given vehicle.

Conclusions: We identified an immune-related gene expression pattern in liver tissues of patients with early-stage HCC, called the ICF, that associates with risk of HCC development in patients with cirrhosis. Administration of nintedanib or aspirin and clopidogrel to mice with chronic liver inflammation caused loss of this gene expression pattern and developed fewer and smaller liver tumors. Agents that alter immune regulatory gene expression patterns associated with carcinogenesis might be tested as chemopreventive agents in patients with cirrhosis.

Keywords: cancer, microenvironment, cytokines, lymphocytes, immune exhaustion

INTRODUCTION

Liver cancer is the fourth leading cause of cancer-related mortality worldwide[1]. Hepatocellular carcinoma (HCC) accounts for more than 90% of liver cancers and is the main cause of death in patients with cirrhosis[2,3]. HCC arise from chronic liver inflammation, fibrosis and eventually cirrhosis in 70-80% of cases[2]. In developed countries, curative treatments are feasible in 30-40% of cases, but recurrence is high and no effective adjuvant therapies are available[2,4]. In addition, ~40-50% of patients are diagnosed at advanced stages when currently approved molecular therapies yield limited survival benefits (~1 year)[3]. Despite recent advances in the management and clearance of HCV infection, there is an unmet need for early detection and application of chemopreventive approaches in patients at high-risk of HCC development.

To date, there are no established preventive strategies for HCC in patients at risk beyond prevention with anti-viral therapies[5]. Once cirrhosis is established, anti-viral therapies reduce but do not eliminate the risk of HCC[4,6,7]. Individual risk assessment is a key first step in the successful development of any chemopreventive strategy. In this regard, increasing evidence suggests the existence of the so-called “cancer field-effect” or field cancerization which consists of predisposing oncogenic and inflammatory signals occurring during chronic liver injury and ultimately leading to malignant transformation[8–10]. Gene signatures derived from the cirrhotic tissue adjacent to HCC tumors have been designed to predict poor outcome, particularly in HCV-infected cirrhotic patients at higher risk of HCC development[9,11–14]. Overall, these studies support the feasibility of using molecular scores of the carcinogenic field to identify patients at high risk of HCC development. However, the carcinogenic roles of inflammation and immune response in the context of the field cancerization have been poorly explored. Understanding the immune features governing the unresolved cancer field-effect is crucial for identifying potential therapeutic targets in patients at high risk of HCC development.

In this study, the analysis of the inflammatory *milieu* that characterizes the underlying liver disease in which HCC tumors arise has led to the identification of an immune-mediated cancer field (ICF) in 60% of early HCC patients and 50% of cirrhotic patients without HCC. This ICF comprises three distinct molecular subtypes including the *High Infiltrate ICF* subtype with increased infiltration of effector T cells, the *Immunosuppressive ICF* subtype with activation of stroma and TGF-β signaling, and the *Pro-inflammatory ICF* subtype with up-regulation of IFN-γ signaling. These immune profiles, particularly the *Immunosuppressive* cancer field, predict increased risk of HCC development in cirrhotic patients. Inhibition of this carcinogenic field significantly reduced HCC onset in two mouse models of chronic liver damage and hepatocarcinogenesis.

Overall, our study provides the rationale to explore chemopreventive strategies in cirrhotic patients at high-risk of HCC development.

MATERIALS AND METHODS

Human cohort

Gene expression data from a cohort of 167 surgically resected fresh-frozen samples (Heptromic dataset, GSE63898) with matched tumor and adjacent non-tumor tissue were analyzed. Samples were previously collected (1998-2008) in the setting of the HCC Genomic Consortium upon institutional review board approval. Full description of the cohort and RNA profiling data are available in previous publications[15,16]. **Supplementary Table 1** provides a summary of the clinical-pathological variables of the samples used in the current study (training cohort, n=167). Validation of the identified molecular profiles was then performed in an independent set of 225 adjacent non-tumor liver tissues previously characterized by our group (GSE10143)[9]. Finally, to identify those non-neoplastic patients at higher risk of HCC development and most likely to benefit from chemopreventive strategies, our findings were evaluated in a previously characterized cohort of patients with early cirrhosis (n=216, GSE15654)[14] and a publicly available dataset of fibrotic liver tissues (n=124, GSE84044)[17].

Modeling the immune-mediated cancer field

Enrichment scores of 4872 gene sets that represent cell states and perturbations of the immune system (Collection C7 of MSigDB, Broad Institute)[18] were calculated by Single-sample Gene Set Enrichment Analysis (ssGSEA) in the non-tumor liver tissue of the training cohort. Next, unsupervised clustering analysis by non-negative matrix factorization (NMF consensus)[19] method was performed to identify the presence of an immune-mediated cancer field. To characterize the samples presenting an ICF and to identify different immune-mediated field subtypes, a second unsupervised clustering was performed using ssGSEA scores obtained for a curated set of gene signatures representative of individual cell types[20,21] ,cancer immune-related signaling pathways[22], and inflammation- or immune-specific biological processes (Hallmark collection of MSigDB, Broad Institute).

Generation of an immune-mediated field gene signature

An ICF field gene signature was generated using top differentially expressed genes in each molecular group (FDR<0.05; Fold-change ≥2), which was then validated in an independent dataset using Nearest Template Prediction (NTP) analysis (p-value<0.05) (Gene Pattern modules)[23].

Molecular characterization of the ICF subtypes and identification of candidate therapies

To characterize the ICF subtypes, gene expression signatures [available in MSigDB (Broad Institute) or previously reported (**Supplementary Table 2**)] were assessed by GSEA, ssGSEA, NTP and Ingenuity Pathway Analyses (IPA). CIBERSORT[20] was used to estimate the relative fraction of 22 immune cell types within the leukocyte compartment of non-tumor liver tissues. The Immunophenoscore (IPS) algorithm[24] was used to analyze the major immunogenic determinants. An *in silico* analysis based on ssGSEA scores of ~1230 gene sets (DSigDB) recapitulating targets of approved therapies was also performed for the screening of candidate targeted therapies.

Histological evaluation of infiltrating inflammation

Histopathological analysis was performed in 98 out of 167 cases. Specifically, hematoxylin and eosin (H&E) staining of formalin-fixed paraffin embedded (FFPE) tissue section of HCCs and their matched adjacent non-tumor livers were evaluated by two expert pathologists (CM and MS). The presence of inflammation (portal/septal, interface, pericentral and lobular) as well as the lymphoid aggregates were assessed in the non-tumor liver tissue sections. More details on the histological evaluation of the samples have been included in **Supplementary material**.

Animal models

We generated a chemically-induced model of HCC and fibrosis in male C57BL/6J mice (Harlan Laboratories, n=55) by a single injection of Diethylnitrosamine (DEN) followed by weekly dosing with carbon tetrachloride (CCl_4), as previously described[25]. Once fibrosis was established, mice were randomized to receive vehicle or nintedanib (50 mg/kg, Boehringer Ingelheim). Mice were sacrificed at different time-points and liver and tumor tissue samples were collected and processed for histological, transcriptomic and protein expression analyses (see **Supplementary material**). All experimental procedures were carried out following the approval of the institutional ethical committee of the University of Barcelona and Hospital Clinic of Barcelona. Additionally, liver samples of a choline-deficient high-fat diet (CD-HFD) fed mouse model reported in a recent study[26] were collected. A total of 25 samples were processed for transcriptomic profiling, including mice fed a chow diet (n=5) or CD-HFD for 12 months and given: vehicle (n=4); aspirin/clopidogrel (Asp/Clo) (n=6) or sulindac (n=10).

Statistical analysis

All analyses were performed using SPSS software version 23 (IBM) or GraphPad Prism version 5.00 (San Diego, CA). Correlations for categorical and continuous variables were analyzed by Fisher's exact test and Wilcoxon rank-sum test, respectively. The prognostic value of the signatures was assessed using Kaplan-Meier estimates, log-rank test, and Cox regression models. In *in vivo* studies, the Mann-Whitney U test was used to compare differences in body weights, liver function, tumor number, tumor size and CD4/CD8 stained area in human samples. Fisher exact test was performed for analysis of HCC incidence and pERK staining. Student T-Test was used to compare the differences in Sirius Red quantification, CD31 staining, CD4/CD8 staining proportion of immune cell infiltrate in mice and relative gene expression.

RESULTS

Identification of a novel immune-mediated cancer field effect in non-tumor liver tissue of patients with early HCC.

In order to characterize the immune features governing the unresolved cancer-field in which new cancers arise, transcriptome-based analysis of a compendium of ~5,000 annotated immunology-specific gene-sets[18] was performed in the non-tumor liver tissue of patients with early stage HCC. This analysis revealed the presence of an immune-mediated cancer field (ICF) in ~60% (98/167) of samples (**Figure 1A and Supplementary Figure 1**). Specifically, these samples were characterized by enrichment of several gene-sets recapitulating the presence of activated immune cells, up-regulation of core signaling pathways involved in immune response (both innate and adaptive) as well as those involved in the modulation of inflammatory response (i.e. IL2-STAT5, IL6-STAT3, IL17, IFN-γ, CSF, TNF-α, and TGF-β signaling) (**Figure 1A-B** and **Supplementary Figure 1**). Moreover, histological evaluation confirmed that liver tissues with ICF contained a higher frequency of moderate to marked inflammatory infiltrate (74% in ICF vs. 52% in non ICF, p=0.034) and lymphoid aggregates (80% in ICF and vs. 55% in non ICF, p=0.009) (**Figure 1C-1D and Supplementary Table 3**). Immunostaining for CD4+ and CD8+ further confirmed significantly higher levels of T cell infiltrates in the adjacent livers of patients with the ICF (**Supplementary Figure 2A**). In contrast, histological evaluation of the tumor showed no significant correlation between the presence of the ICF and the detection of intratumoral or peritumoral infiltration (**Supplementary Table 3**). This is in accordance with our recent publication[15], where the tumor immune-based profile did not correlate with presence or absence of immune gene signatures in the surrounding non-tumor tissue.

While characterizing the ICF we detected that, in addition to immunogenic features, several well-known carcinogenic signals such as epithelial-to-mesenchymal transition, KRAS, EGFR, and VEGF signaling were also significantly enriched in liver tissues containing the ICF (**Supplementary Table 4**). In line with these oncogenic signals, a significant enrichment of previously reported prognostic signatures derived from the adjacent non-tumoral liver were also detected. These signatures included the 186-gene cancer-field signature[9], activated hepatic stellate cells (HSCs)[11], hepatic injury and regeneration (HIR)[13], and multicentric occurrence of HCCs[27] (**Figure 1A**). The presence of the ICF significantly correlated with HCV infection, features indicative of liver dysfunction such as high bilirubin, low platelet count and albumin levels (**Supplementary Table 5**) and poor survival [median OS 43.4 mo in the ICF group vs 94.8 mo in non ICF; p=0.001]**,** (**Supplementary Table 6** and **Supplementary Figure 1B**). Altogether, our

data highlight the presence of an immune-mediated cancer field in 60% of early HCC patients. This ICF is characterized by activation of immunomodulatory signaling cascades (i.e. IFN-γ, TNF-α, TGF-β, IL6) along with cancer promoting signaling pathways (i.e. EMT, EGFR and VEGFR), and is associated with HCV infection and poor prognosis.

The immune-mediated cancer field contains 3 distinct molecular subtypes.

Further dissection of the key immune-modulating signaling pathways and immune-cell infiltrates in those samples harboring the immune-mediated cancer field revealed the existence of three distinct molecular subtypes. The first molecular subtype, henceforth called the "*High Infiltrate ICF*" subtype (23% of the ICF), showed a significant enrichment of several previously established gene signatures mirroring the presence and/or activation of immune cell infiltrates such as lymphocytes (T and B cells)[22,28] or macrophages[29] (**Figure 2A-2B**). Consistently, immunogenicity, herein captured either by the cytolytic activity score (**Figure 2A**)[30] or using the immunophenoscore algorithm[24] (**Figure 2B**), was also significantly higher in these samples ($p<0.001$). Specifically, non-tumor liver samples belonging to the *High Infiltrate ICF* subtype showed significant infiltration of effector T cells (**Figure 2B,** $p\leq0.001$), including increased levels of cytotoxic CD8+ T cells assessed both by transcriptomic ($p=0.03$) and immunohistochemistry ($p=0.0002$) (**Figure 2C** and **Supplementary Figure 2B**). This subtype also was characterized by enrichment of the previously reported ectopic lymphoid structures (ELS) signature[31] (**Figure 2A**). In addition, the *High Infiltrate ICF* was significantly associated with poor survival in comparison to the rest of the patients (**Supplementary Figure 1C**), although there were no significant differences among the distinct ICF subtypes (**Supplementary Figure 1D**). The second subtype, the so-called "*Immunosuppressive ICF*" (36% of the ICF), was characterized primarily by activation of stroma and HSCs, increased TGF-β signaling and T cell exhaustion (**Figure 2A**). Moreover, several immune-checkpoints (i.e. *CTLA-4, TIGIT, LAG*3) were significantly over-expressed (IPS, $p<0.01$) in this class, along with higher levels of M2 macrophages ($p=0.04$) and CD4+ memory resting cells ($p=0.005$), which are among main mediators of immune tolerance and inhibition (**Figure 2B-2C**). The third subtype (41% of the ICF) showed a clear predominance of IFN-γ signaling ($p<0.001$) and enrichment of the inflammatory M1 macrophages ($p<0.0001$), and was called the "*Pro-inflammatory ICF*" subtype (**Figure 2A-2C**). Interestingly, the *High Infiltrate* and *Immunosuppressive* subtypes shared several molecular features including the enrichment of key signaling pathways involved in modulating the immune response (i.e. IL2 and TNF signaling),

proliferation (i.e. KRAS signaling) and angiogenesis (**Figure 2A,** p<0.001).

In order to further confirm the presence and molecular traits of the identified ICF, we generated a transcriptome-based gene signature able to capture the three immune-mediated cancer field subtypes. Interestingly, this signature only showed minimal overlap (0-5%) with previously reported gene signatures of field cancerization in HCC (**Supplementary Figure 3**)[9,12,14,32]. The resulting 172-gene signature (**Supplementary Table 7**) was then validated in the adjacent non-tumor tissue of 225 patients with early HCC, previously characterized by our group[9,33] (**Supplementary Figure 4A**). Similar to what was previously observed in the training cohort, 58% (130/225) of patients belonged to the ICF. Moreover, in this cohort, the presence of the ICF was an independent predictor of poor survival [HR=2.73; 95 CI: 1.1-6.8; p=0.03] (**Supplementary Figure 4B**, **Supplementary Table 8**). Within the ICF group, ~31% (40/130) presented the *High Infiltrate ICF* profile, ~27% (35/130) the *Immunosuppressive ICF* and ~42% (55/130) the *Pro-inflammatory ICF* subtype (**Supplementary Figure 4A**). Subsequent molecular characterization further confirmed the ability of the signature to capture the main molecular traits defining each subtype, such as increased infiltration of effector T cells in *High Infiltrate* subtype, activation of stroma and TGF-β signaling in *Immunosuppressive* subtype and up-regulation of IFN-γ signaling in *Pro-inflammatory* subtype (**Supplementary Figure 4A**). Overall, our results highlight the presence of a poor prognosis-related immune-mediated cancer field comprised of 3 molecular subtypes with a high degree of lymphocyte infiltration (overall 16% of HCC patients) or predominance of either immunosuppressive (overall 20% of HCC patients) or pro-inflammatory (24% of HCC patients) signaling cascades.

The immune cancer-field, particularly the immunosuppressive subtype, predicts a high risk of HCC development in cirrhotic patients

Following the identification of an immune-mediated cancer field in the livers of 60% of patients with early HCC, we next sought to assess its role in liver disease progression and HCC primary occurrence. To this end, the 172-gene signature was analyzed in a cohort of 216 non-malignant cirrhotic patients with a median follow-up of 10 years in the context of an HCC surveillance program[14]. Overall, 51% (110/216) of cirrhotic patients harbored the ICF, including the *High Infiltrate ICF* subtype in 28% (31/110), the *Immunosuppressive ICF* subtype in 19% (21/110), and the *Pro-inflammatory ICF* subtype in 53% (58/110) of cirrhotic patients harboring the ICF. Next, we tested the capacity of the ICF subtypes to predict the risk of HCC development in cirrhotic patients. Interestingly, the presence of the *Immunosuppressive ICF* subtype (10% of all cirrhotic

patients) was significantly associated with a higher risk of HCC development [median time to HCC development of 7.4 years (95% CI: 3.2-11.7) *vs* 17.1 years (95% CI: 10.6-23.7) in Rest, p<0.0001] and was found to be an independent predictor of HCC occurrence in cirrhotic patients in a multivariate analysis [HR 2.41 (95% CI: 1.2-4.8), p=0.012] (**Figure 3A** and **Table 1**). In addition, the *Immunosuppressive ICF* was also significantly associated with poor survival [median overall survival of 7.1 years (95% CI: 4.5-9.6) *vs* 16.3 years (95% CI: 9.1-23.5) in Rest, p<0.0001] and higher risk of hepatic decompensation [median time to hepatic decompensation of 6.5 years (95% CI: 4.3-8.6) *vs* >15 years in Rest, p<0.0001] (**Figure 3B-3C**). Cirrhotic patients harboring the other two ICF subtypes (*High Infiltrate* and *Pro-inflammatory* subtypes) also showed a non-significant trend towards a higher risk of HCC development compared to those patients lacking the ICF [mean time to HCC development of 12.8 years (95% CI:11.5-14.2) in Other ICF subtypes *vs* 16.3 years (95% CI: 14.2-18.5) in non ICF, p=0.06] (**Supplementary Figure 5A**).

Moreover, the analysis of an additional cohort of 124 non-neoplastic patients with liver fibrosis[17] revealed that the immune-mediated cancer field may occur as a progressive event, as it significantly correlated with increasing levels of fibrosis stage and degree of inflammation (**Supplementary Figure 5B**). Particularly, the presence of the *Immunosuppressive ICF* significantly correlated with the presence of advanced liver fibrosis (Scheuer fibrosis S3-4 score[17], p=0.034) (**Supplementary Figure 5B**).

In conclusion, the immune-mediated cancer field detected in patients with early HCC is also present in the livers of ~50% of cirrhotic patients and captures the presence of a damaging and continuous inflammatory response in the underlying liver disease. Furthermore, our results underscore the critical role of an *Immunosuppressive ICF* (overall, 10% of cirrhotic patients) in defining a 2.4 risk of HCC development, and to a smaller extent of the *High Infiltrate* and *Pro-inflammatory* subtypes.

The immune-mediated field as a target for chemoprevention in a mouse model recapitulating chronic liver inflammation and HCC development

Based on the compelling results described above, we hypothesized that the immune-mediated cancer field, and particularly the *Immunosuppressive ICF* subtype, may represent an ideal target for chemopreventive strategies in cirrhotic patients at high risk of HCC development. To this purpose, an *in silico*-based analysis was performed using our training cohort to identify those candidate therapies most likely to modulate the identified ICF. This analysis was based on the enrichment of a compendium of ~1230

gene sets (DSigDB collections D1 and D2)[34] recapitulating the main targets of 1202 approved drugs. Among the top 10 most significantly enriched drugs **(Supplementary Figure 6**), nintedanib was the only FDA-approved therapy indicated for a non-cancer condition. Specifically, nintedanib is the first molecular targeted therapy with clinical efficacy in patients with idiopathic pulmonary fibrosis as both an anti-fibrogenic and anti-inflammatory agent[35]. Given these considerations, the efficacy of nintedanib in reverting the pro-tumorigenic immune-mediated cancer field was tested in a mouse model of HCC development in the setting of chronic inflammation and liver fibrosis (**Supplementary Figure 7A**). In this model, the macroscopic evaluation of explanted livers in DEN/CCl_4 mice sacrificed at the age of 15, 17 and 18 weeks confirmed the development of numerous hepatic tumors (**Figure 4A**). Tumor penetrance and number of tumors progressively increased, ultimately reaching a 100% incidence at 18 weeks of age (**Figure 4A and 4B**). At all-time points, histological evaluation of the liver sections showed that a portion of the tumors were pre-neoplastic (dysplastic) nodules (**Figure 4C**). In mice sacrificed at 15 weeks of age, **Supplementary Figure 7A**), nintedanib showed a clear trend towards reducing HCC incidence, number and size of tumors (**Figure 4B, D and E**). These differences reached significance at 17 weeks of age (**Figure 4B**), having a marked decrease in both overall tumor burden (30% in nintedanib vs 89% in vehicle group, p=0.019) and specifically in HCC incidence (7% vs 33%, p=0.04). Similarly, at 18 weeks of age, HCC incidence was significantly reduced in treated mice (**Figure 4B**, 22% vs 77%, p<0.001). In addition, nintedanib significantly reduced the overall tumor number and size both at 17 and 18 weeks of age (**Figure 4D-E**). Overall, nintedanib was well tolerated with no significant induction of body weight loss or hepatotoxicity measured by serum ALT and AST levels (**Supplementary Figure 7B-C**). Taken together, our data suggest that nintedanib is safe and efficacious in preventing HCC development in our experimental model.

Nintedanib treatment reverts the immune-mediated cancer field effect

Next, we sought to assess the impact of nintedanib treatment on the immune-mediated cancer field. For this purpose, we analyzed gene expression profiling of non-tumor liver samples from 17 weeks-old DEN/CCl_4 mice given nintedanib (n= 10) or vehicle (n=9), and 3 healthy control mice. First, the comparison between the healthy control group and vehicle group revealed a profile of activated pathways compatible with HCC development within a fibrotic and inflammatory background. In this regard, functional analysis of differentially expressed genes (**Supplementary Table 9**) highlighted the activation of hepatic stellate cells and fibrogenesis, as well as immune system activation

(inflammatory response, chemotaxis, binding of myeloid and leukocytes) in vehicle treated DEN/CCl_4 livers (**Supplementary Table 10**). Notably, our model presented a significant enrichment of the gene-set representing the ICF identified in humans (p=0.001) and faithfully recapitulated the human immune-mediated field subtypes described above (**Figure 5A**)**.** The comparison of the gene expression profiles of adjacent non-tumor liver from mice treated with vehicle or nintedanib demonstrated that nintedanib significantly down-regulated the ICF subtypes and, more specifically the *Pro-Inflammatory* and the *Immunosuppressive ICF* phenotype, which predict risk of HCC development in cirrhotic patients (**Figure 5A,** p=0.02). A non-significant trend was also observed for the High Infiltration subtype (**Figure 5A**). Treatment with nintedanib led to a significant down-regulation of inflammatory cues (IL-6/STAT3, interferon-α, interferon-γ) and immune-related signaling (IL-2/STAT5 activation, allograft rejection) **(Figure 5A).** Among the infiltrating immune cells, nintedanib significantly reduced the presence of B and T cells, activated macrophages, helper T cells and Tregs along with associated immune modulators (i.e. *IL1, CCL5 and PDL1*) (**Figure 5A**). Despite exhibiting similar global levels of inflammatory infiltrates, quantification of CD4 and CD8 positive infiltrating lymphocytes by IHC revealed a significant decrease of CD4+ T cells in nintedanib-treated mice compared to controls (**Figure 5B**, $p<0.05$).

Next, in order to further characterize the chemopreventive effects of nintedanib we assessed the activation status of the main nintedanib targets (i.e. VEGFR2 and PDGFR-β). Western blot of non-tumor liver tissue confirmed that nintedanib blocked the activation of VEGFR2 (**Figure 5C**) and its downstream effectors AKT and ERK (**Supplementary Figure 8A**). Consistently, both liver parenchyma and liver tumors were pERK positive in vehicle-treated mice and pERK negative in nintedanib treated mice (**Supplementary Figure 8B**, $p<0.05$), indicating an anti-proliferative effect of nintedanib as well. Given the strong inhibition of VEGFR signaling observed, we next assessed the anti-angiogenic effect of nintedanib in DEN/CCl_4 mice. In this model, reduced CD31 staining was associated with diminished blood vessel area in both liver parenchyma and liver tumors of nintedanib-treated mice (**Figure 5D**). Altogether, these data suggest that nintedanib exhibits its chemopreventive effects in part by inducing vascular normalization and inhibiting hepatic proliferation. In contrast, no reduction of fibrosis degree, the pro-fibrogenic signaling pathway PDGFR-β, or collagen markers were detected in the livers of nintedanib-treated mice (**Supplementary Figure 8C-E**).

Overall, our data confirm that therapeutic targeting of the immune-mediated cancer field, accompanied by liver vascular normalization and suppression of hepatic proliferation, can prevent the development of HCC associated with advanced chronic liver disease.

Immunomodulatory effects of Asp/Clo treatment revert the immune cancer field effect and prevent hepatocarcinogenesis in vivo

To further support the concept of an ICF in promoting HCC development and its therapeutic immunomodulation as candidate strategy for chemoprevention, we performed gene expression profiling in non-tumor liver derived from the recently described mouse model of choline-deficient high-fat diet (CD-HFD) treated either with the immunomodulatory combination aspirin/clopidogrel (Asp/Clo) or the anti-inflammatory sulindac[26]. Of particular interest, in this model, which presents non-alcoholic fatty liver-related liver inflammation with various degrees of fibrosis and HCC development after 12 months of diet regimen[26,36,37], HCC prevention was achieved only through the combination of the anti-inflammatory drug, aspirin, clopidrogel -an P2Y12 inhibitor-, (25% to 0% 12-mo HCC incidence control vs combo respectively, p=0.01)[26] and not sulindac alone (25% to 20%12-mo HCC incidence control vs sulindac, respectively, p=ns, data not shown). In the context of our study, comparative analysis between the non-tumor liver of healthy control and CD-HFD mice showed a significant enrichment of the ICF signature in CD-HFD mice (p=0.002, **Figure 5E**). Notably, all 3 ICF subtypes were significantly up-regulated in CD-HFD mice compared to healthy controls (**Figure 5E**) along with the enrichment of signaling pathways regulating inflammation (i.e. IL6-STAT3, TNFα), immune infiltration and activation[22,28], and epithelial-to-mesenchymal transition (i.e. TGFβ, p<0.05). These data were consistent with the high intrahepatic influx of metabolically activated CD8+ T cells and NK cells (CD3+NK1.1+) measured in CD-HFD fed mice by flow cytometry[26]. Overall, these data confirm the existence of an ICF in an independent model of chronic liver disease further suggesting a role in hepatocarcinogenesis.

Next, we compared the expression profiles of liver samples from CD-HFD vehicle-treated mice with CD-HFD mice treated with the combination Asp/Clo (n=6) or sulindac alone (n=10). Interestingly, only Asp/Clo, but not sulindac alone, was able to prevent HCC and revert the ICF within the liver microenvironment (p=0.05), being the *Pro-inflammatory* ICF subtype the most significantly down-regulated upon treatment (**Figure 5B**). Particularly, based on previous molecular characterization[26], the inhibition of the ICF seemed to be accompanied by a significant reduction of the degree of liver damage, as well as a significantly reduced number of CD8+ and NKT cells in the liver.

Overall, these data support the role of the ICF in promoting carcinogenesis, and suggest that only those drugs able to simultaneously inhibit several components of the ICF by

targeting mitogenic, angiogenic and immunomodulatory kinases (i.e. nintedanib and Asp/Clo) present a more efficacious therapeutic index for HCC prevention.

DISCUSSION

This study represents an in-depth analysis of the *inflammatory milieu* associated with the "field cancerization" in the chronically injured liver, and investigates its clinical implications in the prediction and prevention of HCC occurrence in cirrhotic patients.

The role of the "cancer field effect" in promoting neoplastic transformation has gained much interest in recent years and currently an altered microenvironment is considered a promoter of cancer[8,10]. Although, under physiological conditions, inflammation is an adaptive response to tissue injury, when the inflammatory stimuli persist, the non-resolved inflammation contributes to carcinogenesis[38,39]. In this line, activation of HSC as well as certain pathways, such as nuclear factor-KB and TGF-β signaling, have been previously associated with liver fibrogenesis, and eventually neoplastic transformation[9,12]. With this study, we move beyond the limits of current knowledge and provide a detailed description of the immune microenvironment underlying the *field cancerization* in the liver. To this end, we first characterized the immune profile of the non-tumor liver parenchyma of 392 early HCCs and then investigated its role in predicting HCC development in 216 cirrhotic patients with long-term surveillance for HCC (median of 10 years)[14]. The analysis revealed that up to 60% of HCCs and 50% of cirrhotic patients showed a deleterious immune-mediated response in the surrounding tissue, which was associated with impaired liver function, activation of specific oncogenic loops, angiogenesis and poor survival. Further characterization identified three distinct subtypes with different levels of lymphocyte infiltration and activation of either *immunosuppressive* or *pro-inflammatory* traits. In particular, the so-called *Immunosuppressive ICF* subtype (~10% of cirrhotic patients) was an independent predictor of HCC development, increasing 2.4 the risk of cancer development, whereas both the *High-Infiltrate* and the *Pro-Inflammatory* subtypes showed a trend towards higher risk of HCC occurrence in cirrhosis. The identification of distinct immune subtypes reflects the complex role of the immune system in hepatocarcinogenesis, with both an activated immune response and an exhausted immune-microenvironment contributing to create a pro-tumorigenic environment and increase the risk of HCC development[40].

Reducing the incidence and mortality of HCC requires advances in chemopreventive approaches at pre-neoplastic stages, in addition to curative treatment options for early

lesions. Universal immunization against HBV and antiviral therapies against HBV and HCV have been associated with very reduced HCC risk[2,41,42]. Once cirrhosis is established, the risk of HCC development remains despite achieving a sustained virologic response in HCV patients[6,7]. In addition, the incidence of other risk factors, such as non-alcoholic steatohepatitis (NASH), is dramatically increasing[2]. Thus, alternative HCC preventive strategies capable of interfering with molecular hepatocarcinogenesis are an unmet need. Furthermore, identifying those patients at high risk of HCC development should enable a cost-effective selection of patients most likely to benefit from chemopreventive approaches. In this scenario, our results are of clinical relevance since the ICF, and specifically the *Immunosuppressive* subtype, may provide a novel companion biomarker to enrich at-risk patients in chemoprevention clinical trials. Given these observations, we then sought to investigate if the molecular forces driving such cancer field could serve as target for chemopreventive strategies. Hence, we first verified that the molecular profiles observed in human cirrhosis were faithfully reproduced in two animal models of chronic liver injury. The DEN/CCl_4 chemically-induced mouse model as well as the recently described NASH-HCC model[26] reliably recapitulated the presence of a carcinogenic phenotype observed in liver tissues from patients belonging to the immune-mediated cancer field.

In order to identify the most promising candidate therapies for novel chemopreventive strategies, we conducted an *in silico* analysis using a large compendium of gene sets[34] recapitulating the main targets of 1202 approved drugs. Among the top ten most significantly enriched drugs, we selected nintedanib, the only FDA therapy approved for non-neoplastic conditions. In the DEN/CCl_4 animal model, oral administration of nintedanib reduced the immune-mediated cancer field, including the *Immunosuppressive ICF* subtype, ultimately reducing HCC incidence and growth. Reversion of the ICF induced by treatment with nintedanib was accompanied by reduction of CD4+ lymphocytes, which could be due to its mechanism of action inhibiting src family of kinases (i.e. LCK, FLT3 and SRC) . These findings are in line with previous reports suggesting that CD4+ cells propagate immune-mediated liver injury in models of chronic liver inflammation or autoimmune liver disease[43,44]. Pretreatment with T cell-specific Abs or immunosuppressive agents, such as anti-CD4 mAb, FK506 (Tacrolimus), or cyclosporine A, have shown to ameliorate hepatitis in these models, further supporting the role of CD4+ T cells in inducing liver damage[43]. Results in a second animal model treated with the combination of the anti-inflammatory drug, aspirin, and clopidrogel – a P2Y12 inhibitor-, confirmed the therapeutic potential of immunomodulating the ICF and supported the pro-tumorigenic role exerted by the immune response. Indeed, only the

treatment able to modulate the ICF, as indicated by the reduction of immune cells (i.e. $CD8^+$ and NKT cells) and the reversion of the ICF signature, successfully reduced liver damage and prevented HCC development. Overall, our study identifies a novel promising chemopreventive strategy for HCC and confirms the validity of using the reversion of the *ICF* as reliable read-out of efficacy. This is of great clinical importance since there is currently no effective method to monitor the short-term effects of chemopreventive drugs[5]. Nintedanib belongs to a new generation of TKIs that, in addition to exerting immune modulation blocks the activation of main angiogenic receptors[45]. Many cytokines and growth factors are involved in modulating the formation of new vessels. Expression of *VEGF* and its receptors is elevated in HCC cell lines and tissues, as well as in the blood circulation of patients with HCC[33,46–48]. In our model, nintedanib exerted its chemopreventive mechanisms in part through the inhibition of VEGF signaling, a major driver of angiogenesis[49].Thus far, independent studies had described that HCC prevention can be achieved in animal models by attenuating liver fibrosis through the inhibition of epidermal growth factor receptor (EGFR)[50,51] or lysophosphatidic acid (LPA)[32] signaling. With the current study, we demonstrate that modulation of the liver microenvironment by molecular targeted drugs, which simultaneously block liver inflammation and angiogenesis, might represent a powerful alternative strategy.

We recently defined the immune class of HCC[15] and the Immune exclusion class (characterized by active Wnt/CTNNB1)[3,15,52], which might predict response and primary resistance to checkpoint inhibitors, respectively[3,52]. We herein explore the immunomodulatory mechanisms underlying HCC occurrence by defining an immune-mediated field effect that conforms a cancer-permissive *milieu*, thus posing them at the highest risk of HCC development. In addition, our pre-clinical data with a drug approved in pulmonology and in non-small cell lung cancer treatment suggest that the permissive microenvironment can be reverted leading to a reduction in HCC occurrence. These data provide the rationale for testing this strategy in early chemoprevention trials targeting cirrhotic patients at high risk of HCC development. In addition, this strategy could also be further explored in the adjuvant setting considering that 60% of HCC undergoing resection also present this permissive *milieu* in the adjacent non-tumoral tissue.

FIGURE LEGEND

Figure 1. Identification of an ICF effect in non-tumoral liver tissue adjacent to early HCCs. A) Heatmap representation of the ICF present in 60% of HCC patients. High and low ssGSEA scores are represented in red and blue, respectively. B) Top predicted upstream cytokine and transcription factors activated in liver tissues of ICF patients. C) Representative images of degree of Portal/Septal infiltrating inflammation. D) Representative images depicting presence or absence of lymphoid aggregates.

Figure 2. The ICF contains 3 distinct molecular subtypes. A) Heatmap representation of the three ICF subtypes. Statistical significance is highlighted. B) Immunophenogram representing the enrichment of immunogenic determinants in the distinct ICF subtypes (MHC: Antigen presenting, EC: Effector cells, CP: Check-points, SC: Suppressor Cells). C) Comparison of estimated proportion of immune cells (CIBERSORT method) between the ICF subtypes, representing those immune populations with estimated average fraction >5% and significant differences between the ICF subtypes. Significant statistical differences observed among the different ICF subtypes are highlighted (High Infiltrate, *Purple*, Immunosuppressive, *Orange*; Pro-inflammatory, *Green*; and both High Infiltrate and Immunosuppressive, *Black*). *=p<0.05, **=p<0.01 and ***=p<0.001.

Figure 3. Association of the presence of the *Immunnosuppressive ICF* with HCC occurrence and prognostic variables in cirrhotic patients. (A) Kaplan-Meier estimates of HCC development, (B) overall survival, (C) hepatic decompensation, according to the presence of the *Immunosuppressive* ICF subtype (orange).

Figure 4. Nintedanib reduces HCC onset in mice. A) Representative pictures of macroscopic evaluation of hepatic tumors in mice given vehicle or nintedanib sacrificed at 15, 17 and 18 weeks of age. Arrows indicate macroscopically visible tumors. B) Evaluation of overall tumor burden and HCC incidence. ($^{\#}$) = statistical significance for overall tumor burden; (*) = statistical significance for HCC incidence. C) Microscopic evaluation of the number of tumors per mouse in each group. D) Number of macroscopic tumors per mouse given vehicle or nintedanib at the different time-points. E) Diameter size of the largest tumor per mouse given vehicle or nintedanib at the three different time-points. $^{\#}$ or *=p<0.05, **=p<0.01 and ***=p<0.001.

Figure 5. Nintedanib and Asp/Clo reduce the *ICF* in animal models of chronic inflammation and HCC development. A) Heatmap representation of high and low

ssGSEA scores for the 172-gene signature and gene-sets recapitulating the ICF subtypes. B) Representative images and quantification of CD4+ and CD8+ infiltrating lymphocytes in the liver of 17 weeks old mice given vehicle (n=5) or nintedanib (n=5). C) Western-blot analysis of VEGFR2 activation in the non-tumor liver parenchyma of 17 weeks old mice given vehicle (n=6) or nintedanib (n=6). D) Morphometric quantification of blood vessel area by CD31 immunostaining in 5 randomly selected low magnification fields in mice given vehicle (n=5) or nintedanib (n=5). E) Single sample GSEA analysis of the ICF signature in the different treatment arms of the CD-HFD model. **=$p<0.01$ and ***=$p<0.001$.

TABLES

Variable	Univariate analysis p-value	Multivariate analysis (cox's regression) HR	CI(95% low-high limits)	p-values
Non-tumoral liver tissue-based transcriptomic profiles				
Immunosuppressive-ICF	**0.03**	**2.41**	**1.21-4.80**	**0.01**
186-gene Poor prognosis signature	**<0.0001**	1.56	0.89-2.7	0.12
Clinicopathological variables				
Age (>median)	0.87			
Gender	0.22			
Diabetes	0.48			
HCV genotype 1b	0.18			
Alcohol consumption (>80 g/day)	0.68			
HCVetiology plus alcohol consumption	0.68			
History of antiviral treatment (interferon-based)	0.65			
Varices	**0.02**	1.49	0.85-2.6	0.17
Spleen	0.13			
Ishaak score 6 vs 5	0.24			
Platelet count (<100,000/mm3)	**0.02**	1.51	0.91-2.64	0.15
Bilirubin (> 1 mg/dL)	**0.00**	**1.85**	**1.07-3.2**	**0.03**
AFP (> 10 ng/mL)	0.87			
Prothrombin time (international normalized ratio >1.2)	0.38			

Table 1. Uni- and Multivariate Analysis of risk of HCC development in cirrhotic patients including gene signatures and clinico-pathological variables (n=216).

REFERENCES

1. Bray F, Ferlay J, Soerjomataram I, et al. Global cancer statistics 2018: GLOBOCAN estimates of incidence and mortality worldwide for 36 cancers in 185 countries. CA Cancer J Clin 2018;68:394–424.

2. Llovet JM, Zucman-Rossi J, Pikarsky E, et al. Hepatocellular carcinoma. Nat Rev Dis Prim 2016;2:16018.

3. Llovet JM, Montal R, Sia D, et al. Molecular therapies and precision medicine for hepatocellular carcinoma. Nat Rev Clin Oncol 2018;15:599–616.

4. Galle PR, Forner A, Llovet JM, et al. EASL Clinical Practice Guidelines: Management of hepatocellular carcinoma. J Hepatol 2018.

5. Fujiwara N, Friedman SL, Goossens N, et al. Risk factors and prevention of hepatocellular carcinoma in the era of precision medicine. J Hepatol 2018;68:526–549.

6. Calvaruso V, Cabibbo G, Cacciola I, et al. Incidence of Hepatocellular Carcinoma in Patients With HCV-Associated Cirrhosis Treated With Direct-Acting Antiviral Agents. Gastroenterology 2018;155:411–421.e4.

7. Kanwal F, Kramer J, Asch SM, et al. Risk of Hepatocellular Cancer in HCV Patients Treated With Direct-Acting Antiviral Agents. Gastroenterology 2017;153:996–1005.e1.

8. Lochhead P, Chan AT, Nishihara R, et al. Etiologic field effect: reappraisal of the field effect concept in cancer predisposition and progression. Mod Pathol 2015;28:14–29.

9. Hoshida Y, Villanueva A, Kobayashi M, et al. Gene expression in fixed tissues and outcome in hepatocellular carcinoma. N Engl J Med 2008;359:1995–2004.

10. Hernandez-Gea V, Toffanin S, Friedman SL, et al. Role of the microenvironment in the pathogenesis and treatment of hepatocellular carcinoma. Gastroenterology 2013;144:512–27.

11. Ji J, Eggert T, Budhu A, et al. Hepatic stellate cell and monocyte interaction contributes to poor prognosis in hepatocellular carcinoma. Hepatology 2015;62:481–95.

12. Zhang DY, Goossens N, Guo J, et al. A hepatic stellate cell gene expression signature associated with outcomes in hepatitis C cirrhosis and hepatocellular carcinoma after curative resection. Gut 2016;65:1754–64.

13. **Kim JH, Sohn BH**, Lee H-S, et al. Genomic predictors for recurrence patterns of hepatocellular carcinoma: model derivation and validation. Beck AH, ed. PLoS Med 2014;11:e1001770.

14. Hoshida Y, Villanueva A, Sangiovanni A, et al. Prognostic gene expression signature for patients with hepatitis C-related early-stage cirrhosis. Gastroenterology 2013;144:1024–1030.

15. Sia D, Jiao Y, Martinez-Quetglas I, et al. Identification of an Immune-specific Class of Hepatocellular Carcinoma, Based on Molecular Features. Gastroenterology 2017;153:812–826.

16. **Villanueva A, Portela A**, Sayols S, et al. DNA Methylation-based prognosis and epidrivers in hepatocellular carcinoma. Hepatology 2015.

17. Wang M, Gong Q, Zhang J, et al. Characterization of gene expression profiles in HBV-related liver fibrosis patients and identification of ITGBL1 as a key regulator of fibrogenesis. Sci Rep 2017;7:43446.

18. Godec J, Tan Y, Liberzon A, et al. Compendium of Immune Signatures Identifies Conserved and Species-Specific Biology in Response to Inflammation. Immunity 2016;44:194–206.

19. Brunet J-P, Tamayo P, Golub TR, et al. Metagenes and molecular pattern discovery using matrix factorization. Proc Natl Acad Sci U S A 2004;101:4164–9.

20. **Newman AM, Liu CL**, Green MR, et al. Robust enumeration of cell subsets from tissue expression profiles. Nat Methods 2015;12:453–7.

21. **Bindea G, Mlecnik B**, Tosolini M, et al. Spatiotemporal dynamics of intratumoral immune cells reveal the immune landscape in human cancer. Immunity 2013;39:782–95.

22. **Thorsson V, Gibbs DL**, Brown SD, et al. The Immune Landscape of Cancer. Immunity 2018;48:812–830.e14.

23. Reich M, Liefeld T, Gould J, et al. GenePattern 2.0. Nat Genet 2006;38:500–501.

24. **Charoentong P, Finotello F, Angelova M**, et al. Pan-cancer Immunogenomic Analyses Reveal Genotype-Immunophenotype Relationships and Predictors of Response to Checkpoint Blockade. Cell Rep 2017;18:248–262.

25. **Dapito DH, Mencin A, Gwak G-Y**, et al. Promotion of hepatocellular carcinoma by the intestinal microbiota and TLR4. Cancer Cell 2012;21:504–16.

26. **Malehmir M, Pfister D, Gallage S**, et al. Platelet GPIbα is a mediator and

potential interventional target for NASH and subsequent liver cancer. Nat Med 2019;25:641–655.

27. Okamoto M, Utsunomiya T, Wakiyama S, et al. Specific gene-expression profiles of noncancerous liver tissue predict the risk for multicentric occurrence of hepatocellular carcinoma in hepatitis C virus-positive patients. Ann Surg Oncol 2006;13:947–54.

28. **Wolf DM, Lenburg ME**, Yau C, et al. Gene Co-Expression Modules as Clinically Relevant Hallmarks of Breast Cancer Diversity Haibe-Kains B, ed. PLoS One 2014;9:e88309.

29. Beck AH, Espinosa I, Edris B, et al. The macrophage colony-stimulating factor 1 response signature in breast carcinoma. Clin Cancer Res 2009;15:778–87.

30. Rooney MS, Shukla SA, Wu CJ, et al. Molecular and genetic properties of tumors associated with local immune cytolytic activity. Cell 2015;160:48–61.

31. Finkin S, Yuan D, Stein I, et al. Ectopic lymphoid structures function as microniches for tumor progenitor cells in hepatocellular carcinoma. Nat Immunol 2015;16:1235–1244.

32. **Nakagawa S, Wei L**, Song WM, et al. Molecular Liver Cancer Prevention in Cirrhosis by Organ Transcriptome Analysis and Lysophosphatidic Acid Pathway Inhibition. Cancer Cell 2016;30:879–890.

33. Chiang DY, Villanueva A, Hoshida Y, et al. Focal gains of VEGFA and molecular classification of hepatocellular carcinoma. Cancer Res 2008;68:6779–88.

34. **Yoo M, Shin J**, Kim J, et al. DSigDB: drug signatures database for gene set analysis: Fig. 1. Bioinformatics 2015;31:3069–3071.

35. Richeldi L, Bois RM du, Raghu G, et al. Efficacy and safety of nintedanib in idiopathic pulmonary fibrosis. N Engl J Med 2014;370:2071–82.

36. Wolf MJ, Adili A, Piotrowitz K, et al. Metabolic Activation of Intrahepatic CD8+ T Cells and NKT Cells Causes Nonalcoholic Steatohepatitis and Liver Cancer via Cross-Talk with Hepatocytes. Cancer Cell 2014;26:549–564.

37. **Brown ZJ, Heinrich B**, Greten TF. Mouse models of hepatocellular carcinoma: an overview and highlights for immunotherapy research. Nat Rev Gastroenterol Hepatol 2018;15:536–554.

38. Coussens LM, Werb Z. Inflammation and cancer. Nature 2002;420:860–7.

39. **Hanahan D, Weinberg RA**. Hallmarks of cancer: The next generation. Cell

2011;144:646–674.

40. Makarova-Rusher O V., Medina-Echeverz J, Duffy AG, et al. The yin and yang of evasion and immune activation in HCC. J Hepatol 2015;62:1420–1429.

41. Papatheodoridis G V, Dalekos GN, Yurdaydin C, et al. Incidence and predictors of hepatocellular carcinoma in Caucasian chronic hepatitis B patients receiving entecavir or tenofovir. J Hepatol 2015;62:363–70.

42. Morgan RL, Baack B, Smith BD, et al. Eradication of hepatitis C virus infection and the development of hepatocellular carcinoma: a meta-analysis of observational studies. Ann Intern Med 2013;158:329–37.

43. Tiegs G, Hentschel J, Wendel A. A T cell-dependent experimental liver injury in mice inducible by concanavalin A. J Clin Invest 1992;90:196–203.

44. Omenetti S, Brogi M, Goodman WA, et al. Dysregulated intrahepatic CD4+ T-cell activation drives liver inflammation in ileitis-prone SAMP1/YitFc mice. Cell Mol Gastroenterol Hepatol 2015;1:406–419.

45. Hilberg F, Roth GJ, Krssak M, et al. BIBF 1120: triple angiokinase inhibitor with sustained receptor blockade and good antitumor efficacy. Cancer Res 2008;68:4774–82.

46. Mas VR, Maluf DG, Archer KJ, et al. Angiogenesis soluble factors as hepatocellular carcinoma noninvasive markers for monitoring hepatitis C virus cirrhotic patients awaiting liver transplantation. Transplantation 2007;84:1262–71.

47. Poon RTP, Ho JWY, Tong CSW, et al. Prognostic significance of serum vascular endothelial growth factor and endostatin in patients with hepatocellular carcinoma. Br J Surg 2004;91:1354–60.

48. Horwitz E, Stein I, Andreozzi M, et al. Human and mouse VEGFA-amplified hepatocellular carcinomas are highly sensitive to sorafenib treatment. Cancer Discov 2014;4(6):730–743.

49. Carmeliet P. VEGF as a key mediator of angiogenesis in cancer. Oncology 2005;69 Suppl 3:4–10.

50. Schiffer E, Housset C, Cacheux W, et al. Gefitinib, an EGFR inhibitor, prevents hepatocellular carcinoma development in the rat liver with cirrhosis. Hepatology 2005;41:307–14.

51. Fuchs BC, **Hoshida Y, Fujii T**, et al. Epidermal growth factor receptor inhibition attenuates liver fibrosis and development of hepatocellular carcinoma. Hepatology

2014;59:1577–90.

52. Pinyol R, Sia D, Llovet JM. Immune exclusion-Wnt/CTNNB1 class predicts resistance to immunotherapies in HCC. Clin Cancer Res 2019.

Author names in bold designate shared co-first authorship.

Figure 1

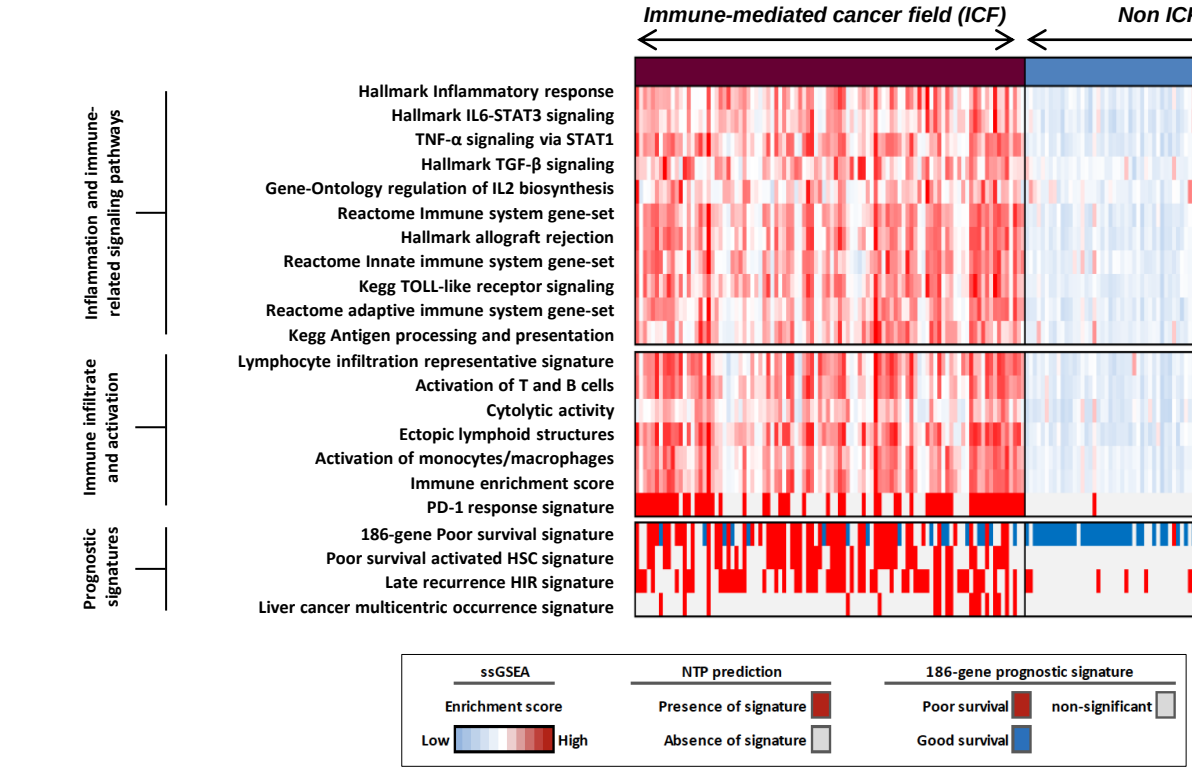
A
Immune-mediated cancer field (ICF)
Non ICF
Inflammation and immune-related signaling pathways
Hallmark Inflammatory response
Hallmark IL6-STAT3 signaling
TNF-α signaling via STAT1
Hallmark TGF-β signaling
Gene-Ontology regulation of IL2 biosynthesis
Reactome Immune system gene-set
Hallmark allograft rejection
Reactome Innate immune system gene-set
Kegg TOLL-like receptor signaling
Reactome adaptive immune system gene-set
Kegg Antigen processing and presentation
Immune infiltrate and activation
Lymphocyte infiltration representative signature
Activation of T and B cells
Cytolytic activity
Ectopic lymphoid structures
Activation of monocytes/macrophages
Immune enrichment score
PD-1 response signature
Prognostic signatures
186-gene Poor survival signature
Poor survival activated HSC signature
Late recurrence HIR signature
Liver cancer multicentric occurrence signature
ssGSEA
Enrichment score
Low
High
NTP prediction
Presence of signature
Absence of signature
186-gene prognostic signature
Poor survival
non-significant
Good survival

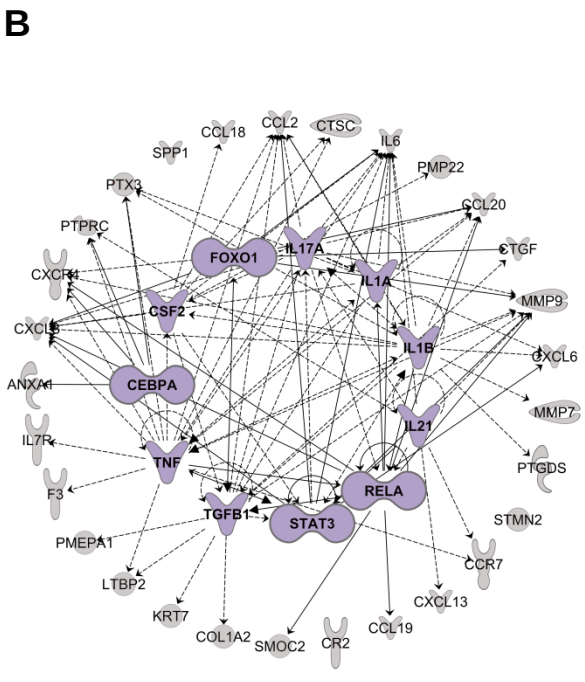
B
CCL18
CCL2
CTSC
SPP1
IL6
PMP22
PTX3
CCL20
PTPRC
FOXO1
IL17A
CTGF
CXCR4
IL1A
CSF2
MMP9
CXCL8
IL1B
CXCL6
ANXA1
CEBPA
MMP7
IL21
IL7R
TNF
PTGDS
F3
RELA
TGFB1
STAT3
STMN2
PMEPA1
CCR7
LTBP2
CXCL13
KRT7
COL1A2
SMOC2
CR2
CCL19

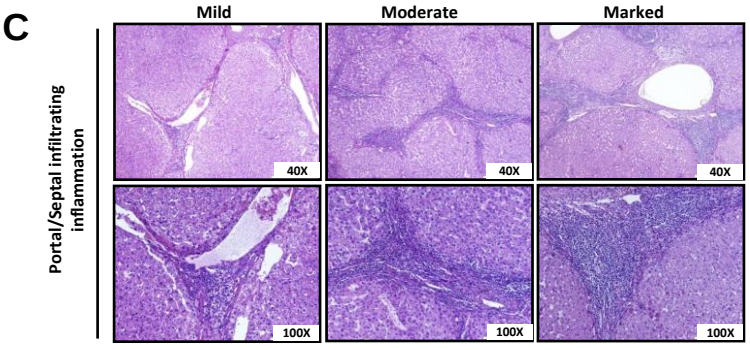
C
Mild
Moderate
Marked
Portal/Septal infiltrating inflammation
40X
100X

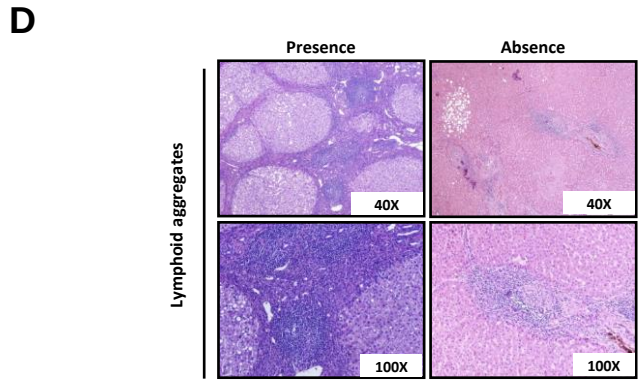
D
Presence
Absence
Lymphoid aggregates
40X
100X

Figure 2

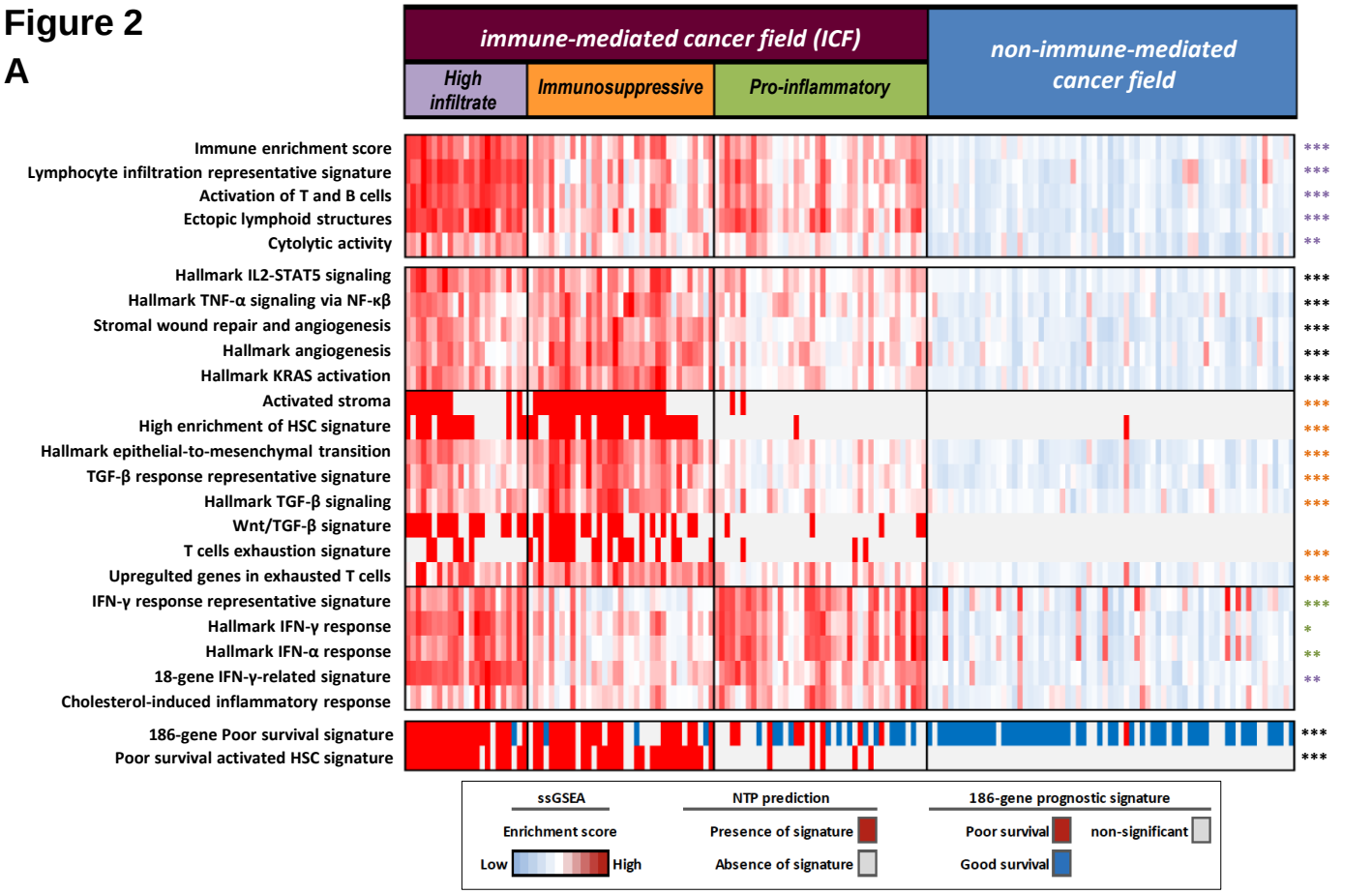
A
immune-mediated cancer field (ICF)
High infiltrate
Immunosuppressive
Pro-inflammatory
non-immune-mediated cancer field
Immune enrichment score
Lymphocyte infiltration representative signature
Activation of T and B cells
Ectopic lymphoid structures
Cytolytic activity
Hallmark IL2-STAT5 signaling
Hallmark TNF-α signaling via NF-κβ
Stromal wound repair and angiogenesis
Hallmark angiogenesis
Hallmark KRAS activation
Activated stroma
High enrichment of HSC signature
Hallmark epithelial-to-mesenchymal transition
TGF-β response representative signature
Hallmark TGF-β signaling
Wnt/TGF-β signature
T cells exhaustion signature
Upregulted genes in exhausted T cells
IFN-γ response representative signature
Hallmark IFN-γ response
Hallmark IFN-α response
18-gene IFN-γ-related signature
Cholesterol-induced inflammatory response
186-gene Poor survival signature
Poor survival activated HSC signature
ssGSEA
Enrichment score
Low
High
NTP prediction
Presence of signature
Absence of signature
186-gene prognostic signature
Poor survival
non-significant
Good survival

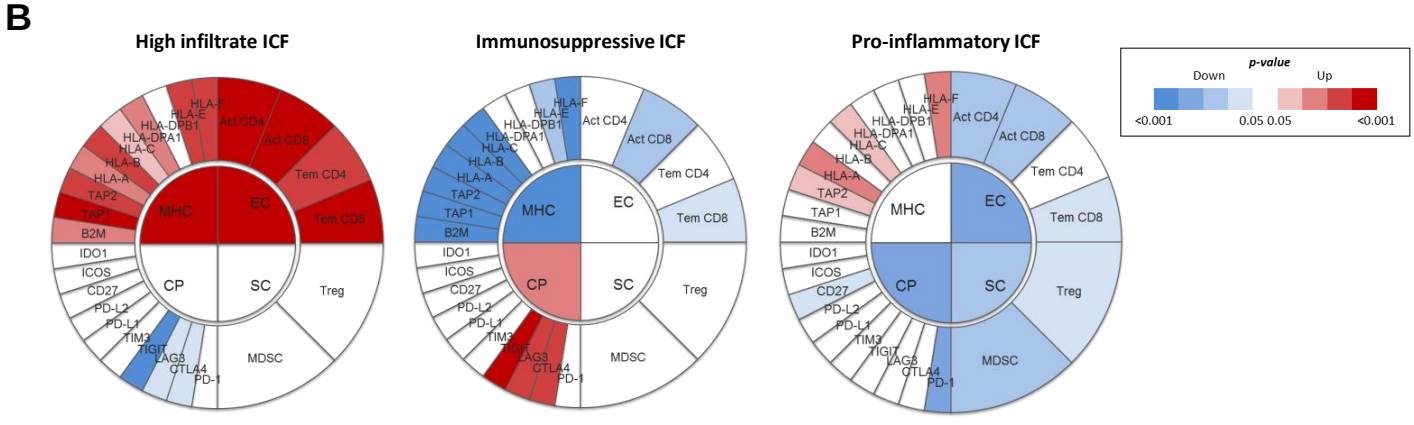
B
High infiltrate ICF
Immunosuppressive ICF
Pro-inflammatory ICF
p-value
Down
Up
<0.001
0.05 0.05
<0.001
MHC
EC
CP
SC
Act CD4
Act CD8
Tem CD4
Tem CD8
Treg
MDSC

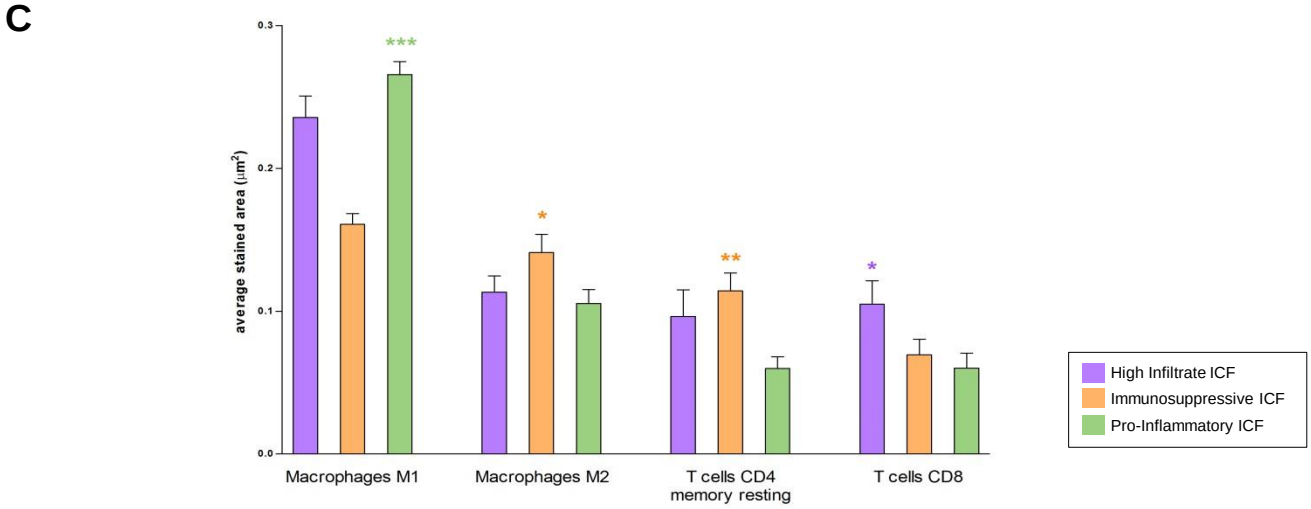
C
average stained area (μm²)
Macrophages M1
Macrophages M2
T cells CD4 memory resting
T cells CD8
High Infiltrate ICF
Immunosuppressive ICF
Pro-Inflammatory ICF

Figure 3

A

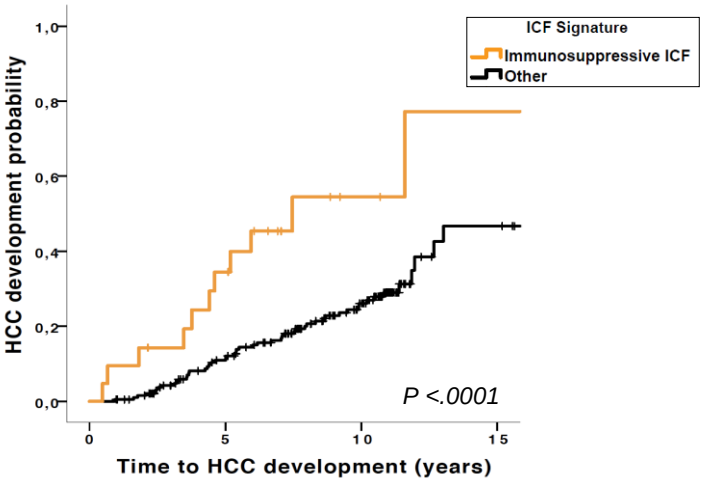

Immunosuppressive ICF	21	13	3	1
Rest	195	154	88	13

B

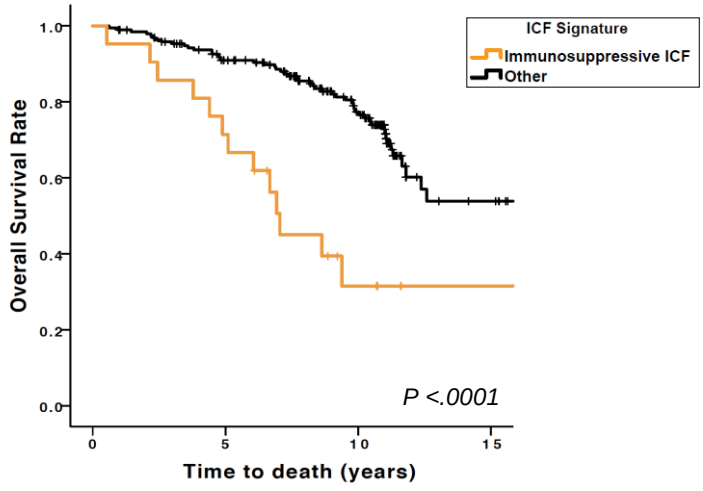

Immunosuppressive ICF	21	15	4	1
Rest	195	163	96	15

C

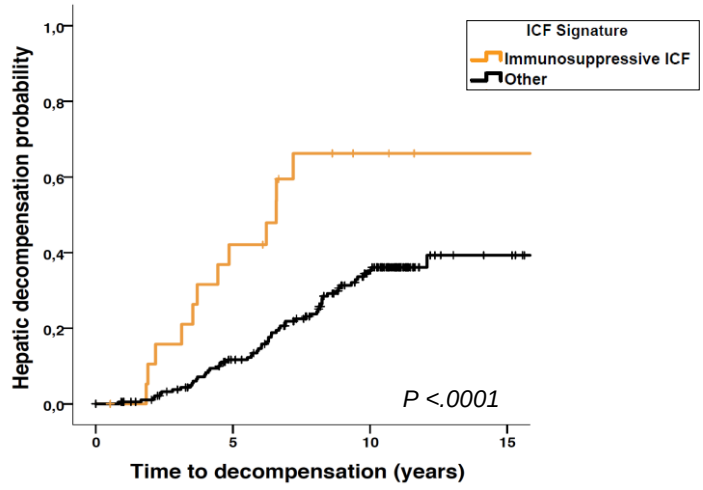

Immunosuppressive ICF	21	11	3	1
Rest	195	152	78	14

Figure 4

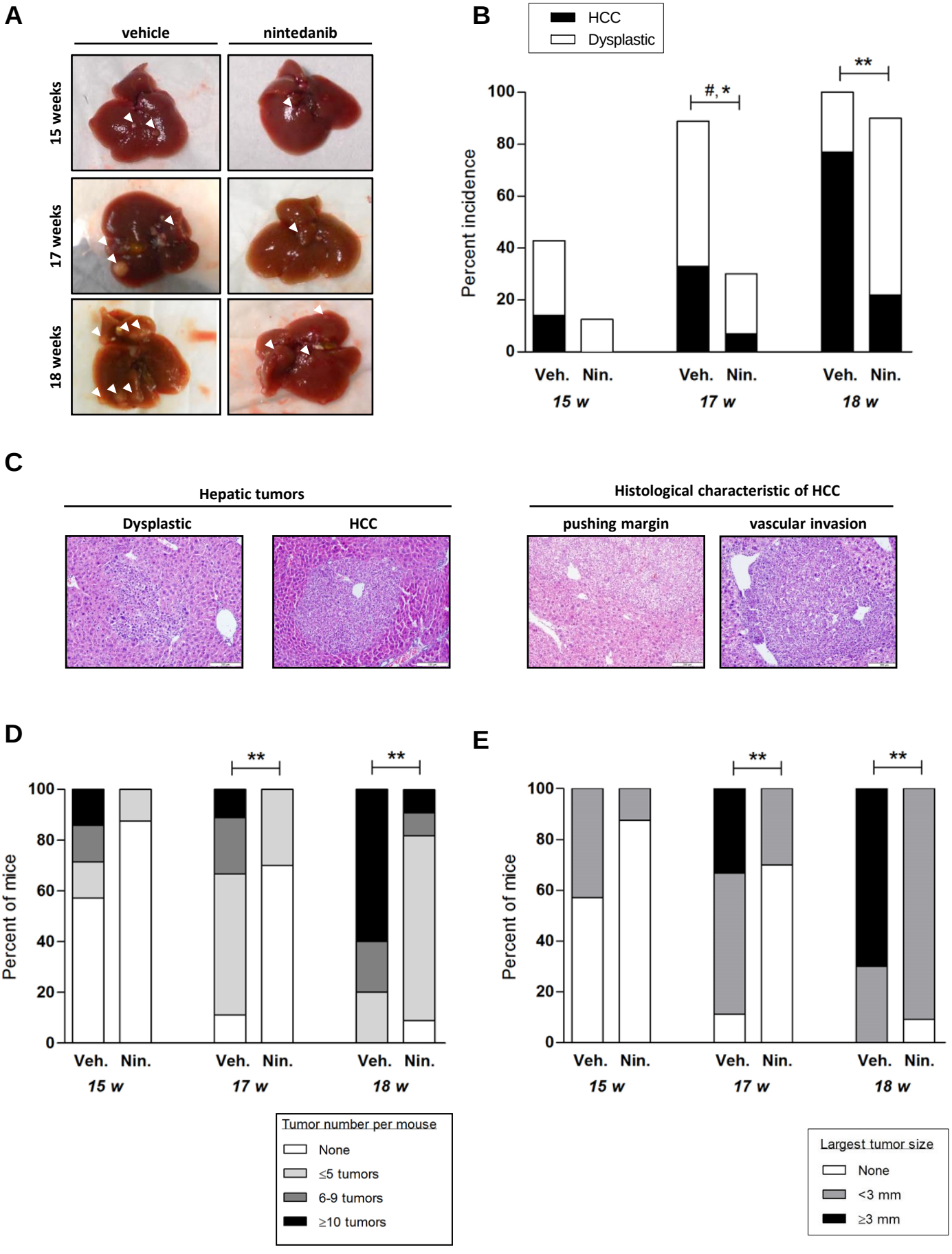
A
vehicle
nintedanib
15 weeks
17 weeks
18 weeks
B
HCC
Dysplastic
Percent incidence
100
80
60
40
20
0
#, *
**
Veh. Nin.
15 w
Veh. Nin.
17 w
Veh. Nin.
18 w
C
Hepatic tumors
Dysplastic
HCC
Histological characteristic of HCC
pushing margin
vascular invasion
D
Percent of mice
100
80
60
40
20
0
**
**
Veh. Nin.
15 w
Veh. Nin.
17 w
Veh. Nin.
18 w
Tumor number per mouse
None
≤5 tumors
6-9 tumors
≥10 tumors
E
Percent of mice
100
80
60
40
20
0
**
**
Veh. Nin.
15 w
Veh. Nin.
17 w
Veh. Nin.
18 w
Largest tumor size
None
<3 mm
≥3 mm

Figure 5

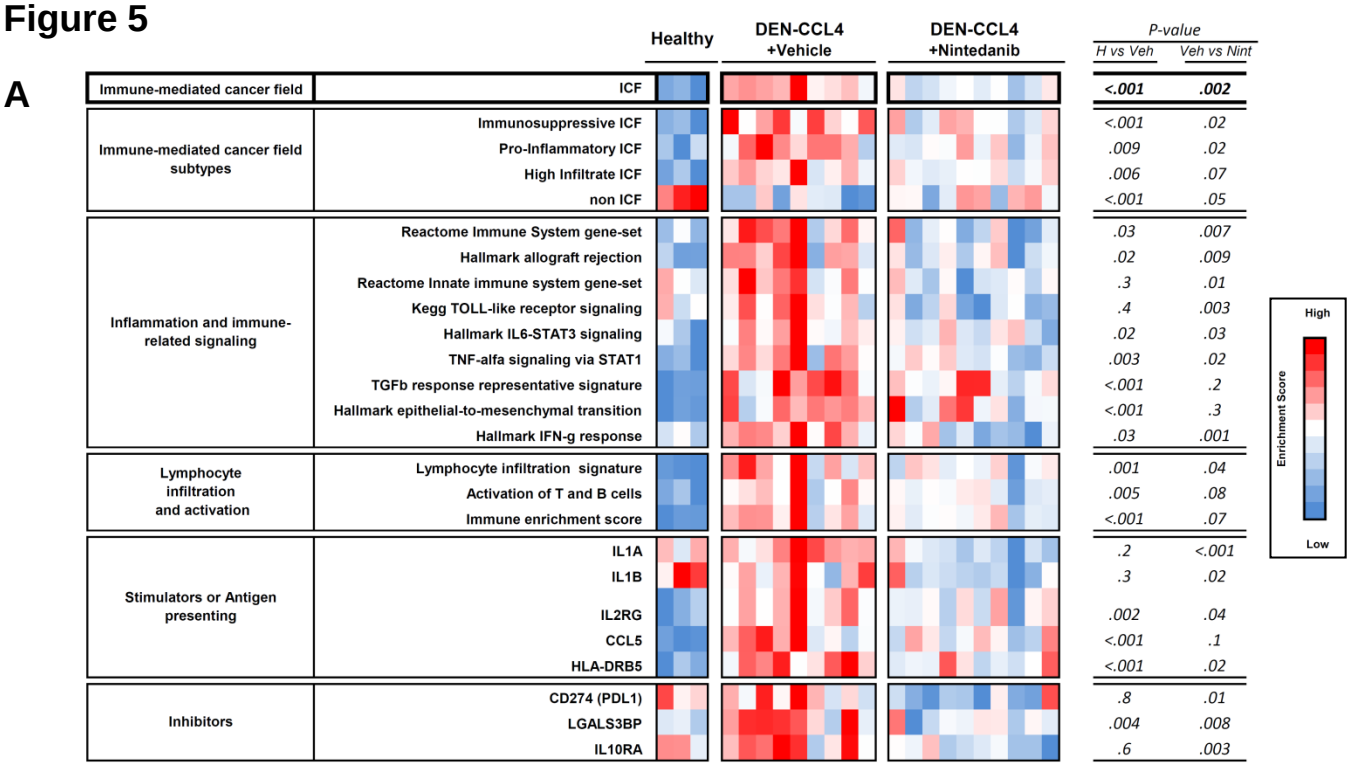
A
Healthy
DEN-CCL4 +Vehicle
DEN-CCL4 +Nintedanib
P-value
H vs Veh
Veh vs Nint
Immune-mediated cancer field
ICF
<.001 .002
Immune-mediated cancer field subtypes
Immunosuppressive ICF <.001 .02
Pro-Inflammatory ICF .009 .02
High Infiltrate ICF .006 .07
non ICF <.001 .05
Inflammation and immune-related signaling
Reactome Immune System gene-set .03 .007
Hallmark allograft rejection .02 .009
Reactome Innate immune system gene-set .3 .01
Kegg TOLL-like receptor signaling .4 .003
Hallmark IL6-STAT3 signaling .02 .03
TNF-alfa signaling via STAT1 .003 .02
TGFb response representative signature <.001 .2
Hallmark epithelial-to-mesenchymal transition <.001 .3
Hallmark IFN-g response .03 .001
Lymphocyte infiltration and activation
Lymphocyte infiltration signature .001 .04
Activation of T and B cells .005 .08
Immune enrichment score <.001 .07
Stimulators or Antigen presenting
IL1A .2 <.001
IL1B .3 .02
IL2RG .002 .04
CCL5 <.001 .1
HLA-DRB5 <.001 .02
Inhibitors
CD274 (PDL1) .8 .01
LGALS3BP .004 .008
IL10RA .6 .003
High
Enrichment Score
Low

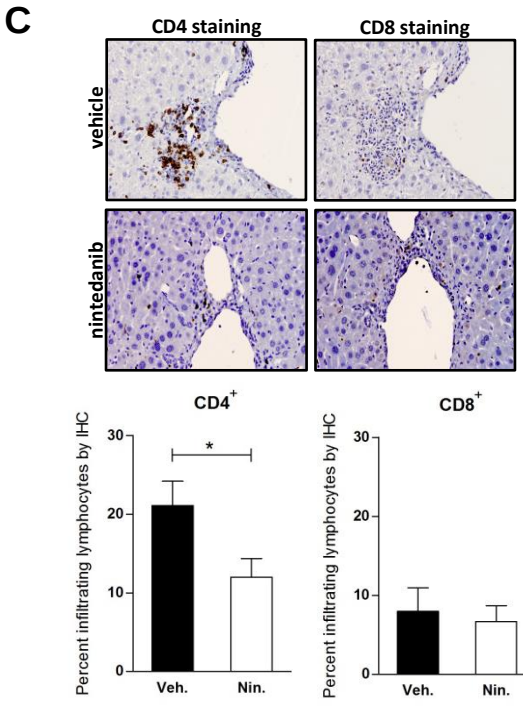
C
CD4 staining
CD8 staining
vehicle
nintedanib
CD4+
CD8+
Percent infiltrating lymphocytes by IHC
30
20
10
0
*
Veh.
Nin.

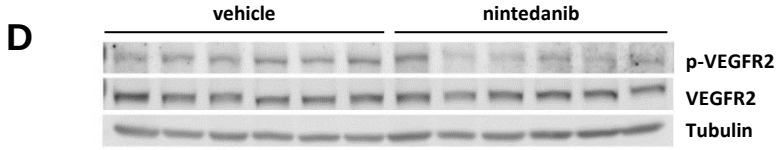
D
vehicle
nintedanib
p-VEGFR2
VEGFR2
Tubulin

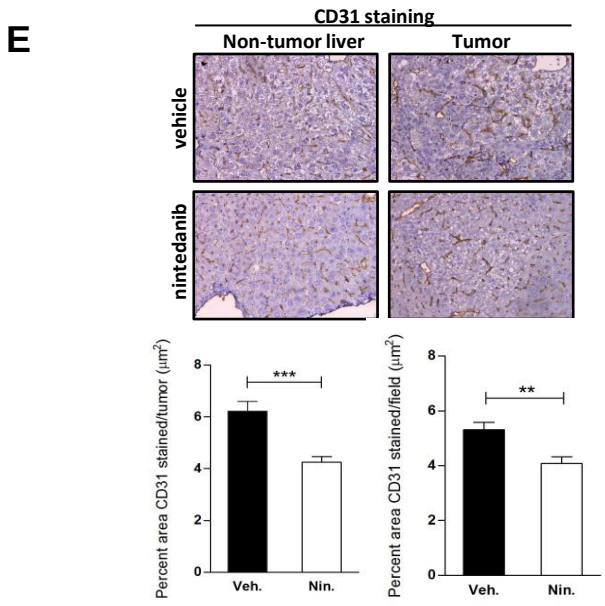
E
CD31 staining
Non-tumor liver
Tumor
vehicle
nintedanib
Percent area CD31 stained/tumor (μm²)
Percent area CD31 stained/field (μm²)
8
6
4
2
0
***
**
Veh.
Nin.

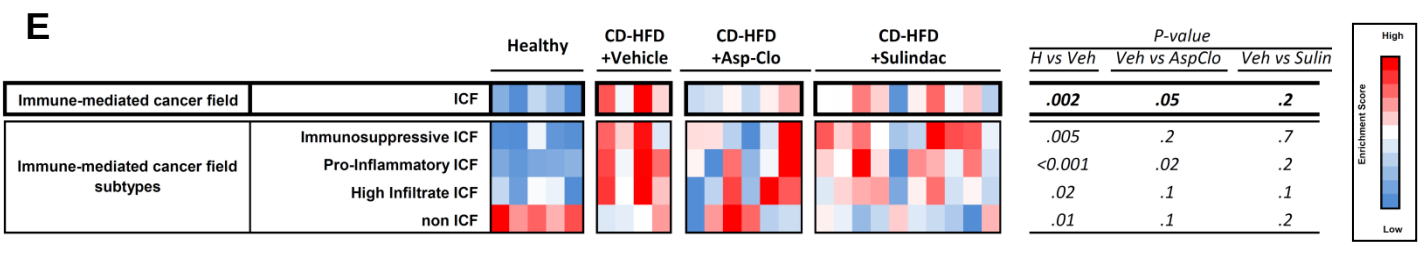
E
Healthy
CD-HFD +Vehicle
CD-HFD +Asp-Clo
CD-HFD +Sulindac
P-value
H vs Veh
Veh vs AspClo
Veh vs Sulin
Immune-mediated cancer field
ICF
.002 .05 .2
Immune-mediated cancer field subtypes
Immunosuppressive ICF .005 .2 .7
Pro-Inflammatory ICF <0.001 .02 .2
High Infiltrate ICF .02 .1 .1
non ICF .01 .1 .2
High
Enrichment Score
Low

SUPPLEMENTARY MATERIAL

SUPPLEMENTARY METHODS

Histological analysis of human samples

Histological evaluation was performed in 98 tissue samples obtained from patients with early HCC included in the study cohort. The Portal/septal, pericentral and lobular Inflammation were assessed as follows: 0=absent; 1= mild; 2= moderate; and 3= marked. The presence or absence (1 or 0, respectively) of interface inflammation, as well as lymphoid aggregates was also evaluated. The latter structures were mainly found in the periportal/periseptal areas. An inflammatory infiltrate score was created by summing the values given by the portal/septal, lobular and interface inflammation. Pericentral inflammation was not considered for the scoring system since 57% of patients were cirrhotic. According to the final score, we defined two inflammatory categories: the absent-mild category if the score was < 3, and the moderate-marked category if the score was ≥3. The presence or absence of cirrhosis was defined according to METAVIR algorithm[1] (F0-1-2-3/F4). Ductular proliferation was also considered. Steatosis was assessed based on the size of the fat vesicles (macrovesicular or microvesicular) and the localization of the fat droplets in the liver parenchyma (periseptal/periportal, pericentral or lobular). The presence or absence of ballooning, apoptotic bodies and oncocytic change was also evaluated. Immunohistochemistry for CD4 and CD8 was performed in a subset of 70 patients of the training cohort. Staining was carried out on 3µm-thick FFPE tissue sections collected from an 40-44ºC flotation bath containing deionized water and mounted on 25 X 75 mm positively (+) charged slides. The slides were dried at 60ºC in convection oven for 30min. Deparaffinization was performed followed by standard cell conditioning 1 (ULTRA CC1 from Ventana Medical Systems, Inc.). Staining was performed using Ventana BenchMark ULTRA system with the primary antibody approximately 20min, 36ºC. Signal was captured using ultraview universal diaminobenzidine (DAB) detection kit and blocked with antibody diluent (REF 251-018) for 8 min. Samples were counterstained with hematoxylin for 4 min and post counterstained with Bluing Reagent for 4 min. The primary antibodies used were anti-CD4 (Roche, clone SP35) and anti-CD8 (Roche, clone SP57). The quantification was done automatically (Image J) by calculating the positive areas (μm^2) -considering 5 random areas within lobular and portal/septal infiltrates of the non-tumor liver tissue- at 200X magnification and using the same threshold for all samples.

Generation of the DEN/CCl_4 animal Model

The chemically-induced (DEN/CCl_4) model was generated as previously described[2,3]. HCC was induced by a single intraperitoneal (i.p.) injection of N-diethylnitrosamine (DEN; Sigma-Aldrich, MO; 25 mg/kg i.p. dissolved in 0.9% sodium chloride solution) given at day 15 postpartum followed by 11-14 weekly injections of carbon tetrachloride (CCl_4 0.5 ml/kg i.p., dissolved in corn oil) starting at 4 weeks of age (**Supplementary Figure 7A**). Mice (n=55) were randomized at 12 weeks of age to receive 50 mg/kg/day of nintedanib (Boehringer Ingelheim) (n=29) or vehicle (n=26). The vehicle solution was formulated as follows: 1.8 % Hydroxypropyl Beta Cyclodextrin (HPß-CD), 5% acetic acid (10%) and Natrosol (0.5%). At 15, 17 and 18 weeks of age mice were sacrificed 48h after the last dose of CCl_4, having been treated with nintedanib for 3, 5 and 6 weeks, respectively (n=15-21 per time-point). Immediately after sacrifice, livers were explanted, digitally photographed and weighed. The evaluation of macroscopic malignant nodules was assessed by two independent investigators. Based on visual criteria, a hepatic lesion with a diameter >0.5 mm and with dysmorphic and/or dyschromic surface was considered a hepatic tumor. The diameter of tumors was measured with a hand caliper. The biological end-points for chemopreventive efficacy were a) incidence of hepatic tumors, b) number of tumors and c) size, considering the largest diameter of all counted tumors. The largest liver lobe was fixed in buffered 4% paraformaldehyde (PFA) for 24 hours for posterior histological and immunohistochemical analysis. In addition, samples of adjacent non-tumor liver were snap frozen at -80ºC for subsequent RNA and protein analysis. Potential treatment-related toxicity was evaluated by monitoring body weight losses and quantitative determination of serum aspartate aminotransferase (AST) and alanine aminotransferase (ALT).

Histological and Immunohistochemical analysis of the mouse samples

Formalin-fixed paraffin-embedded (FFPE) mouse liver samples were cut in 4 µm sections and stained with hematoxylin and eosin (H&E) for further histological examination. The samples were assessed taking into consideration non-tumor and tumor tissue by two expert liver pathologists (CM, MS) blinded to the treatments. In the non-tumor tissue, the number of lymphoid aggregates was determined. These were defined as polarized aggregates composed mainly of lymphocytes with scant plasma cells, neutrophils and macrophages localized in the periportal and pericentral areas with a measure no bigger than 0.1 mm. The presence of inflammatory infiltrates was also

determined for the periportal, pericentral and lobular area using a scoring system as follows: 0=absence or rare; 1=mild; 2=mild-moderate; 3=moderate; 4=moderate-marked; and 5=marked. Other variables such as the presence of microabscesses, ductular proliferation (0=absence; 1=<25% of portal tracts involved; 2=25-50% of portal tracts involved; 3=>50% of portal tracts involved), necrosis, steatosis, apoptotic bodies, were also determined. Ballooning was defined according to the following scale being 0= absence; 1= focal; 2= multiple foci; 3= diffuse. Hepatic fibrosis was assessed by Sirius Red staining. The METAVIR algorithm[1] was used to grade hepatic fibrosis from F0 (no scarring) to F4 (cirrhosis or severe fibrosis). Also, perisinusoidal fibrosis was evaluated as follows 1= 0-5%; 2= 5-33%; 3= 33-66% and 4= >60%. Histologically, hepatic tumors presented a high cellular density composed of small cells with altered nuclear/cytoplasmic ratio, and a clear cytoplasm. Among these hepatic tumors, those circular well-defined lesions with pushing margins were diagnosed as HCCs whereas a dysplastic nodule was considered when the lesion had an ill-defined shape within the liver parenchyma. The presence of vascular invasion was a characteristic attributed to HCC. The size of both lesions was not used to make a distinction between them, although HCC tend to be larger than dysplastic nodules. Finally, for the evaluation of the chemopreventive effects of a TKI in adjacent liver tissue, FFPE sections from mice sacrificed at 17 weeks of age were analyzed by immunohistochemistry (n=5 mice per treatment arm). Heat-induced antigen retrieval was performed with 10 mM sodium citrate buffer (pH 6.0) or 0.5 M Tris buffer (pH 10.0) for 15 minutes (5 minutes, 3 times), and the reaction was quenched using hydrogen peroxide 3%. After washing with PBS, samples were incubated with anti-pERK (phosphoThr202/Tyr204) (from Cell Signaling, Danvers, MA), anti-CD31 (Abcam plc, Cambridge, UK), and anti-CD4 and anti-CD8 (both from Cell Signaling, Danvers, MA). DAB (3,3'-diaminobenzidine) was used as detection system (EnVision+ System-HRP, Dako). Morphometric quantification of percentage area of liver vasculature (n=5 mice per treatment arm) was performed by evaluating the mean area of CD31 staining, in randomly selected low magnification fields (n=5, 10X fields for CD31 staining; n=10, 20x fields for collagen) using ImageJ software.

RNA extraction and gene expression profiling of mice livers

Total RNA from the two mouse models herein described was extracted from 20 mg fresh-frozen non-tumoral liver tissue with Trizol reagent (Invitrogen) and purified with RNeasy

columns (Qiagen, Valencia, CA). RNA sample concentration and quality were assessed by NanoDrop ND-1000 spectrometer (NanoDrop, Wilmington, DE) and bioanalyzer (Agilent, Palo Alto, CA), respectively. Gene expression microarray studies were conducted using the Gene Chip HT MG-430 (Affymetrix). The raw .cel files were background corrected and normalized using the Robust Multiarray Averaging (RMA) procedure [4], with a custom chip definition file (.cdf) from the Custom CDF project (HTMG430PM_Mm_ENTREZG v18.0)[5]. To assess ICF-signature enrichment through ssGSEA (GenePattern), mice genes were humanized and intensity values were log transformed. For qRT-PCR analysis, cDNA was synthesized from 1 µg purified total RNA using SuperScript III reverse transcriptase (Invitrogen). Relative gene expression levels were measured by TaqMan Gene Expression Assays (Applied Biosystems, Foster City, CA) using specific probes for *Col1a1* (Mm00801666_g1), *Col1a2* (Mm00483888_m1), *Acta2* (Mm01546133_m1), and *Pdgfrb* (Mm00435546_m1). The housekeeping gene *GAPDH* (Mm99999915_g1) was used for normalization. Microarray data of these newly profiled samples are in GEO under accession number (GSE125975).

Western-blot analysis

Whole-cell extracts were collected in lysis buffer (50 mM Tris pH 7.4, 150 mM NaCl, 1% Triton X-100, 0.1% SDS, 0.25 mM EDTA, 1% Sodium deoxycholate) containing phosphatases and proteases inhibitors (Roche). 30-70 µg of total protein were resolved in polyacrylamide gels and transferred to nitrocellulose membranes (Pierce, Rockford, IL). Membranes were BSA-blocked and hybridized overnight at 4 °C with primary antibodies against VEGFR-2, phospho-VEGFR-2 (Tyr951), Akt, phospho-Akt (Ser473), ERK-1/2, phospho-ERK-1/2 (Thr202/Tyr204), Bcl-xL, PARP (all from Cell Signaling), and tubulin (Sigma). Appropriate HRP-conjugated secondary antibodies (Dako) were incubated for 1h at room temperature and immunoreactivity was detected with a LAS-3000 imaging system (Fujifilm, Tokyo, Japan) using Amersham™ ECL™ Prime western Blotting Detection Reagent (GE Healthcare, United Kingdom).

SUPPLEMENTARY FIGURE LEGENDS

Supplementary Figure 1. Identification of an immune-mediated cancer field in the non-tumor liver tissues and its association with overall survival in patients with early HCC. A) Consensus-clustered analysis of gene-sets recapitulating the different perturbation states of immune. The figure includes a subgroup of representative gene-sets among the ~5000 gene-sets evaluated (Collection C7 of MsigDB). **B)** Kaplan-Meier estimates of overall survival according to the presence of the immune-mediated cancer field, **B)** the presence of High-Infiltrate subtype, and **C)** the different ICF subtypes. ICF: immune-mediated cancer field. C)

Supplementary Figure 2. Immunohistochemistry assessment of CD4 and CD8 positivity in non-tumor liver tissues. Average stained area was automatically quantified and compared in **A)** samples from patients belonging to the ICF and non ICF subgroups, and **B)** between ICF subtypes. n= 15-19 samples per group. ***=p<0.001.

Supplementary Figure 3. Gene-overlapping between the 172 ICF gene-expression signature and other previously reported poor-prognosis expression signatures in non-tumor liver tissue. Signatures are denoted by the name of the first authors in each of the publications[6–10]. Numbers in brackets indicate the total number of genes constitute each signature, whereas bold numbers represent the number of genes that overlap between each signature and the ICF signature (herein referred as *Moeini*).

Supplementary Figure 4. External validation of the molecular and clinical features of the immune-mediated cancer field and its subtypes. A) Main molecular characteristics of the immune-mediated cancer field and the 3 distinct molecular subtypes were validated in a previously reported cohort including 225 FFPE non-tumoral liver tissue from patients with early HCC profiled by DASL array. **B)** Kaplan-Meier estimates of overall survival according to the presence of the immune-mediated cancer field. ICF: immune-mediated cancer field.

Supplementary Figure 5. Association of the presence of immune-mediated cancer field subtypes with risk of HCC development and advanced liver disease in fibrotic patients. A) Kaplan-Meier analysis of the correlation of the immune-mediated cancer

field subtypes with risk of HCC development. **B)** Correlation of the prediction of immune-mediated cancer field subtypes with fibrosis and inflammation degree. Fibrosis degree was classified as: none (S0), low (S1-S2) and high (S3-S4). Inflammation degree was classified as: none (G0), low (G1-G2) and high (G3-G4). other ICF: High Infiltrate and Pro-inflammatory ICFs. Non ICF: non ICF subtype and unclassified cases.

Supplementary Figure 6. I*n silico* enrichment analysis of gene sets recapitulating the targets of approved molecular therapies in non-tumor liver of patients with early HCC. A) Heatmap representing the enrichment scores of gene sets recapitulating the molecular targets of top enriched therapies in non-tumor liver of HCC patients harboring the immune-mediated cancer field (ICF) in comparison to non ICF/other. **B)** Constellation map representation of enrichment of gene set of main targets of top scored therapies centered around the immune-mediated cancer field phenotype. The Blue lines denote presence of overlapping genes among the different gene sets. NMI: Normalized mutual information. AUC.pval: Area under the curve p-value. t.stat: t-statistic. t.pval: t-statistic p-value.

Supplementary Figure 7. Prolonged treatment with nintedanib does not induce significant toxicity in DEN/CCl_4 induced mouse models. **A)** Experimental design of the murine model of DEN/CCl4 induced hepatocarcinogenesis in the context of liver fibrosis. **B)** Monitoring of body weight in all mice from each experimental group during the administration of nintedanib or vehicle at the longest time-point, 18-weeks of age. **C)** Evaluation of the serum levels of alanine transaminase (ALT) and aspartate transaminase (AST) in each experimental group.

Supplementary Figure 8. Nintedanib inhibits downstream MAPK pathway but has no effect on reverting DEN/CCl4 induced PDGF signaling nor hepatic fibrosis. A) Western-blot analysis of downstream MAPK(AKT and ERK) signaling. **B)** Representative images and quantification of pERK staining in 17 weeks old mice treated with vehicle or nintedanib. In the vehicle arm the tumors and the adjacent non-tumor tissue are positive with patchy nuclear and cytoplasmic staining, while in the nintedanib arm both are negative. T: tumor. NT: non-tumor. **C)** Western-blot analysis of the pro-fibrogenic PDGFR signaling**. D)** Representative images of Sirius Red staining in mice treated with vehicle or nintedanib. Nintedanib did not exert any significant effect on liver fibrosis. **E)** Gene expression levels of pro-fibrogenic marker genes by quantitative RT-PCR in livers

of mice sacrificed at 15, 17 and 18 weeks of age treated with vehicle or nintedanib. The *GAPDH* gene was used as a housekeeper for normalization. Significant statistical differences are defined as follows: *<0.05 and ***=p<0.001.

SUPPLEMENTARY REFERENCES

1. Bedossa P, Poynard T. An algorithm for the grading of activity in chronic hepatitis C. The METAVIR Cooperative Study Group. Hepatology 1996;24:289–93.
2. Uehara T, Ainslie GR, Kutanzi K, et al. Molecular Mechanisms of Fibrosis-Associated Promotion of Liver Carcinogenesis. Toxicol Sci 2013;132:53–63.
3. Dapito DH, Mencin A, Gwak G-Y, et al. Promotion of hepatocellular carcinoma by the intestinal microbiota and TLR4. Cancer Cell 2012;21:504–16.
4. Irizarry RA, Hobbs B, Collin F, et al. Exploration, normalization, and summaries of high density oligonucleotide array probe level data. Biostatistics 2003;4:249–64.
5. Dai M, Wang P, Boyd AD, et al. Evolving gene/transcript definitions significantly alter the interpretation of GeneChip data. Nucleic Acids Res 2005;33:e175.
6. Nakagawa S, Wei L, Song WM, et al. Molecular Liver Cancer Prevention in Cirrhosis by Organ Transcriptome Analysis and Lysophosphatidic Acid Pathway Inhibition. Cancer Cell 2016;30:879–890.
7. Hoshida Y, Villanueva A, Kobayashi M, et al. Gene expression in fixed tissues and outcome in hepatocellular carcinoma. N Engl J Med 2008;359:1995–2004.
8. Kim JH, Sohn BH, Lee H-S, et al. Genomic predictors for recurrence patterns of hepatocellular carcinoma: model derivation and validation. Beck AH, ed. PLoS Med 2014;11:e1001770.
9. Ji J, Eggert T, Budhu A, et al. Hepatic stellate cell and monocyte interaction contributes to poor prognosis in hepatocellular carcinoma. Hepatology 2015;62:481–95.
10. Zhang DY, Goossens N, Guo J, et al. A hepatic stellate cell gene expression signature associated with outcomes in hepatitis C cirrhosis and hepatocellular carcinoma after curative resection. Gut 2016;65:1754–64.

Supplementary Figure 1

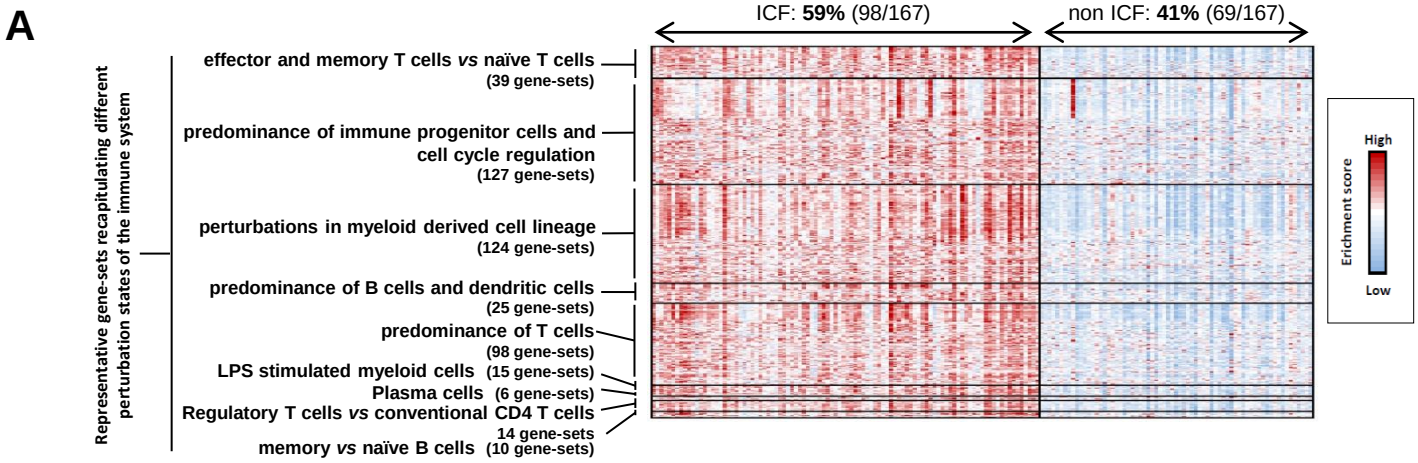

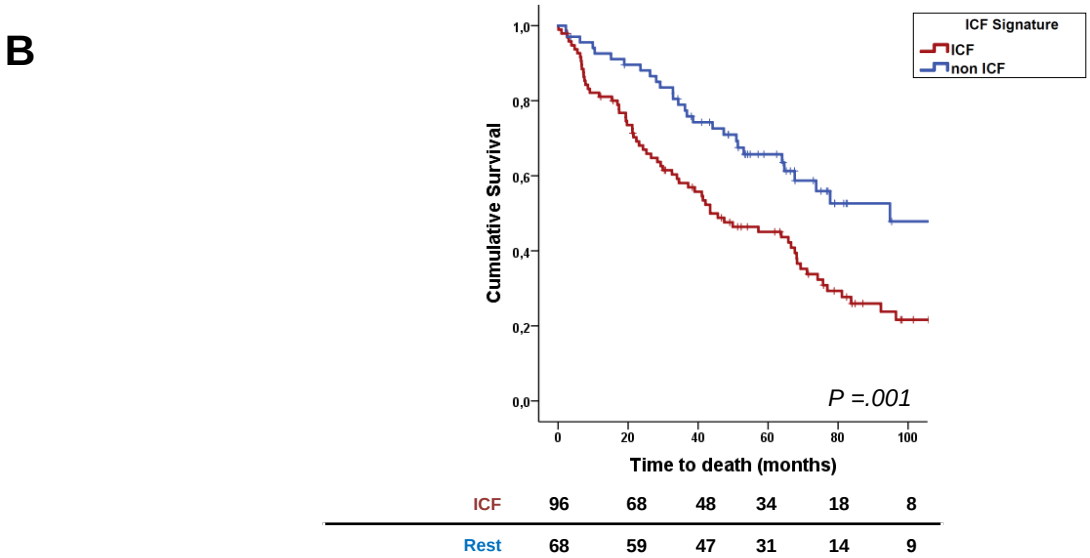

ICF	96	68	48	34	18	8
Rest	68	59	47	31	14	9

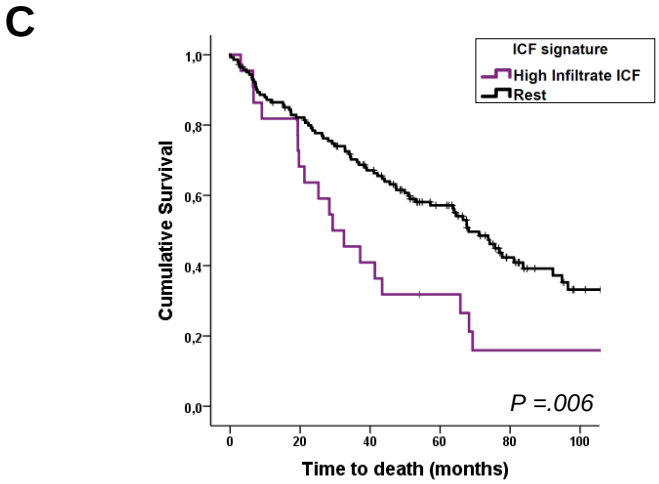

High Infiltrate ICF	22	15	9	6	3	3
Rest	142	112	86	59	29	14

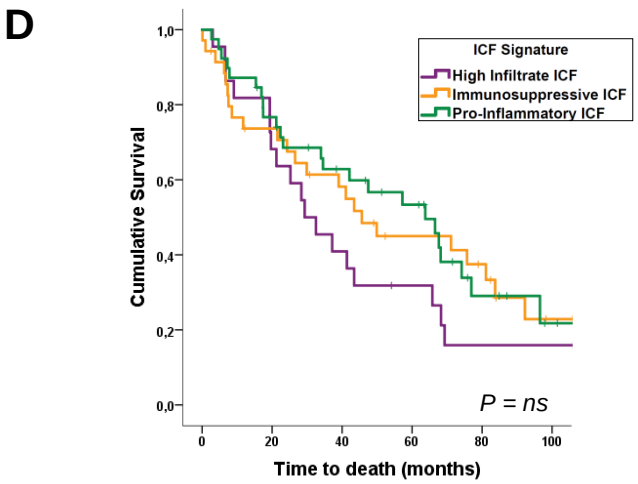

High Infiltrate ICF	22	15	9	6	3	3
Immunosuppressive ICF	35	24	18	12	9	3
Pro-Inflammatory ICF	39	29	21	16	6	2

Supplementary Figure 2

A

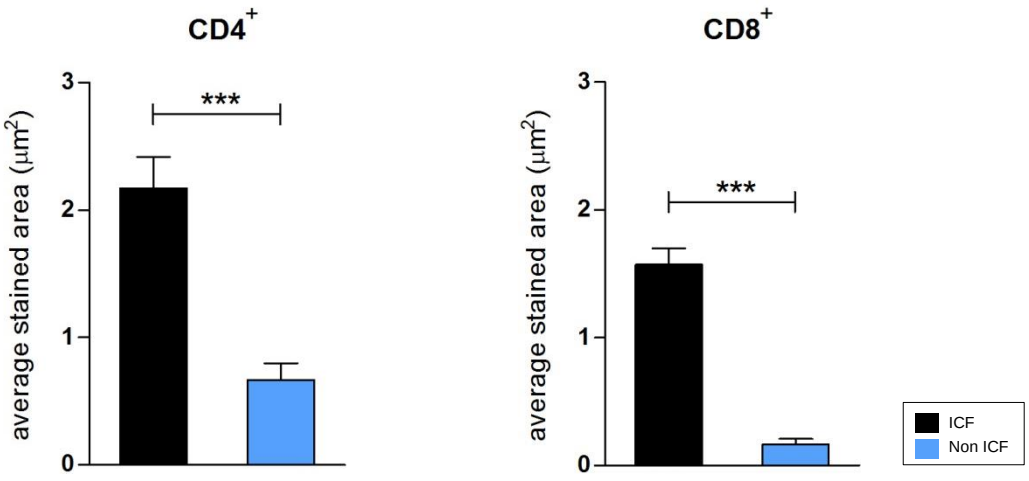

B

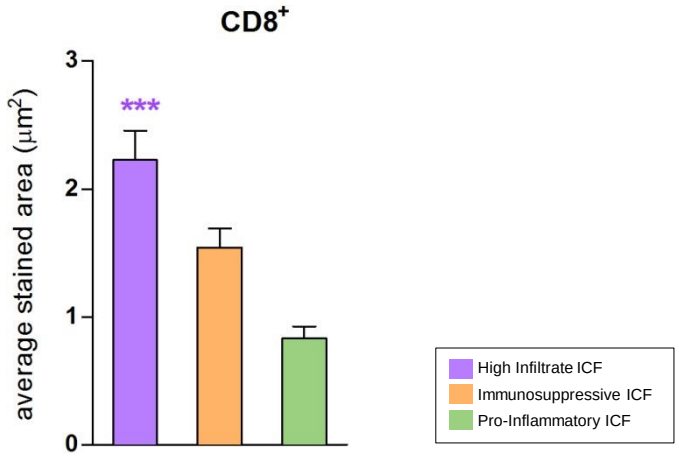

Supplementary Figure 3

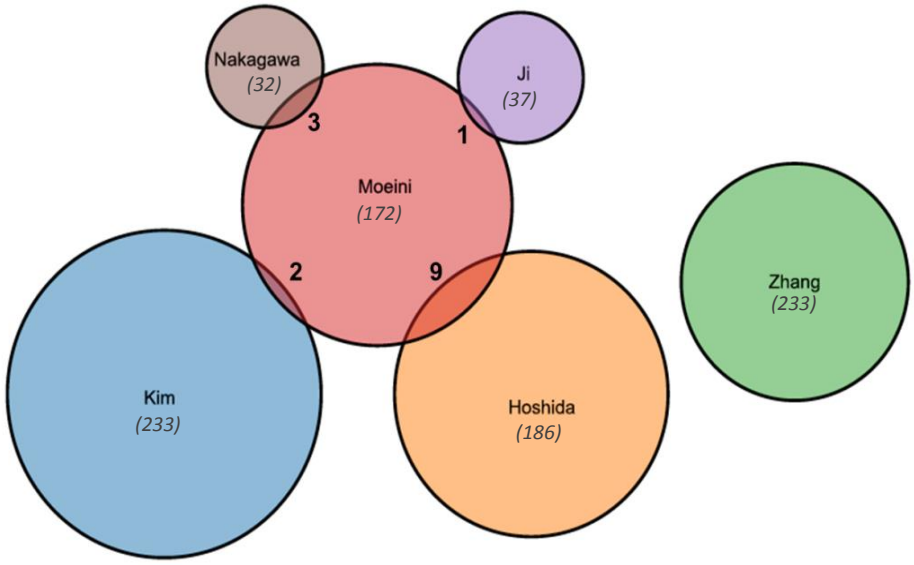

Supplementary Figure 4

A

Validation cohort (GSE10143, n=225 non-tumor liver tissues)

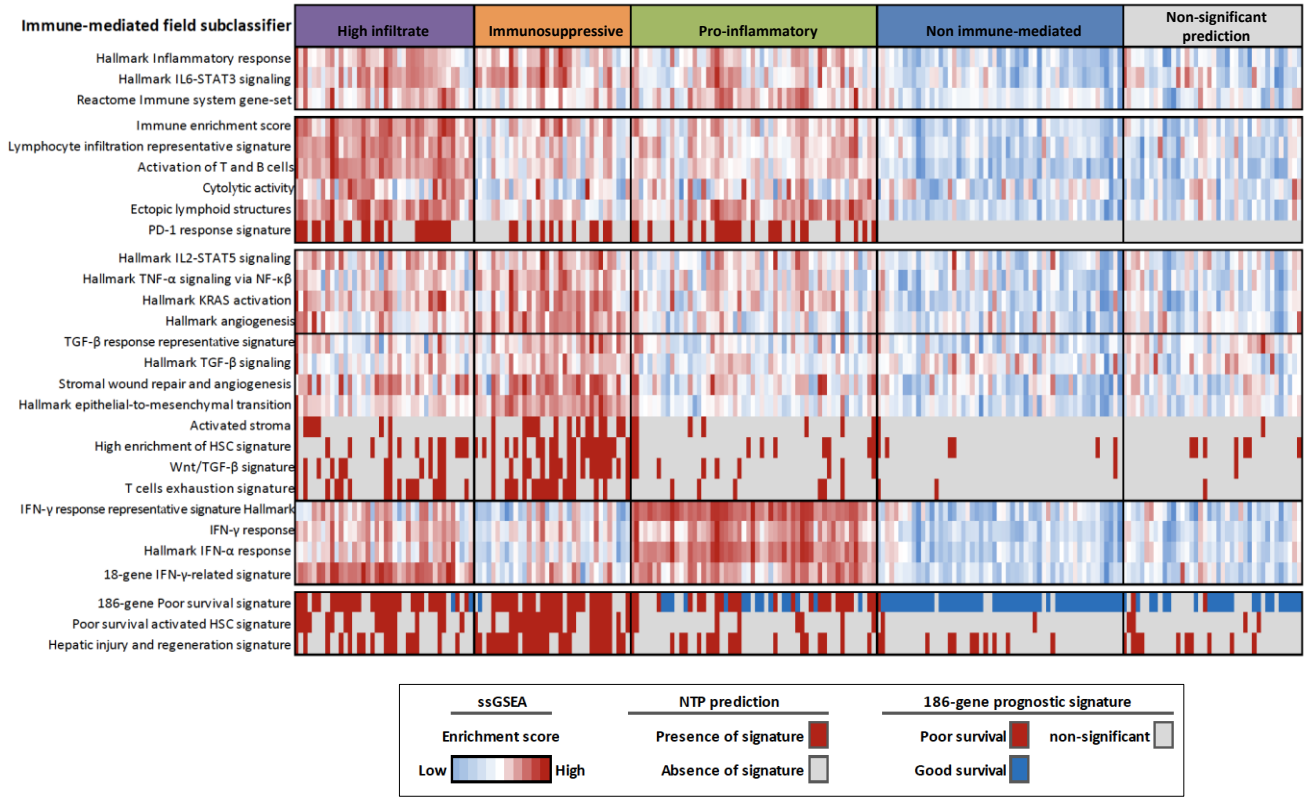

B

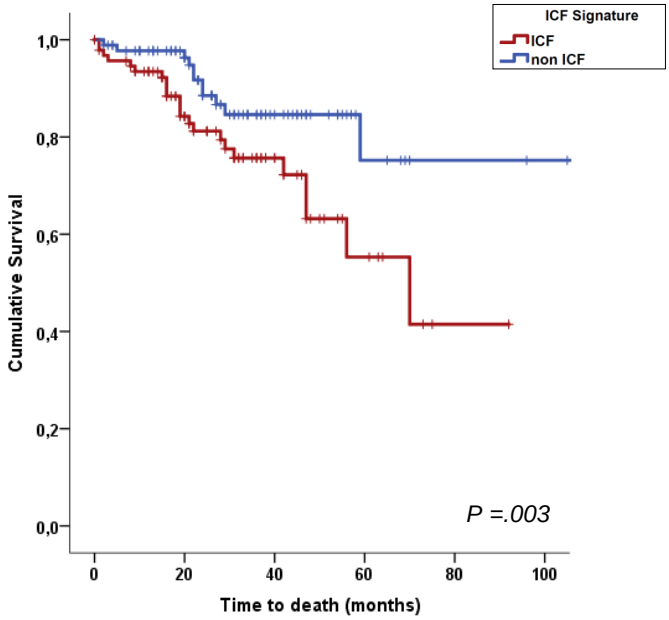

ICF	94	57	22	7	1	0
Non ICF	90	64	25	8	4	3

Supplementary Figure 5

A

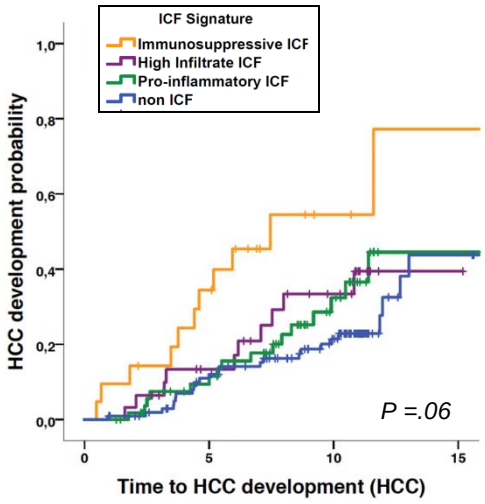

Immunosuppressive ICF	21	13	3	1
High Infiltrate ICF	31	23	13	1
Pro-Inflammatory ICF	58	45	18	3
Non ICF	106	87	57	10

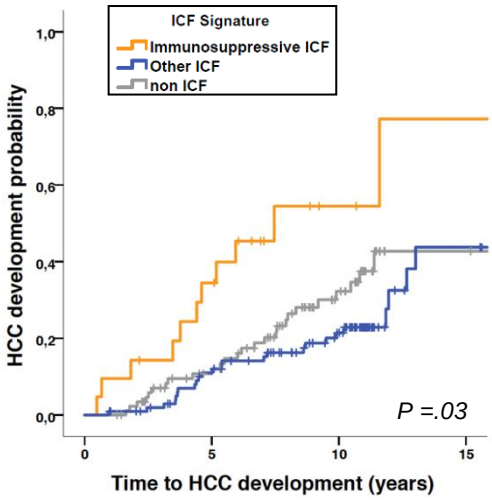

Immunosuppressive ICF	21	13	3	1
Other ICF	89	68	31	3
Non ICF	106	87	57	10

B

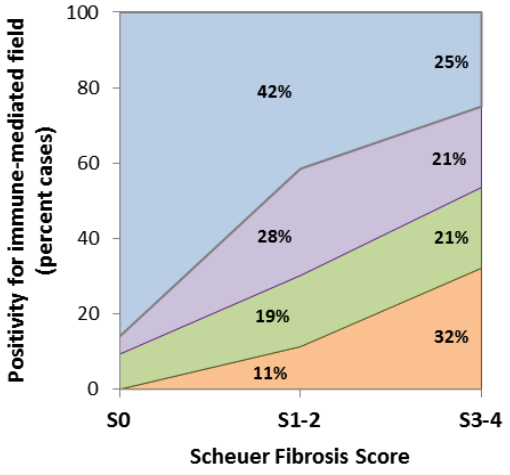

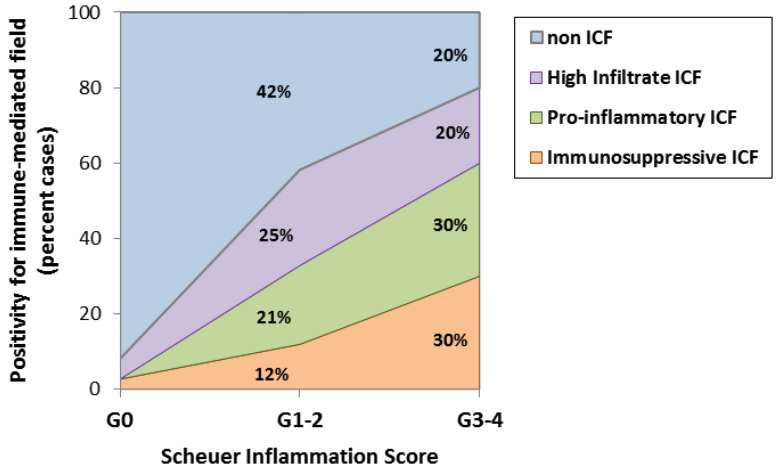

Supplementary Figure 6

A

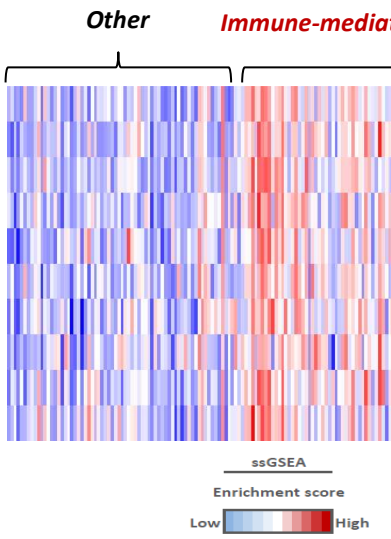

	NMI	AUC.pval	t.pval
Cabozantinib	0.2484	1.30E-14	3.03E-07
Crizotinib	0.2471	1.63E-14	7.92E-12
Nilotinib	0.2097	2.48E-13	2.31E-16
Dabrafenib	0.2	3.16E-12	1.06E-16
Bosutinib	0.1967	4.24E-12	5.03E-14
Vandetanib	0.1925	2.57E-12	1.61E-07
Gefitinib	0.1817	1.76E-10	8.22E-06
Pazopanib	0.171	6.93E-11	5.18E-11
Nintedanib	0.1662	2.25E-11	0.0007306
Ponatinib	0.1333	2.38E-09	4.51E-15

B

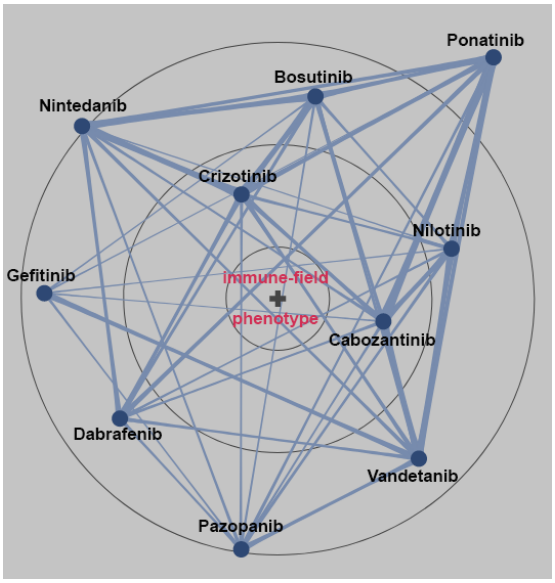

Supplementary Figure 7

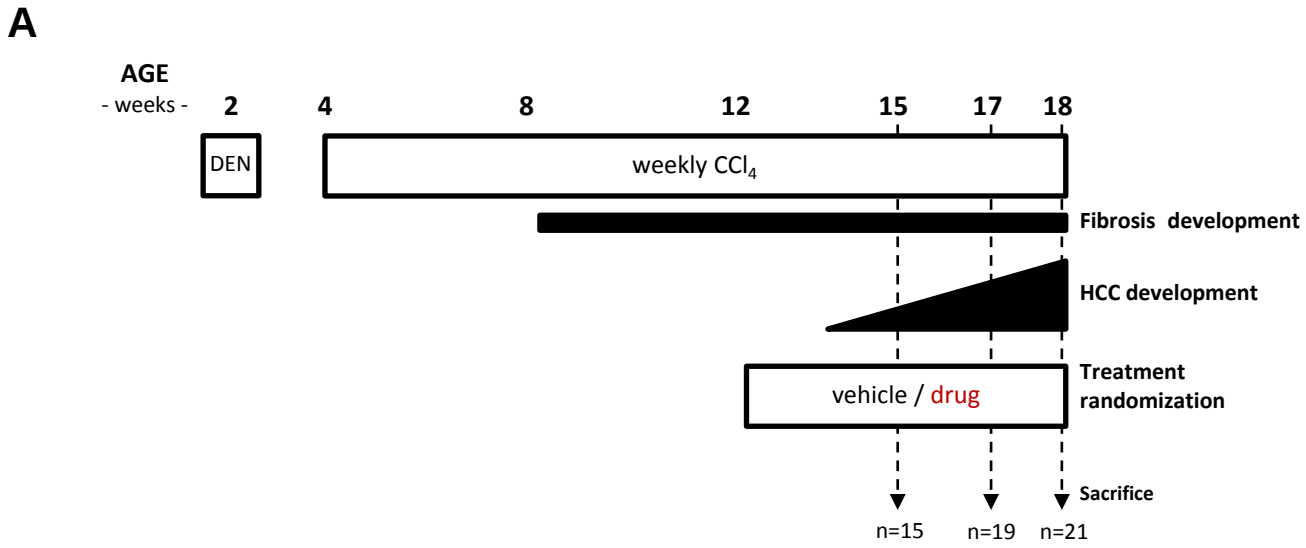

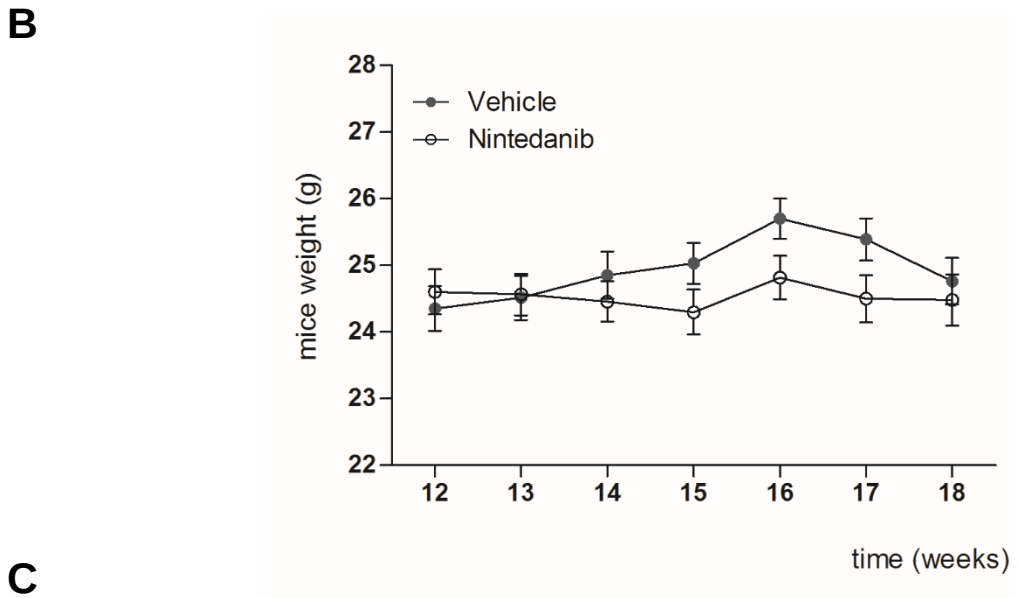

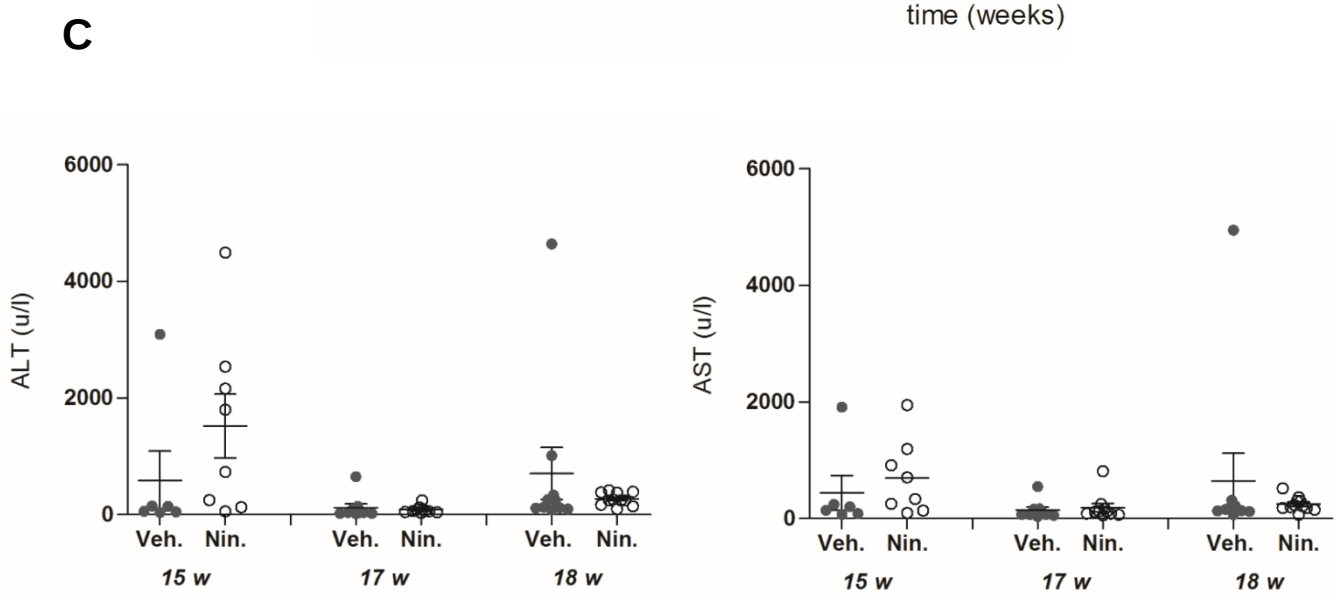

Supplementary Figure 8

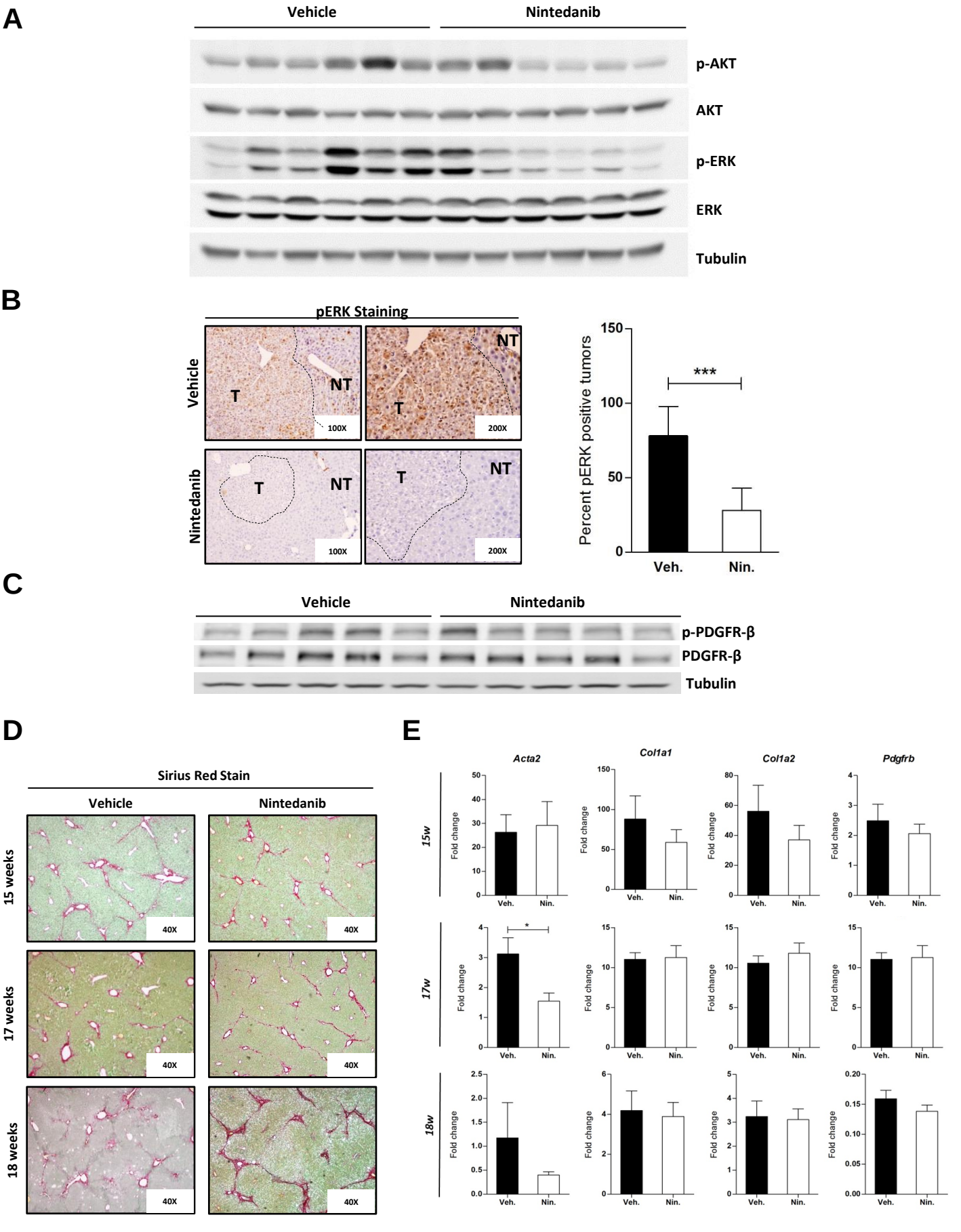

Supplementary Table 1. Clinicopathological characteristics of study cohort (n=167).

Variable	Value
Median age (years)	65.2
Gender, male (%n)	77
Etiology (%)	
Hepatitis C	46
Hepatitis B	25
Alcohol	14
Others	15
Child-Pugh score (%)	
A	99
B	1
Tumor size, cm (%)	
<2	11
2-3	28
>3	60
Multple Nodules (%)	
Absent	70
Present	30
Microvascular Invasion (%)	
Absent	69
Present	31
Satellites (%)	
Absent	70
Present	30
BCLC early stage, 0-A (%)	82
Degree of tumor differentiation (%)	
Well	16
Moderate	35
Poor	15
Bilirrubin, >1 mg/dL (%)	43
Albumin, <3.5 g/L (%)	12
Platelet Count, <100.000/mm3 (%)	22
AFP, >100 mg/dL (%)	24
Events (%)	
Recurrence	67
Death	59
Follow-up, median months (range)	67 (53-80)

Missing data: etiology (n=5), Child Pugh score (n=3, tumo size (n=2), multiple nodules (n=2), microvascular invasion (n=4), degree of tumor differentiation (n=31), bilirrubin (n=5), albumin (n=5), platelet count (n=5), AFP (n=5), recurrence (n=9) death (n=3), follow-up (n=3).

Supplementary Table 2. Previously reported gene signatures used in this study.

Signature Name	Publication
Signatures used in non-tumor tissue	
Activated stroma	Moffitt RA, et al. Nat Genet 2015;47:1168-78
Activation of monocytes/macrophages	Beck AH, et al. Clin Cancer Res 2009;15:778–87
Activation of T and B cells	Wolf DM, et al. PLoS One 2014;9:e88309
Cholesterol-induced inflammatory response	Wunder C, et al. Nat Med 2006;12:1030-8
Cytolytic activity	Rooney MS, et al. Cell 2015;160:48-61
Ectopic lymphoid structures (ELS)	Finkin S, et al. Nat Immunol 2015;16(12):1235
Hepatic injury and regeneration (HIR) signature	Kim JH, et al. PloS Med 2014;11:e1001770
Hepatic Stellate Cell (HSC) signature	Zhang DY, et al. Gut 2016;65:1754-64
Immune enrichment score	Yoshihara K, et al. Nat Commun 2013;4:2612
Liver cancer multicentric occurrence	Okamoto M, et al Ann Surg Oncol 2006;13:947-54
Lymphocyte infiltration representative signature	Thorsson V, et al. Immunity 2018;48:812-30
PD-1 response signature	Quigley M, et al. Nat Med 2010;16:1147-51
Poor survival activated HSC signature	Ji J, et al. Hepatology 2015;62:481-95
Stromal enrichment score	Yoshihara K, et al. Nat Commun 2013;4:2612
Stromal wound repair and angiogenesis	Wolf DM, et al. PLoS One 2014;9:e88309
T cell exhaustion signature	Quigley M, et al. Nat Med 2010;16:1147-51
TGF-β response representative signature	Thorsson V, et al. Immunity 2018;48:812-30
Upregulated genes in exhausted T cells	Wherry EJ, et al. Immunity 2007;27:670–684
Wnt/TGF-β signature	Lachenmayer A, et al. Clin Cancer Res 2012;18:4997-5007
18-gene IFN-γ-related signature	Ayers M, et al. J Clin Invest 2017; 127:2930–40
186-gene Poor survival signature	Hoshida Y, et al. N Engl J Med 2008;359:1995-2004
Signatures of HCC molecular subclasses	
Boyault G3 class	Boyault S, et al. Hepatology 2007;45:42-52
Chiang HCC 5 classes	Chiang DY, et al. Cancer Res 2008;68:6779-88
Coulouarn late vs early TGF-β	Coulouarn C, et al. Hepatology. 2008;47:2059-67
Hoshida S1-S2-S3	Hoshida Y, et al. Cancer Res 2009;69:7385-92
Lee Cluster A	Lee JS, et al. Hepatology 2004;40:667–76
Minguez vascular invasion	Minguez B, et al. J Hepatol. 2011;55:1325-31
Sia HCC Immune class	Sia D, et al. Gastroenterology 2017;153:812-26
Villanueva CK19 positive	Villanueva A, et al. Gastroenterology 2011;140:1501-12.e2
Villanueva NOTCH	Villanueva A, et al. Gastroenterology 2012;143:1660-1669.e7
Woo early recurrence	Woo HG, et al. Clin Cancer Res 2008;14:2056–64
Yamashita EpCAM	Yamashita T, et al. Cancer Res 2008;68:1451–61

Supplementary Table 3. Correlation of the immune-mediated cancer field (ICF) with histological characteristics.

Variable	ICF		non ICF		Fisher test
	%	n patients	%	n patients	p-value
Non-tumor tissue characteristics					
Fibrosis degree and cirrhosis					
F1-F2	11%	(7/71)	29%	(17/59)	**0.01**
F3	17%	(12/71)	22%	(13/59)	0.37
F4 (cirrhosis)	75%	(9/71)	49%	(29/59)	**0.002**
Portal/Septal Inflammation					
Absent-mild	26%	(14/54)	50%	(22/44)	
Moderate-Marked	74%	(40/54)	50%	(22/44)	**0.02**
Lobular Inflammation					
Absent-mild	94%	(51/54)	98%	(43/44)	
Moderate-Marked	6%	(3/54)	2%	(1/44)	0.63
Interface Inflammation					
Present	37%	(20/54)	23%	(10/44)	
Absent	63%	(34/54)	77%	(34/44)	0.19
Non-tumoral Inflammatory infiltrate score					
Absent-Mild	26%	(14/54)	48%	(21/44)	
Moderate-Marked	74%	(40/54)	52%	(23/44)	**0.03**
Non-Tumoral lymphoid aggregates					
Absent	20%	(11/54)	45%	(20/44)	
Present	80%	(43/54)	55%	(24/44)	**0.01**
Apoptotic bodies					
Absent	83%	(45/54)	77%	(34/44)	0.61
Present	17%	(9/54)	23%	(10/44)	
Tumor tissue characteristics					
Number of lesions					
Single	63%	(62/98)	78%	(54/69)	
Multinodular	35%	(34/98)	22%	(15/69)	*0.08*
Tumor size					
>3.5cm	58%	(56/97)	45%	(31/69)	
<3.5cm	42%	(41/97)	54%	(37/69)	0.15
Tumor satellites					
Yes	34%	(33/97)	25%	(17/69)	0.23
No	66%	(64/97)	75%	(52/69)	
Microscopic vascular invasion					
Yes	42%	(41/98)	30%	(21/69)	0.19
No	56%	(55/98)	67%	(46/69)	
Histological grade					
Well	15%	(15/98)	10%	(7/69)	0.63
Moderate	48%	(47/98)	46%	(32/69)	0.59
Poor	22%	(22/98)	19%	(13/69)	1.00
Intratumoral inflammatory infiltrate					
Mild	19%	(10/54)	21%	(9/42)	0.80
Moderate	41%	(22/54)	55%	(23/42)	0.30
Marked	37%	(20/54)	24%	(10/42)	0.18
Intratumoral Neutrophilic infiltrate					
Absent-rare	78%	(42/54)	64%	(27/42)	
Present	22%	(12/54)	36%	(15/42)	0.17
Peritumoral inflammatory infiltrate					
Mild	37%	(20/54)	24%	(10/42)	0.18
Moderate	41%	(22/54)	55%	(23/42)	0.30
Marked	19%	(10/54)	21%	(9/42)	0.80
Tertiary Lymphoid Structures (TLS)					
Present	22%	(12/54)	8%	(8/42)	
Absent	77%	(42/54)	35%	(34/42)	0.80

Supplementary Table 4. Pathways enriched by GSEA in immune-mediated cancer field.

NAME	MSigDB collection	SIZE	ES	NES
HALLMARK_ALLOGRAFT_REJECTION	Hallmark	198	0.69	1.98
HALLMARK_IL2_STAT5_SIGNALING	Hallmark	196	0.56	1.86
HALLMARK_INFLAMMATORY_RESPONSE	Hallmark	200	0.61	1.85
HALLMARK_COMPLEMENT	Hallmark	200	0.53	1.80
HALLMARK_KRAS_SIGNALING_UP	Hallmark	199	0.53	1.80
HALLMARK_INTERFERON_GAMMA_RESPONSE	Hallmark	200	0.70	1.78
HALLMARK_EPITHELIAL_MESENCHYMAL_TRANSITION	Hallmark	199	0.64	1.77
HALLMARK_TGF_BETA_SIGNALING	Hallmark	54	0.61	1.74
HALLMARK_IL6_JAK_STAT3_SIGNALING	Hallmark	87	0.61	1.73
HALLMARK_ANGIOGENESIS	Hallmark	36	0.67	1.73
HALLMARK_APOPTOSIS	Hallmark	160	0.50	1.68
HALLMARK_TNFA_SIGNALING_VIA_NFKB	Hallmark	198	0.64	1.65
JAATINEN_HEMATOPOIETIC_STEM_CELL_DN	C2	220	0.64	1.96
REACTOME_IMMUNOREGULATORY_INTERACTIONS_BETWEEN_A_LYMPHOID_AND_A_NON_LYMPHOID_CE	C2	60	0.69	1.96
KHETCHOUMIAN_TRIM24_TARGETS_UP	C2	45	0.79	1.96
TONKS_TARGETS_OF_RUNX1_RUNX1T1_FUSION_HSC_DN	C2	182	0.57	1.96
CHIANG_LIVER_CANCER_SUBCLASS_PROLIFERATION_UP	C2	173	0.67	1.96
KEGG_FC_GAMMA_R_MEDIATED_PHAGOCYTOSIS	C2	91	0.59	1.96
PASQUALUCCI_LYMPHOMA_BY_GC_STAGE_DN	C2	164	0.62	1.95
BASSO_CD40_SIGNALING_UP	C2	99	0.72	1.95
LINDGREN_BLADDER_CANCER_CLUSTER_2B	C2	375	0.67	1.95
FINAK_BREAST_CANCER_SDPP_SIGNATURE	C2	24	0.82	1.94
MCLACHLAN_DENTAL_CARIES_UP	C2	236	0.72	1.94
FIGUEROA_AML_METHYLATION_CLUSTER_5_DN	C2	42	0.54	1.94
LI_INDUCED_T_TO_NATURAL_KILLER_UP	C2	297	0.55	1.93
KEGG_VIRAL_MYOCARDITIS	C2	68	0.64	1.93
HENDRICKS_SMARCA4_TARGETS_DN	C2	48	0.62	1.93
KEGG_PATHOGENIC_ESCHERICHIA_COLI_INFECTION	C2	51	0.70	1.93
KEGG_LEUKOCYTE_TRANSENDOTHELIAL_MIGRATION	C2	113	0.57	1.93
BOYLAN_MULTIPLE_MYELOMA_C_D_DN	C2	246	0.54	1.92
FLECHNER_BIOPSY_KIDNEY_TRANSPLANT_REJECTED_VS_OK_UP	C2	87	0.81	1.92
ICHIBA_GRAFT_VERSUS_HOST_DISEASE_35D_UP	C2	128	0.72	1.92
PASINI_SUZ12_TARGETS_DN	C2	312	0.62	1.92
DUNNE_TARGETS_OF_AML1_MTG8_FUSION_UP	C2	50	0.66	1.92
AMUNDSON_POOR_SURVIVAL_AFTER_GAMMA_RADIATION_2G	C2	168	0.56	1.92
BOYLAN_MULTIPLE_MYELOMA_D_DN	C2	75	0.62	1.92
FAELT_B_CLL_WITH_VH_REARRANGEMENTS_UP	C2	46	0.60	1.91
WALLACE_PROSTATE_CANCER_RACE_UP	C2	281	0.70	1.91
HOSHIDA_LIVER_CANCER_SURVIVAL_UP	C2	73	0.72	1.91
HUANG_GATA2_TARGETS_UP	C2	147	0.60	1.91
DIAZ_CHRONIC_MEYLOGENOUS_LEUKEMIA_DN	C2	115	0.64	1.91
MARSON_FOXP3_TARGETS_UP	C2	65	0.68	1.91
HUANG_DASATINIB_RESISTANCE_UP	C2	78	0.69	1.90
HOFMANN_MYELODYSPLASTIC_SYNDROM_RISK_DN	C2	22	0.66	1.90
SU_THYMUS	C2	20	0.79	1.90
GAURNIER_PSMD4_TARGETS	C2	70	0.68	1.90
KEGG_INTESTINAL_IMMUNE_NETWORK_FOR_IGA_PRODUCTION	C2	45	0.69	1.90
SCHUETZ_BREAST_CANCER_DUCTAL_INVASIVE_UP	C2	345	0.73	1.90
AMUNDSON_POOR_SURVIVAL_AFTER_GAMMA_RADIATION_8G	C2	93	0.57	1.90
VERHAAK_AML_WITH_NPM1_MUTATED_DN	C2	240	0.57	1.90
REACTOME_HEMOSTASIS	C2	442	0.46	1.90
JOHANSSON_GLIOMAGENESIS_BY_PDGFB_UP	C2	56	0.66	1.89
GRUETZMANN_PANCREATIC_CANCER_UP	C2	352	0.61	1.89
NAKAYAMA_SOFT_TISSUE_TUMORS_PCA1_UP	C2	73	0.75	1.89
VALK_AML_CLUSTER_11	C2	36	0.61	1.89
WU_CELL_MIGRATION	C2	180	0.61	1.89
HADDAD_T_LYMPHOCYTE_AND_NK_PROGENITOR_DN	C2	62	0.64	1.89
KEGG_ANTIGEN_PROCESSING_AND_PRESENTATION	C2	77	0.64	1.89
PID_IL12_2PATHWAY	C2	62	0.65	1.89
PID_CXCR4_PATHWAY	C2	102	0.60	1.88
TAKEDA_TARGETS_OF_NUP98_HOXA9_FUSION_16D_UP	C2	167	0.54	1.88
ONO_FOXP3_TARGETS_DN	C2	42	0.68	1.88
REACTOME_INFLAMMASOMES	C2	16	0.76	1.88
RUTELLA_RESPONSE_TO_HGF_VS_CSF2RB_AND_IL4_DN	C2	240	0.55	1.88
PID_GLYPICAN_1PATHWAY	C2	26	0.74	1.88
RUTELLA_RESPONSE_TO_HGF_DN	C2	229	0.57	1.88
KIM_GLIS2_TARGETS_UP	C2	84	0.74	1.88
ONO_AML1_TARGETS_DN	C2	41	0.64	1.88
REACTOME_INTERFERON_SIGNALING	C2	151	0.63	1.88
YU_MYC_TARGETS_DN	C2	53	0.68	1.87
WANG_ESOPHAGUS_CANCER_VS_NORMAL_UP	C2	117	0.58	1.87
CHARAFE_BREAST_CANCER_LUMINAL_VS_MESENCHYMAL_DN	C2	451	0.63	1.87
LINDSTEDT_DENDRITIC_CELL_MATURATION_D	C2	67	0.64	1.87
LU_IL4_SIGNALING	C2	89	0.61	1.87
OSADA_ASCL1_TARGETS_DN	C2	24	0.75	1.87
KEGG_CELL_ADHESION_MOLECULES_CAMS	C2	130	0.53	1.87
DER_IFN_GAMMA_RESPONSE_UP	C2	71	0.72	1.87
HELLER_SILENCED_BY_METHYLATION_UP	C2	269	0.52	1.87
REACTOME_PLATELET_ACTIVATION_SIGNALING_AND_AGGREGATION	C2	196	0.53	1.87
REACTOME_SEMAPHORIN_INTERACTIONS	C2	63	0.64	1.87
LIU_VAV3_PROSTATE_CARCINOGENESIS_UP	C2	88	0.63	1.87
PID_IL12_STAT4_PATHWAY	C2	33	0.71	1.87
LIANG_SILENCED_BY_METHYLATION_UP	C2	30	0.65	1.87
WIERENGA_STAT5A_TARGETS_DN	C2	202	0.52	1.87
DEMAGALHAES_AGING_UP	C2	53	0.68	1.86
ZHAN_EARLY_DIFFERENTIATION_GENES_DN	C2	42	0.63	1.86
SWEET_KRAS_TARGETS_UP	C2	82	0.63	1.86
GNATENKO_PLATELET_SIGNATURE	C2	45	0.71	1.86
SERVITJA_ISLET_HNF1A_TARGETS_UP	C2	162	0.56	1.86
RASHI_RESPONSE_TO_IONIZING_RADIATION_6	C2	81	0.59	1.86
RAGHAVACHARI_PLATELET_SPECIFIC_GENES	C2	70	0.66	1.86
JACKSON_DNMT1_TARGETS_UP	C2	77	0.63	1.86
BOSCO_TH1_CYTOTOXIC_MODULE	C2	112	0.57	1.86
CHEOK_RESPONSE_TO_HD_MTX_UP	C2	22	0.76	1.86
DER_IFN_BETA_RESPONSE_UP	C2	102	0.71	1.86
KEGG_CHEMOKINE_SIGNALING_PATHWAY	C2	179	0.55	1.86

IGLESIAS_E2F_TARGETS_UP	C2	149	0.66	1.86
DAVICIONI_TARGETS_OF_PAX_FOXO1_FUSIONS_UP	C2	253	0.54	1.86
KEGG_ASTHMA	C2	28	0.69	1.86
REACTOME_INTEGRIN_CELL_SURFACE_INTERACTIONS	C2	79	0.63	1.86
MUNSHI_MULTIPLE_MYELOMA_UP	C2	81	0.57	1.86
REACTOME_SEMA4D_IN_SEMAPHORIN_SIGNALING	C2	28	0.68	1.86
CROONQUIST_NRAS_SIGNALING_UP	C2	39	0.72	1.86
MORI_SMALL_PRE_BII_LYMPHOCYTE_UP	C2	85	0.55	1.85
PID_CD8_TCR_PATHWAY	C2	52	0.69	1.85
ICHIBA_GRAFT_VERSUS_HOST_DISEASE_D7_UP	C2	107	0.72	1.85
KEGG_LEISHMANIA_INFECTION	C2	68	0.67	1.85
YAN_ESCAPE_FROM_ANOIKIS	C2	24	0.74	1.85
PID_RAC1_PATHWAY	C2	51	0.58	1.85
REACTOME_CYTOKINE_SIGNALING_IN_IMMUNE_SYSTEM	C2	260	0.56	1.85
BORLAK_LIVER_CANCER_EGF_UP	C2	55	0.65	1.85
REACTOME_TCR_SIGNALING	C2	49	0.69	1.85
BASSO_HAIRY_CELL_LEUKEMIA_UP	C2	80	0.63	1.85
SCHRAETS_MLL_TARGETS_DN	C2	33	0.66	1.85
GOLDRATH_ANTIGEN_RESPONSE	C2	337	0.54	1.85
WIELAND_UP_BY_HBV_INFECTION	C2	98	0.80	1.85
REACTOME_GPVI_MEDIATED_ACTIVATION_CASCADE	C2	30	0.73	1.85
LINDSTEDT_DENDRITIC_CELL_MATURATION_C	C2	68	0.60	1.85
TONKS_TARGETS_OF_RUNX1_RUNX1T1_FUSION_HSC_UP	C2	180	0.57	1.85
GUENTHER_GROWTH_SPHERICAL_VS_ADHERENT_DN	C2	25	0.71	1.84
PID_TCR_PATHWAY	C2	65	0.66	1.84
SASSON_RESPONSE_TO_FORSKOLIN_DN	C2	87	0.62	1.84
KEGG_SMALL_CELL_LUNG_CANCER	C2	84	0.54	1.84
CHARAFE_BREAST_CANCER_LUMINAL_VS_BASAL_DN	C2	441	0.57	1.84
RADMACHER_AML_PROGNOSIS	C2	77	0.60	1.84
REN_ALVEOLAR_RHABDOMYOSARCOMA_DN	C2	406	0.61	1.84
KEGG_AUTOIMMUNE_THYROID_DISEASE	C2	48	0.61	1.84
LEE_DIFFERENTIATING_T_LYMPHOCYTE	C2	187	0.68	1.84
HELLER_HDAC_TARGETS_DN	C2	284	0.51	1.84
LEE_LIVER_CANCER_DENA_UP	C2	59	0.67	1.84
DIRMEIER_LMP1_RESPONSE_LATE_UP	C2	56	0.70	1.84
PID_ILK_PATHWAY	C2	45	0.65	1.84
CHAUHAN_RESPONSE_TO_METHOXYESTRADIOL_DN	C2	100	0.64	1.84
HELLEBREKERS_SILENCED_DURING_TUMOR_ANGIOGENESIS	C2	80	0.59	1.84
DER_IFN_ALPHA_RESPONSE_UP	C2	74	0.74	1.84
WOO_LIVER_CANCER_RECURRENCE_UP	C2	105	0.77	1.84
PETROVA_PROX1_TARGETS_DN	C2	64	0.72	1.84
PID_PI3KCI_PATHWAY	C2	48	0.63	1.84
MA_MYELOID_DIFFERENTIATION_UP	C2	39	0.65	1.84
VANASSE_BCL2_TARGETS_DN	C2	72	0.51	1.84
BARIS_THYROID_CANCER_DN	C2	58	0.59	1.84
HE_PTEN_TARGETS_UP	C2	16	0.74	1.84
MORI_LARGE_PRE_BII_LYMPHOCYTE_DN	C2	57	0.71	1.84
ROSS_ACUTE_MYELOID_LEUKEMIA_CBF	C2	79	0.55	1.84
ROSS_AML_WITH_CBFB_MYH11_FUSION	C2	50	0.66	1.84
PID_NFAT_3PATHWAY	C2	53	0.60	1.83
KEGG_NATURAL_KILLER_CELL_MEDIATED_CYTOTOXICITY	C2	127	0.51	1.83
SASSON_RESPONSE_TO_GONADOTROPHINS_DN	C2	87	0.62	1.83
FERRANDO_T_ALL_WITH_MLL_ENL_FUSION_UP	C2	85	0.56	1.83
PANGAS_TUMOR_SUPPRESSION_BY_SMAD1_AND_SMAD5_UP	C2	132	0.54	1.83
RORIE_TARGETS_OF_EWSR1_FLI1_FUSION_UP	C2	30	0.64	1.83
GEORGANTAS_HSC_MARKERS	C2	66	0.60	1.83
SHIN_B_CELL_LYMPHOMA_CLUSTER_2	C2	30	0.63	1.83
RAY_TARGETS_OF_P210_BCR_ABL_FUSION_DN	C2	15	0.79	1.83
PID_PDGFRB_PATHWAY	C2	126	0.56	1.83
WIKMAN_ASBESTOS_LUNG_CANCER_DN	C2	28	0.67	1.83
RODWELL_AGING_KIDNEY_NO_BLOOD_UP	C2	211	0.62	1.83
JI_CARCINOGENESIS_BY_KRAS_AND_STK11_DN	C2	17	0.77	1.82
GRAHAM_CML_DIVIDING_VS_NORMAL_QUIESCENT_DN	C2	90	0.65	1.82
PHONG_TNF_RESPONSE_NOT_VIA_P38	C2	337	0.51	1.82
THUM_SYSTOLIC_HEART_FAILURE_UP	C2	405	0.58	1.82
DEURIG_T_CELL_PROLYMPHOCYTIC_LEUKEMIA_DN	C2	307	0.61	1.82
XU_RESPONSE_TO_TRETINOIN_AND_NSC682994_UP	C2	17	0.79	1.82
VALK_AML_CLUSTER_4	C2	28	0.69	1.82
REACTOME_INTERFERON_GAMMA_SIGNALING	C2	59	0.68	1.82
FLECHNER_PBL_KIDNEY_TRANSPLANT_REJECTED_VS_OK_UP	C2	61	0.65	1.82
BYSTROEM_CORRELATED_WITH_IL5_UP	C2	49	0.59	1.82
NIELSEN_LEIOMYOSARCOMA_CNN1_DN	C2	20	0.77	1.82
GILDEA_METASTASIS	C2	30	0.77	1.82
CROONQUIST_IL6_DEPRIVATION_UP	C2	20	0.69	1.82
CHIARADONNA_NEOPLASTIC_TRANSFORMATION_KRAS_CDC25_UP	C2	57	0.63	1.81
LE_SKI_TARGETS_UP	C2	17	0.76	1.81
SNIJDERS_AMPLIFIED_IN_HEAD_AND_NECK_TUMORS	C2	37	0.66	1.81
LEE_EARLY_T_LYMPHOCYTE_DN	C2	54	0.74	1.81
BOSCO_ALLERGEN_INDUCED_TH2_ASSOCIATED_MODULE	C2	141	0.57	1.81
PID_FCER1_PATHWAY	C2	60	0.65	1.81
BIOCARTA_MEF2D_PATHWAY	C2	18	0.72	1.81
ISSAEVA_MLL2_TARGETS	C2	59	0.59	1.81
HAN_JNK_SINGALING_UP	C2	35	0.68	1.81
OSMAN_BLADDER_CANCER_DN	C2	376	0.55	1.81
REACTOME_DOWNSTREAM_TCR_SIGNALING	C2	33	0.66	1.81
FRIDMAN_SENESCENCE_UP	C2	76	0.60	1.81
REACTOME_CHEMOKINE_RECEPTORS_BIND_CHEMOKINES	C2	51	0.63	1.81
LEE_LIVER_CANCER_SURVIVAL_DN	C2	170	0.71	1.81
SMIRNOV_RESPONSE_TO_IR_6HR_DN	C2	111	0.56	1.81
MORI_MATURE_B_LYMPHOCYTE_UP	C2	89	0.62	1.81
BURTON_ADIPOGENESIS_8	C2	85	0.65	1.81
WU_HBX_TARGETS_2_DN	C2	16	0.77	1.81
YAGI_AML_WITH_T_8_21_TRANSLOCATION	C2	362	0.47	1.81
NAKAMURA_METASTASIS	C2	46	0.63	1.81
SHIN_B_CELL_LYMPHOMA_CLUSTER_8	C2	36	0.63	1.81
BIOCARTA_TH1TH2_PATHWAY	C2	19	0.72	1.81
STEIN_ESRRA_TARGETS_DN	C2	102	0.58	1.81
LEE_LIVER_CANCER_MYC_E2F1_UP	C2	55	0.62	1.81

MORI_IMMATURE_B_LYMPHOCYTE_UP	C2	52	0.71	1.81
DANG_REGULATED_BY_MYC_DN	C2	250	0.51	1.81
TING_SILENCED_BY_DICER	C2	30	0.63	1.81
BURTON_ADIPOGENESIS_9	C2	90	0.61	1.81
ZHU_CMV_ALL_UP	C2	119	0.61	1.81
HUMMERICH_SKIN_CANCER_PROGRESSION_UP	C2	86	0.60	1.81
ZHAN_MULTIPLE_MYELOMA_HP_UP	C2	46	0.61	1.81
IZADPANAH_STEM_CELL_ADIPOSE_VS_BONE_UP	C2	124	0.58	1.81
LINDSTEDT_DENDRITIC_CELL_MATURATION_B	C2	51	0.72	1.81
HAHTOLA_CTCL_PATHOGENESIS	C2	15	0.83	1.80
VERRECCHIA_EARLY_RESPONSE_TO_TGFB1	C2	55	0.65	1.80
LENAOUR_DENDRITIC_CELL_MATURATION_UP	C2	112	0.53	1.80
TARTE_PLASMA_CELL_VS_B_LYMPHOCYTE_DN	C2	37	0.74	1.80
ONO_FOXP3_TARGETS_UP	C2	23	0.69	1.80
REACTOME_NUCLEOTIDE_BINDING_DOMAIN_LEUCINE_RICH_REPEAT_CONTAINING_RECEPTOR_NLR_SIG	C2	44	0.60	1.80
ALONSO_METASTASIS_EMT_UP	C2	36	0.67	1.80
REACTOME_PHOSPHORYLATION_OF_CD3_AND_TCR_ZETA_CHAINS	C2	15	0.85	1.80
DELYS_THYROID_CANCER_UP	C2	434	0.52	1.80
PETROVA_ENDOTHELIUM_LYMPHATIC_VS_BLOOD_DN	C2	162	0.61	1.80
VANTVEER_BREAST_CANCER_ESR1_DN	C2	234	0.53	1.80
REACTOME_METABOLISM_OF_MRNA	C2	206	0.65	1.80
SYED_ESTRADIOL_RESPONSE	C2	18	0.72	1.80
BOYAULT_LIVER_CANCER_SUBCLASS_G5_DN	C2	27	0.82	1.80
ZHANG_PROLIFERATING_VS_QUIESCENT	C2	49	0.62	1.80
PICCALUGA_ANGIOIMMUNOBLASTIC_LYMPHOMA_UP	C2	204	0.63	1.80
KUNINGER_IGF1_VS_PDGFB_TARGETS_DN	C2	45	0.59	1.80
HELLER_HDAC_TARGETS_SILENCED_BY_METHYLATION_DN	C2	272	0.50	1.80
GRANDVAUX_IRF3_TARGETS_DN	C2	19	0.67	1.80
MARKEY_RB1_ACUTE_LOF_DN	C2	222	0.57	1.80
VALK_AML_CLUSTER_15	C2	30	0.59	1.80
PID_CD40_PATHWAY	C2	31	0.63	1.80
NEMETH_INFLAMMATORY_RESPONSE_LPS_UP	C2	88	0.64	1.80
BIOCARTA_P38MAPK_PATHWAY	C2	39	0.60	1.80
BIOCARTA_IL17_PATHWAY	C2	15	0.72	1.80
GU_PDEF_TARGETS_UP	C2	71	0.61	1.80
PID_SYNDECAN_2_PATHWAY	C2	33	0.65	1.80
JIANG_TIP30_TARGETS_UP	C2	45	0.62	1.80
NUTT_GBM_VS_AO_GLIOMA_UP	C2	46	0.63	1.80
TONKS_TARGETS_OF_RUNX1_RUNX1T1_FUSION_ERYTHROCYTE_UP	C2	155	0.54	1.80
HESS_TARGETS_OF_HOXA9_AND_MEIS1_DN	C2	76	0.63	1.79
WINTER_HYPOXIA_DN	C2	49	0.75	1.79
NAKAMURA_METASTASIS_MODEL_UP	C2	43	0.60	1.79
WUNDER_INFLAMMATORY_RESPONSE_AND_CHOLESTEROL_UP	C2	55	0.65	1.79
LEE_AGING_CEREBELLUM_UP	C2	83	0.54	1.79
MORI_PLASMA_CELL_DN	C2	32	0.69	1.79
REACTOME_CELL_SURFACE_INTERACTIONS_AT_THE_VASCULAR_WALL	C2	84	0.53	1.79
HAHTOLA_MYCOSIS_FUNGOIDES_SKIN_UP	C2	176	0.62	1.79
POMEROY_MEDULLOBLASTOMA_DESMOPLASIC_VS_CLASSIC_DN	C2	59	0.64	1.79
BRUECKNER_TARGETS_OF_MIRLET7A3_DN	C2	76	0.60	1.79
REACTOME_METABOLISM_OF_RNA	C2	250	0.65	1.79
BIOCARTA_MCALPAIN_PATHWAY	C2	25	0.61	1.79
KEGG_VASOPRESSIN_REGULATED_WATER_REABSORPTION	C2	44	0.58	1.79
DELPUECH_FOXO3_TARGETS_UP	C2	68	0.57	1.79
GAZDA_DIAMOND_BLACKFAN_ANEMIA_PROGENITOR_UP	C2	38	0.65	1.79
BOQUEST_STEM_CELL_DN	C2	215	0.57	1.79
SHIN_B_CELL_LYMPHOMA_CLUSTER_3	C2	27	0.71	1.79
LI_WILMS_TUMOR_VS_FETAL_KIDNEY_2_DN	C2	51	0.64	1.79
WORSCHECH_TUMOR_REJECTION_UP	C2	54	0.61	1.79
WATTEL_AUTONOMOUS_THYROID_ADENOMA_DN	C2	55	0.63	1.79
BIOCARTA_RHO_PATHWAY	C2	31	0.62	1.79
SHETH_LIVER_CANCER_VS_TXNIP_LOSS_PAM2	C2	151	0.50	1.79
KEGG_CHRONIC_MYELOID_LEUKEMIA	C2	72	0.52	1.79
LEE_NEURAL_CREST_STEM_CELL_UP	C2	146	0.48	1.79
VILIMAS_NOTCH1_TARGETS_UP	C2	50	0.68	1.78
MORI_PRE_BI_LYMPHOCYTE_DN	C2	75	0.59	1.78
TONKS_TARGETS_OF_RUNX1_RUNX1T1_FUSION_MONOCYTE_DN	C2	54	0.65	1.78
REACTOME_AXON_GUIDANCE	C2	239	0.48	1.78
KEEN_RESPONSE_TO_ROSIGLITAZONE_DN	C2	104	0.64	1.78
KEGG_NOD_LIKE_RECEPTOR_SIGNALING_PATHWAY	C2	62	0.59	1.78
MA_PITUITARY_FETAL_VS_ADULT_DN	C2	19	0.71	1.78
PID_AVB3_OPN_PATHWAY	C2	31	0.69	1.78
KANG_AR_TARGETS_UP	C2	17	0.73	1.78
BIOCARTA_TCR_PATHWAY	C2	43	0.65	1.78
KAPOSI_LIVER_CANCER_MET_UP	C2	17	0.75	1.78
DAVIES_MULTIPLE_MYELOMA_VS_MGUS_DN	C2	27	0.76	1.78
HSIAO_HOUSEKEEPING_GENES	C2	384	0.66	1.78
TORCHIA_TARGETS_OF_EWSR1_FLI1_FUSION_DN	C2	309	0.47	1.78
PID_CD8_TCR_DOWNSTREAM_PATHWAY	C2	64	0.55	1.78
AKL_HTLV1_INFECTION_DN	C2	65	0.60	1.77
DORSEY_GAB2_TARGETS	C2	31	0.66	1.77
HERNANDEZ_MITOTIC_ARREST_BY_DOCETAXEL_1_UP	C2	34	0.61	1.77
KEGG_HEMATOPOIETIC_CELL_LINEAGE	C2	85	0.52	1.77
GERHOLD_ADIPOGENESIS_DN	C2	63	0.68	1.77
MORI_SMALL_PRE_BII_LYMPHOCYTE_DN	C2	74	0.57	1.77
WATANABE_RECTAL_CANCER_RADIOTHERAPY_RESPONSIVE_DN	C2	91	0.61	1.77
ZHENG_BOUND_BY_FOXP3	C2	479	0.54	1.77
BURTON_ADIPOGENESIS_7	C2	50	0.63	1.77
TOMLINS_PROSTATE_CANCER_DN	C2	40	0.67	1.77
KEGG_FOCAL_ADHESION	C2	196	0.54	1.77
HERNANDEZ_MITOTIC_ARREST_BY_DOCETAXEL_2_UP	C2	60	0.51	1.77
WIERENGA_STAT5A_TARGETS_GROUP2	C2	56	0.60	1.77
RUTELLA_RESPONSE_TO_CSF2RB_AND_IL4_UP	C2	332	0.50	1.77
LIM_MAMMARY_LUMINAL_MATURE_DN	C2	97	0.60	1.77
BILANGES_SERUM_RESPONSE_TRANSLATION	C2	36	0.69	1.77
CHIARETTI_T_ALL_REFRACTORY_TO_THERAPY	C2	28	0.61	1.77
LIU_SMARCA4_TARGETS	C2	59	0.56	1.77
JISON_SICKLE_CELL_DISEASE_DN	C2	174	0.60	1.77
BASSO_CD40_SIGNALING_DN	C2	66	0.54	1.77

BIOCARTA_FCER1_PATHWAY	C2	38	0.64	1.77
BERTUCCI_MEDULLARY_VS_DUCTAL_BREAST_CANCER_UP	C2	200	0.54	1.77
MATSUDA_NATURAL_KILLER_DIFFERENTIATION	C2	471	0.44	1.77
BIOCARTA_IL2RB_PATHWAY	C2	38	0.62	1.77
REACTOME_SIGNALING_BY_ILS	C2	105	0.56	1.77
PID_BCR_5PATHWAY	C2	65	0.60	1.77
RASHI_RESPONSE_TO_IONIZING_RADIATION_2	C2	126	0.58	1.76
BOYAULT_LIVER_CANCER_SUBCLASS_G3_UP	C2	185	0.65	1.76
WIEDERSCHAIN_TARGETS_OF_BMI1_AND_PCGF2	C2	57	0.62	1.76
KYNG_RESPONSE_TO_H2O2	C2	69	0.60	1.76
ST_INTEGRIN_SIGNALING_PATHWAY	C2	81	0.54	1.76
ZUCCHI_METASTASIS_DN	C2	44	0.70	1.76
REACTOME_COSTIMULATION_BY_THE_CD28_FAMILY	C2	61	0.56	1.76
WESTON_VEGFA_TARGETS	C2	106	0.56	1.76
CHIARADONNA_NEOPLASTIC_TRANSFORMATION_KRAS_UP	C2	125	0.56	1.76
ALONSO_METASTASIS_NEURAL_UP	C2	17	0.71	1.76
FLECHNER_PBL_KIDNEY_TRANSPLANT_OK_VS_DONOR_UP	C2	151	0.53	1.76
HORIUCHI_WTAP_TARGETS_UP	C2	290	0.51	1.76
LENAOUR_DENDRITIC_CELL_MATURATION_DN	C2	127	0.58	1.76
CHYLA_CBFA2T3_TARGETS_UP	C2	374	0.43	1.76
SANA_TNF_SIGNALING_DN	C2	88	0.62	1.76
CASORELLI_ACUTE_PROMYELOCYTIC_LEUKEMIA_UP	C2	170	0.51	1.76
PID_EPHA_FWDPATHWAY	C2	34	0.58	1.76
CHIARADONNA_NEOPLASTIC_TRANSFORMATION_KRAS_CDC25_DN	C2	50	0.65	1.76
ALCALA_APOPTOSIS	C2	86	0.62	1.76
ZHOU_TNF_SIGNALING_4HR	C2	54	0.65	1.76
RUTELLA_RESPONSE_TO_CSF2RB_AND_IL4_DN	C2	309	0.53	1.76
LINDVALL_IMMORTALIZED_BY_TERT_UP	C2	74	0.58	1.76
PID_TXA2PATHWAY	C2	57	0.59	1.76
MISSIAGLIA_REGULATED_BY_METHYLATION_UP	C2	118	0.58	1.76
REACTOME_INFLUENZA_LIFE_CYCLE	C2	134	0.71	1.76
CAIRO_HEPATOBLASTOMA_UP	C2	202	0.57	1.75
PARK_HSC_AND_MULTIPOTENT_PROGENITORS	C2	48	0.59	1.75
DOANE_RESPONSE_TO_ANDROGEN_DN	C2	230	0.45	1.75
KEGG_ALLOGRAFT_REJECTION	C2	35	0.71	1.75
ROZANOV_MMP14_TARGETS_SUBSET	C2	33	0.69	1.75
KEGG_T_CELL_RECEPTOR_SIGNALING_PATHWAY	C2	107	0.52	1.75
JECHLINGER_EPITHELIAL_TO_MESENCHYMAL_TRANSITION_UP	C2	70	0.62	1.75
SWEET_LUNG_CANCER_KRAS_DN	C2	426	0.50	1.75
RHEIN_ALL_GLUCOCORTICOID_THERAPY_UP	C2	74	0.66	1.75
PID_INTEGRIN_A4B1_PATHWAY	C2	33	0.65	1.75
HINATA_NFKB_TARGETS_KERATINOCYTE_UP	C2	91	0.62	1.75
TIEN_INTESTINE_PROBIOTICS_6HR_UP	C2	55	0.69	1.75
KLEIN_PRIMARY_EFFUSION_LYMPHOMA_DN	C2	58	0.68	1.75
HOELZEL_NF1_TARGETS_UP	C2	130	0.50	1.75
TONKS_TARGETS_OF_RUNX1_RUNX1T1_FUSION_GRANULOCYTE_DN	C2	15	0.78	1.75
GOLUB_ALL_VS_AML_UP	C2	24	0.68	1.75
APRELIKOVA_BRCA1_TARGETS	C2	47	0.65	1.75
SHIPP_DLBCL_VS_FOLLICULAR_LYMPHOMA_DN	C2	45	0.66	1.75
BIOCARTA_CTLA4_PATHWAY	C2	19	0.73	1.75
REACTOME_GENERATION_OF_SECOND_MESSENGER_MOLECULES	C2	25	0.76	1.75
HASLINGER_B_CLL_WITH_CHROMOSOME_12_TRISOMY	C2	24	0.66	1.75
SANA_TNF_SIGNALING_UP	C2	82	0.61	1.75
FOSTER_TOLERANT_MACROPHAGE_DN	C2	403	0.53	1.75
BENPORATH_ES_CORE_NINE_CORRELATED	C2	100	0.53	1.75
KEGG_EPITHELIAL_CELL_SIGNALING_IN_HELICOBACTER_PYLORI_INFECTION	C2	68	0.53	1.75
XU_RESPONSE_TO_TRETINOIN_UP	C2	15	0.69	1.75
THEILGAARD_NEUTROPHIL_AT_SKIN_WOUND_DN	C2	225	0.53	1.75
ZHAN_MULTIPLE_MYELOMA_DN	C2	40	0.61	1.75
MARKEY_RB1_CHRONIC_LOF_DN	C2	117	0.53	1.75
TAKEDA_TARGETS_OF_NUP98_HOXA9_FUSION_10D_UP	C2	185	0.52	1.75
GHO_ATF5_TARGETS_DN	C2	16	0.69	1.75
LIAN_NEUTROPHIL_GRANULE_CONSTITUENTS	C2	25	0.66	1.74
BROWNE_HCMV_INFECTION_8HR_DN	C2	45	0.58	1.74
KLEIN_TARGETS_OF_BCR_ABL1_FUSION	C2	45	0.65	1.74
YAGI_AML_FAB_MARKERS	C2	187	0.49	1.74
CHIBA_RESPONSE_TO_TSA_UP	C2	51	0.64	1.74
FUJII_YBX1_TARGETS_UP	C2	41	0.57	1.74
BROCKE_APOPTOSIS_REVERSED_BY_IL6	C2	141	0.61	1.74
ZHANG_RESPONSE_TO_IKK_INHIBITOR_AND_TNF_UP	C2	217	0.56	1.74
NADLER_OBESITY_UP	C2	59	0.73	1.74
BOYLAN_MULTIPLE_MYELOMA_D_CLUSTER_DN	C2	40	0.55	1.74
SIG_REGULATION_OF_THE_ACTIN_CYTOSKELETON_BY_RHO_GTPASES	C2	35	0.57	1.74
YAMASHITA_LIVER_CANCER_WITH_EPCAM_UP	C2	51	0.63	1.74
ROSS_LEUKEMIA_WITH_MLL_FUSIONS	C2	76	0.55	1.74
ZHAN_MULTIPLE_MYELOMA_LB_DN	C2	39	0.68	1.74
WILENSKY_RESPONSE_TO_DARAPLADIB	C2	28	0.75	1.74
MARSON_FOXP3_CORE_DIRECT_TARGETS	C2	19	0.78	1.74
KANG_GIST_WITH_PDGFRA_UP	C2	50	0.53	1.74
LIU_TARGETS_OF_VMYB_VS_CMYB_DN	C2	40	0.68	1.74
PLASARI_TGFB1_SIGNALING_VIA_NFIC_1HR_UP	C2	33	0.63	1.73
TAKEDA_TARGETS_OF_NUP98_HOXA9_FUSION_8D_DN	C2	199	0.52	1.73
LEE_LIVER_CANCER_E2F1_UP	C2	60	0.60	1.73
ABRAHAM_ALPC_VS_MULTIPLE_MYELOMA_UP	C2	26	0.61	1.73
LINDVALL_IMMORTALIZED_BY_TERT_DN	C2	79	0.56	1.73
REACTOME_ANTIVIRAL_MECHANISM_BY_IFN_STIMULATED_GENES	C2	64	0.66	1.73
ALTEMEIER_RESPONSE_TO_LPS_WITH_MECHANICAL_VENTILATION	C2	125	0.60	1.73
OZANNE_AP1_TARGETS_UP	C2	16	0.74	1.73
GRAHAM_NORMAL_QUIESCENT_VS_NORMAL_DIVIDING_UP	C2	63	0.64	1.73
REACTOME_IL_3_5_AND_GM_CSF_SIGNALING	C2	43	0.61	1.73
REACTOME_FACTORS_INVOLVED_IN_MEGAKARYOCYTE_DEVELOPMENT_AND_PLATELET_PRODUCTION	C2	120	0.40	1.73
KEGG_B_CELL_RECEPTOR_SIGNALING_PATHWAY	C2	75	0.55	1.73
PID_GMCSF_PATHWAY	C2	37	0.60	1.73
WANG_SMARCE1_TARGETS_UP	C2	274	0.53	1.73
LEE_NAIVE_T_LYMPHOCYTE	C2	19	0.67	1.73
KEGG_TOLL_LIKE_RECEPTOR_SIGNALING_PATHWAY	C2	98	0.50	1.73
STEARMAN_LUNG_CANCER_EARLY_VS_LATE_DN	C2	59	0.58	1.73
LINDGREN_BLADDER_CANCER_CLUSTER_2A_DN	C2	137	0.55	1.73

REACTOME_SEMA4D_INDUCED_CELL_MIGRATION_AND_GROWTH_CONE_COLLAPSE	C2	24	0.64	1.73
ZHU_CMV_24_HR_UP	C2	93	0.60	1.73
ROSS_AML_WITH_AML1_ETO_FUSION	C2	75	0.49	1.73
WANG_TARGETS_OF_MLL_CBP_FUSION_UP	C2	42	0.53	1.73
YAMAZAKI_TCEB3_TARGETS_UP	C2	173	0.51	1.73
SHETH_LIVER_CANCER_VS_TXNIP_LOSS_PAM3	C2	68	0.53	1.72
PATTERSON_DOCETAXEL_RESISTANCE	C2	28	0.64	1.72
HOLLEMAN_ASPARAGINASE_RESISTANCE_ALL_DN	C2	24	0.74	1.72
BIOCARTA_FAS_PATHWAY	C2	30	0.63	1.72
FRIDMAN_IMMORTALIZATION_DN	C2	33	0.62	1.72
JEON_SMAD6_TARGETS_UP	C2	23	0.67	1.72
PID_IL2_PI3K_PATHWAY	C2	34	0.56	1.72
WESTON_VEGFA_TARGETS_12HR	C2	33	0.64	1.72
GENTILE_UV_RESPONSE_CLUSTER_D1	C2	18	0.68	1.72
RIGGI_EWING_SARCOMA_PROGENITOR_UP	C2	414	0.43	1.72
WU_HBX_TARGETS_3_UP	C2	18	0.70	1.72
BAELDE_DIABETIC_NEPHROPATHY_DN	C2	427	0.52	1.72
HOLLEMAN_ASPARAGINASE_RESISTANCE_ALL_UP	C2	22	0.59	1.72
PID_SYNDECAN_1_PATHWAY	C2	46	0.66	1.72
ZHENG_FOXP3_TARGETS_IN_T_LYMPHOCYTE_DN	C2	36	0.67	1.72
PARK_APL_PATHOGENESIS_DN	C2	49	0.60	1.72
DAVICIONI_TARGETS_OF_PAX_FOXO1_FUSIONS_DN	C2	66	0.51	1.72
REACTOME_MHC_CLASS_II_ANTIGEN_PRESENTATION	C2	89	0.54	1.72
SASAI_RESISTANCE_TO_NEOPLASTIC_TRANSFROMATION	C2	49	0.67	1.72
KEGG_CYTOKINE_CYTOKINE_RECEPTOR_INTERACTION	C2	251	0.44	1.72
JISON_SICKLE_CELL_DISEASE_UP	C2	180	0.54	1.72
ZHU_CMV_8_HR_UP	C2	46	0.64	1.72
TAVOR_CEBPA_TARGETS_DN	C2	30	0.58	1.72
WAMUNYOKOLI_OVARIAN_CANCER_GRADES_1_2_DN	C2	65	0.62	1.72
WOTTON_RUNX_TARGETS_UP	C2	21	0.57	1.72
LY_AGING_PREMATURE_DN	C2	29	0.65	1.72
ZEMBUTSU_SENSITIVITY_TO_VINCRISTINE	C2	17	0.64	1.72
PODAR_RESPONSE_TO_ADAPHOSTIN_UP	C2	143	0.56	1.72
REACTOME_IL_2_SIGNALING	C2	41	0.60	1.72
VISALA_AGING_LYMPHOCYTE_DN	C2	19	0.67	1.72
REACTOME_NONSENSE_MEDIATED_DECAY_ENHANCED_BY_THE_EXON_JUNCTION_COMPLEX	C2	103	0.74	1.72
BIOCARTA_BCR_PATHWAY	C2	34	0.60	1.71
HERNANDEZ_ABERRANT_MITOSIS_BY_DOCETACEL_2NM_UP	C2	80	0.51	1.71
REACTOME_G_ALPHA_Z_SIGNALLING_EVENTS	C2	43	0.54	1.71
DORN_ADENOVIRUS_INFECTION_48HR_DN	C2	40	0.64	1.71
PID_ERBB1_DOWNSTREAM_PATHWAY	C2	103	0.49	1.71
MCBRYAN_PUBERTAL_BREAST_4_5WK_UP	C2	269	0.48	1.71
HOFFMANN_PRE_BI_TO_LARGE_PRE_BII_LYMPHOCYTE_DN	C2	72	0.51	1.71
KEGG_SPLICEOSOME	C2	124	0.61	1.71
TSAI_RESPONSE_TO_RADIATION_THERAPY	C2	32	0.67	1.71
MARSON_FOXP3_TARGETS_STIMULATED_UP	C2	29	0.70	1.71
TAKEDA_TARGETS_OF_NUP98_HOXA9_FUSION_8D_UP	C2	148	0.51	1.71
CROONQUIST_STROMAL_STIMULATION_UP	C2	57	0.68	1.71
PID_FAK_PATHWAY	C2	58	0.55	1.71
TURASHVILI_BREAST_LOBULAR_CARCINOMA_VS_LOBULAR_NORMAL_DN	C2	73	0.65	1.71
LAIHO_COLORECTAL_CANCER_SERRATED_UP	C2	112	0.68	1.71
CAIRO_LIVER_DEVELOPMENT_UP	C2	166	0.53	1.71
MCCABE_HOXC6_TARGETS_DN	C2	21	0.58	1.71
BROWN_MYELOID_CELL_DEVELOPMENT_UP	C2	161	0.51	1.71
FULCHER_INFLAMMATORY_RESPONSE_LECTIN_VS_LPS_DN	C2	438	0.51	1.71
KEGG_GRAFT_VERSUS_HOST_DISEASE	C2	36	0.70	1.71
GAVIN_FOXP3_TARGETS_CLUSTER_P3	C2	153	0.46	1.71
KEGG_PRIMARY_IMMUNODEFICIENCY	C2	35	0.68	1.71
ODONNELL_TARGETS_OF_MYC_AND_TFRC_UP	C2	81	0.55	1.71
REACTOME_PD1_SIGNALING	C2	17	0.74	1.71
CHANG_POU5F1_TARGETS_UP	C2	15	0.70	1.71
KUMAR_TARGETS_OF_MLL_AF9_FUSION	C2	393	0.42	1.71
LEE_TARGETS_OF_PTCH1_AND_SUFU_UP	C2	52	0.52	1.71
ZHANG_ANTIVIRAL_RESPONSE_TO_RIBAVIRIN_DN	C2	49	0.59	1.71
GOTZMANN_EPITHELIAL_TO_MESENCHYMAL_TRANSITION_UP	C2	68	0.54	1.71
KORKOLA_TERATOMA_UP	C2	15	0.74	1.71
WIERENGA_STAT5A_TARGETS_UP	C2	209	0.46	1.71
ST_ERK1_ERK2_MAPK_PATHWAY	C2	32	0.59	1.71
HASLINGER_B_CLL_WITH_13Q14_DELETION	C2	23	0.67	1.71
MIYAGAWA_TARGETS_OF_EWSR1_ETS_FUSIONS_UP	C2	249	0.43	1.71
HEIDENBLAD_AMPLICON_12P11_12_UP	C2	33	0.59	1.71
BOYLAN_MULTIPLE_MYELOMA_C_DN	C2	54	0.54	1.71
CHUNG_BLISTER_CYTOTOXICITY_DN	C2	43	0.57	1.71
PID_INTEGRIN3_PATHWAY	C2	43	0.61	1.71
PID_KIT_PATHWAY	C2	52	0.54	1.71
BOYAULT_LIVER_CANCER_SUBCLASS_G123_UP	C2	44	0.63	1.70
LEE_AGING_NEOCORTEX_UP	C2	87	0.54	1.70
MCBRYAN_PUBERTAL_BREAST_3_4WK_DN	C2	36	0.55	1.70
KAYO_CALORIE_RESTRICTION_MUSCLE_UP	C2	94	0.51	1.70
ZHAN_MULTIPLE_MYELOMA_CD2_UP	C2	43	0.54	1.70
MULLIGHAN_MLL_SIGNATURE_2_DN	C2	272	0.46	1.70
OKUMURA_INFLAMMATORY_RESPONSE_LPS	C2	180	0.46	1.70
LE_EGR2_TARGETS_UP	C2	107	0.51	1.70
REACTOME_POST_CHAPERONIN_TUBULIN_FOLDING_PATHWAY	C2	16	0.72	1.70
BHATTACHARYA_EMBRYONIC_STEM_CELL	C2	85	0.56	1.70
JUBAN_TARGETS_OF_SPI1_AND_FLI1_DN	C2	86	0.55	1.70
WEIGEL_OXIDATIVE_STRESS_BY_TBH_AND_H2O2	C2	35	0.65	1.70
MODY_HIPPOCAMPUS_PRENATAL	C2	41	0.67	1.70
AMIT_SERUM_RESPONSE_240_MCF10A	C2	56	0.55	1.70
GENTLES_LEUKEMIC_STEM_CELL_UP	C2	28	0.65	1.70
KEGG_TYPE_I_DIABETES_MELLITUS	C2	40	0.63	1.70
HAHTOLA_SEZARY_SYNDROM_UP	C2	96	0.56	1.70
OKAMOTO_LIVER_CANCER_MULTICENTRIC_OCCURRENCE_UP	C2	25	0.69	1.70
DELASERNA_MYOD_TARGETS_DN	C2	56	0.53	1.70
BIOCARTA_MPR_PATHWAY	C2	33	0.58	1.70
VALK_AML_CLUSTER_10	C2	32	0.61	1.70
LU_TUMOR_ANGIOGENESIS_UP	C2	25	0.73	1.70
ACEVEDO_LIVER_CANCER_WITH_H3K27ME3_UP	C2	269	0.44	1.70

TENEDINI_MEGAKARYOCYTE_MARKERS	C2	66	0.53	1.70
FARMER_BREAST_CANCER_CLUSTER_4	C2	19	0.81	1.70
GENTILE_UV_RESPONSE_CLUSTER_D6	C2	35	0.64	1.70
GAVIN_FOXP3_TARGETS_CLUSTER_P4	C2	98	0.49	1.70
CAIRO_PML_TARGETS_BOUND_BY_MYC_UP	C2	23	0.67	1.70
GAJATE_RESPONSE_TO_TRABECTEDIN_UP	C2	65	0.57	1.70
SIG_CHEMOTAXIS	C2	45	0.52	1.70
BOHN_PRIMARY_IMMUNODEFICIENCY_SYNDROM_DN	C2	40	0.55	1.70
LINDSTEDT_DENDRITIC_CELL_MATURATION_A	C2	65	0.66	1.70
ROY_WOUND_BLOOD_VESSEL_UP	C2	49	0.65	1.70
HINATA_NFKB_TARGETS_FIBROBLAST_UP	C2	84	0.59	1.70
YANG_BREAST_CANCER_ESR1_DN	C2	25	0.67	1.70
PID_INTEGRIN_CS_PATHWAY	C2	26	0.65	1.69
PAPASPYRIDONOS_UNSTABLE_ATEROSCLEROTIC_PLAQUE_UP	C2	52	0.65	1.69
PID_ALK1_PATHWAY	C2	26	0.61	1.69
REACTOME_RESPONSE_TO_ELEVATED_PLATELET_CYTOSOLIC_CA2_	C2	81	0.54	1.69
DAVICIONI_MOLECULAR_ARMS_VS_ERMS_DN	C2	177	0.48	1.69
SIG_PIP3_SIGNALING_IN_B_LYMPHOCYTES	C2	36	0.62	1.69
REACTOME_PROTEIN_FOLDING	C2	49	0.63	1.69
GRAHAM_CML_QUIESCENT_VS_NORMAL_QUIESCENT_DN	C2	44	0.61	1.69
SCHAEFFER_SOX9_TARGETS_IN_PROSTATE_DEVELOPMENT_DN	C2	45	0.59	1.69
VERRECCHIA_RESPONSE_TO_TGFB1_C1	C2	17	0.71	1.69
GAVIN_FOXP3_TARGETS_CLUSTER_T4	C2	90	0.58	1.69
TURASHVILI_BREAST_LOBULAR_CARCINOMA_VS_DUCTAL_NORMAL_UP	C2	67	0.66	1.69
MCDOWELL_ACUTE_LUNG_INJURY_UP	C2	45	0.65	1.69
ONO_AML1_TARGETS_UP	C2	24	0.65	1.69
TURASHVILI_BREAST_DUCTAL_CARCINOMA_VS_DUCTAL_NORMAL_UP	C2	44	0.64	1.69
HOLLMANN_APOPTOSIS_VIA_CD40_UP	C2	194	0.50	1.69
KEGG_NEUROTROPHIN_SIGNALING_PATHWAY	C2	125	0.46	1.69
LEI_MYB_TARGETS	C2	312	0.50	1.69
POS_HISTAMINE_RESPONSE_NETWORK	C2	32	0.60	1.69
JIANG_AGING_CEREBRAL_CORTEX_DN	C2	52	0.57	1.69
PID_TNF_PATHWAY	C2	46	0.57	1.69
REACTOME_L1CAM_INTERACTIONS	C2	83	0.46	1.69

Supplementary Table 5. Correlation of the immune-mediated cancer field with clinicopathological characteristics.

Variable	ICF	non ICF	Fisher test
	% n# patients	% n# patients	p-value
General Clinicopathological variables			
Age			
≥65 years	53% (52/98)	47% (46/98)	
<65 years	46% (45/98)	23% (23/98)	0.11
Gender			
Female	29% (28/97)	14% (10/69)	**0.04**
Male	71% (69/97)	86% (59/69)	
Etiology			
HCV	58% (57/98)	26% (18/69)	**<0.0001**
HBV	16% (16/98)	36% (25/69)	**0.01**
Alcohol	9% (9/98)	19% (13/69)	0.10
Others	13% (13/98)	16% (11/69)	0.66
BCLC stage			
BCLC 0 or A	76% (74/98)	91% (63/69)	
BCLC B or C	22% (22/98)	7% (5/69)	**0.01**
Blood tests			
AFP levels (>100 mg/dL)	24% (23/96)	24% (16/67)	1.00
Albumin levels (<3.5 gr/L)	18% (17/95)	4% (3/68)	**0.01**
Bilirubin (>1 mg/dL)	53% (50/94)	28% (19/68)	**0.00**
Platelet count (<100,000/mm3)	29% (28/96)	12% (8/68)	**0.01**

Supplementary Table 6. Uni- and Multivariate Analysis of Survival in HCC Patients (Heptromic cohort, n=167)

	Univariate analysis	Multivariate analysis (cox's regression)		
Variable	**p-value**	**HR**	**CI (95% low-high limits)**	**p-values**
Clinicopathological variables				
Vascular invasion	<0.001	**1.79**	**1.11-2.92**	**0.018**
Multinodularity	<0.001	**2.67**	**1.56-4.58**	**<0.001**
BCLC stage B or C	0.006			
HCV etiology	0.009			
Platelet count (<100,000/mm3)	0.012	**2.23**	**1.32-3.78**	**0.003**
Satellites	0.016			
Gender	0.024			
Albumin levels (<3.5 gr/L)	0.029			
Tumor size (>3.5cm)	0.039			
Prognostic liver tissue-based transcriptomic profiles				
Immune-mediated cancer-field (ICF, *current manuscript*)	0.001			

Supplementary Table 7. 172-gene signatures of immune-mediated cancer field.

Gene name	Immune-mediated field	Immune-mediated field subtype
PTX3	ICF	Immunosuppressive
IL6	ICF	Immunosuppressive
MMP7	ICF	Immunosuppressive
IL8	ICF	Immunosuppressive
S100A9	ICF	Immunosuppressive
CXCL3	ICF	Immunosuppressive
SPP1	ICF	Immunosuppressive
IL1B	ICF	Immunosuppressive
FNDC1	ICF	Immunosuppressive
PTGS2	ICF	Immunosuppressive
CFTR	ICF	Immunosuppressive
AREG	ICF	Immunosuppressive
THBS2	ICF	Immunosuppressive
FABP4	ICF	Immunosuppressive
LOH3CR2A	ICF	Immunosuppressive
COL15A1	ICF	Immunosuppressive
HBG1	ICF	Immunosuppressive
EMP1	ICF	Immunosuppressive
VCAN	ICF	Immunosuppressive
S100A8	ICF	Immunosuppressive
COL1A2	ICF	Immunosuppressive
FHL2	ICF	Immunosuppressive
CD93	ICF	Immunosuppressive
CLIC6	ICF	Immunosuppressive
TAC1	ICF	Immunosuppressive
NTS	ICF	Immunosuppressive
AKR1B10	ICF	Immunosuppressive
DEFA1	ICF	Immunosuppressive
HSPA6	ICF	Immunosuppressive
STMN2	ICF	Immunosuppressive
EFEMP1	ICF	Immunosuppressive
HSPA7	ICF	Immunosuppressive
GREM1	ICF	Immunosuppressive
CH25H	ICF	Immunosuppressive
SERPINB2	ICF	Immunosuppressive
CCDC80	ICF	Immunosuppressive
PMEPA1	ICF	Immunosuppressive
CCL2	ICF	Immunosuppressive
FCGR3B	ICF	Immunosuppressive
IFI6	ICF	Proinflammatory
CXCL10	ICF	Proinflammatory
OASL	ICF	Proinflammatory
IFI27	ICF	Proinflammatory
IFIT3	ICF	Proinflammatory
EPSTI1	ICF	Proinflammatory
ISG15	ICF	Proinflammatory
MX1	ICF	Proinflammatory
DDX60	ICF	Proinflammatory
RSAD2	ICF	Proinflammatory
OAS1	ICF	Proinflammatory

IFIT1	ICF	Proinflammatory
OAS2	ICF	Proinflammatory
HERC5	ICF	Proinflammatory
IFIT2	ICF	Proinflammatory
STAT1	ICF	Proinflammatory
OAS3	ICF	Proinflammatory
CXCL9	ICF	Proinflammatory
IFI44	ICF	Proinflammatory
CXCL11	ICF	Proinflammatory
RTP4	ICF	Proinflammatory
GABBR1	ICF	Proinflammatory
UBD	ICF	Proinflammatory
GBP4	ICF	Proinflammatory
LAMP3	ICF	Proinflammatory
B2M	ICF	Proinflammatory
PSME1	ICF	Proinflammatory
UBE2L6	ICF	Proinflammatory
PSMB9	ICF	Proinflammatory
HLA-B	ICF	Proinflammatory
HLA-A	ICF	Proinflammatory
IFITM1	ICF	Proinflammatory
RARRES3	ICF	Proinflammatory
TAP1	ICF	Proinflammatory
GBP1	ICF	Proinflammatory
CYP3A7	ICF	Proinflammatory
HLA-F	ICF	Proinflammatory
BST2	ICF	Proinflammatory
TDRD7	ICF	Proinflammatory
IFI35	ICF	Proinflammatory
CXCL13	ICF	High Infiltrate
MS4A1	ICF	High Infiltrate
CR2	ICF	High Infiltrate
BANK1	ICF	High Infiltrate
FCRL3	ICF	High Infiltrate
C4orf7	ICF	High Infiltrate
IGKV3D-11	ICF	High Infiltrate
AIM2	ICF	High Infiltrate
POU2AF1	ICF	High Infiltrate
CCR7	ICF	High Infiltrate
MMP9	ICF	High Infiltrate
CD52	ICF	High Infiltrate
TRBC1	ICF	High Infiltrate
ITK	ICF	High Infiltrate
CCL21	ICF	High Infiltrate
CCL19	ICF	High Infiltrate
GZMK	ICF	High Infiltrate
BCL11B	ICF	High Infiltrate
LY75	ICF	High Infiltrate
FYB	ICF	High Infiltrate
PRKCH	ICF	High Infiltrate
CD3D	ICF	High Infiltrate
TRBC2	ICF	High Infiltrate

RGS10	ICF	High Infiltrate
TRAC	ICF	High Infiltrate
TRAJ17	ICF	High Infiltrate
TRAV20	ICF	High Infiltrate
TRAF5	ICF	High Infiltrate
DOCK10	ICF	High Infiltrate
NLRC5	ICF	High Infiltrate
RHOH	ICF	High Infiltrate
PVRIG	ICF	High Infiltrate
STAG3	ICF	High Infiltrate
CD8A	ICF	High Infiltrate
GPR18	ICF	High Infiltrate
RAC2	ICF	High Infiltrate
LAPTM5	ICF	High Infiltrate
WDFY4	ICF	High Infiltrate
CD48	ICF	High Infiltrate
CD2	ICF	High Infiltrate
LTB	ICF	High Infiltrate
IRF4	ICF	High Infiltrate
GIMAP7	ICF	High Infiltrate
EMB	ICF	High Infiltrate
EMBP1	ICF	High Infiltrate
DOCK11	ICF	High Infiltrate
LCK	ICF	High Infiltrate
CST7	ICF	High Infiltrate
CCL5	ICF	High Infiltrate
CD53	ICF	High Infiltrate
PRKCB	ICF	High Infiltrate
PTPRC	ICF	High Infiltrate
GZMA	ICF	High Infiltrate
UGT2B17	non-ICF	Non-immune-mediated
SLC16A12	non-ICF	Non-immune-mediated
ALPK2	non-ICF	Non-immune-mediated
CYP2C19	non-ICF	Non-immune-mediated
FAM151A	non-ICF	Non-immune-mediated
LOC646982	non-ICF	Non-immune-mediated
DHRS2	non-ICF	Non-immune-mediated
TRIM55	non-ICF	Non-immune-mediated
CYP4A22	non-ICF	Non-immune-mediated
CYP26A1	non-ICF	Non-immune-mediated
ADCY1	non-ICF	Non-immune-mediated
PPP1R3G	non-ICF	Non-immune-mediated
C5orf27	non-ICF	Non-immune-mediated
MOGAT1	non-ICF	Non-immune-mediated
FITM1	non-ICF	Non-immune-mediated
USH2A	non-ICF	Non-immune-mediated
CYP1A1	non-ICF	Non-immune-mediated
CPS1-IT	non-ICF	Non-immune-mediated
RAPH1	non-ICF	Non-immune-mediated
CNDP1	non-ICF	Non-immune-mediated
SULT1E1	non-ICF	Non-immune-mediated
ABCC6P1	non-ICF	Non-immune-mediated

KCNN2	non-ICF	Non-immune-mediated
PCOLCE2	non-ICF	Non-immune-mediated
BCHE	non-ICF	Non-immune-mediated
HEPACAM	non-ICF	Non-immune-mediated
LPAL2	non-ICF	Non-immune-mediated
ADAMTS17	non-ICF	Non-immune-mediated
MME	non-ICF	Non-immune-mediated
SLC22A25	non-ICF	Non-immune-mediated
LPA	non-ICF	Non-immune-mediated
IDO2	non-ICF	Non-immune-mediated
BBOX1	non-ICF	Non-immune-mediated
CUX2	non-ICF	Non-immune-mediated
AKR1D1	non-ICF	Non-immune-mediated
PPP1R1A	non-ICF	Non-immune-mediated
SNORA59A	non-ICF	Non-immune-mediated
SNORA59B	non-ICF	Non-immune-mediated
GPR125	non-ICF	Non-immune-mediated
CYP1A2	non-ICF	Non-immune-mediated

Supplementary Table 8. Uni- and Multivariate Analysis of Survival in HCC Patients (Validation cohort, n=225)

	Univariate analysis	Multivariate analysis (cox's regression)		
Variable	**p-value**	**HR**	**CI (95% low-high limits)**	**p-values**
Clinicopathological variables				
Vascular invasion	0.02			
Multinodularity	0.13			
Satellites	<0.001	2.22	0.87-5.67	0.096
Albumin levels (<3.5 gr/L)	0.016	2.6	0.89-7.58	0.08
Tumor size (>3.5cm)	0.003	**2.66**	**1.13-6.25**	**0.025**
AFP (>100mg/dL)	0.059	2.28	0.96-5.56	0.064
Prognostic liver tissue-based transcriptomic profiles				
Immune-mediated cancer-field (ICF, *current manuscript*)	0.001	**2.73**	**1.09-6.83**	**0.032**

Supplementary Table 9. List of 300 differentially expressed genes in non-tumor liver parenchyma of DEN/CCl4 mice, treated with vehicle vs liver of healthy control mice (FC ≥1.5, FDR q<0.05).

Symbol	Fold change	p value	FDR q value
Up-regulated			
Gpnmb	5.01	0.00	0.00
Apoa4	4.86	0.00	0.00
Mmp12	4.05	0.00	0.00
Col1a2	3.9	0.00	0.00
Ly6d	3.88	0.00	0.00
S100a8	3.82	0.00	0.00
Ccl5	3.7	0.00	0.01
Mt2	3.61	0.00	0.03
Dpt	3.61	0.00	0.00
2010003K11Rik	3.57	0.00	0.00
Gstm3	3.45	0.00	0.00
Mt1	3.14	0.00	0.02
Ms4a7	3.11	0.00	0.01
Cpe	3.11	0.00	0.00
Ubd	3.1	0.00	0.00
Hamp2	3.07	0.00	0.00
Tuba8	3.06	0.00	0.00
Mtmr11	3.01	0.00	0.00
Mfsd2a	2.94	0.00	0.00
Tinag	2.92	0.00	0.01
Lum	2.91	0.00	0.00
Ccnd1	2.91	0.00	0.00
Akr1c18	2.87	0.00	0.04
Crtap	2.78	0.00	0.01
Cdkn2c	2.71	0.00	0.00
Ifi27l2b	2.69	0.00	0.00
Mmp2	2.67	0.00	0.00
Abcd2	2.67	0.00	0.00
Cyp7a1	2.62	0.00	0.02
Emp1	2.59	0.00	0.01
Cd24a	2.58	0.00	0.00
Col3a1	2.58	0.00	0.00
Igha	2.57	0.00	0.01
Prom1	2.56	0.00	0.01
S100a9	2.56	0.00	0.00
Lepr	2.53	0.00	0.00
Nek2	2.48	0.00	0.04
Ccdc80	2.44	0.00	0.00
Cdk1	2.39	0.00	0.00
2210013O21Rik	2.39	0.00	0.00
Ms4a6b	2.37	0.00	0.00
Tmem86a	2.36	0.00	0.01
Sparcl1	2.34	0.00	0.01
Rnf145	2.3	0.00	0.01
Hsd17b6	2.3	0.00	0.01
Cenpa	2.23	0.00	0.00

Clec7a	2.2	0.00	0.00
Blnk	2.17	0.00	0.04
Cyp39a1	2.17	0.00	0.00
Slco1a4	2.15	0.00	0.04
Igkc	2.12	0.00	0.03
Sftpd	2.11	0.00	0.04
Olfml3	2.1	0.00	0.04
Lgals3	2.1	0.00	0.00
Jchain	2.1	0.00	0.03
Lgals4	2.08	0.00	0.00
Ttc39aos1	2.08	0.00	0.01
Col5a2	2.08	0.00	0.00
S100a6	2.08	0.00	0.02
Sgce	2.07	0.00	0.00
Klf4	2.06	0.00	0.03
Gpc1	2.04	0.00	0.02
Tceal8	2.02	0.00	0.00
Fstl1	2.01	0.00	0.00
Slc39a4	2.01	0.00	0.01
Pygb	1.98	0.00	0.04
Cbr3	1.98	0.00	0.01
Golm1	1.98	0.00	0.00
Lipo1	1.98	0.00	0.04
Coro1a	1.97	0.00	0.01
Lyve1	1.96	0.00	0.02
Sulf2	1.96	0.00	0.01
Spink1	1.96	0.00	0.05
Cbr1	1.95	0.00	0.00
Col6a3	1.95	0.00	0.01
Abcc4	1.95	0.00	0.00
Cyp4a31	1.93	0.00	0.02
Pf4	1.92	0.00	0.00
Il2rg	1.91	0.00	0.02
Vim	1.91	0.00	0.01
Serpina3g	1.9	0.00	0.01
Plat	1.89	0.00	0.01
Rhbdf1	1.89	0.00	0.01
Uap1l1	1.87	0.00	0.01
Ptprc	1.87	0.00	0.03
Hvcn1	1.86	0.00	0.02
Ltbp2	1.85	0.00	0.02
Fbn1	1.85	0.00	0.01
Defb1	1.84	0.00	0.04
Tpm1	1.84	0.00	0.00
Nipa1	1.84	0.00	0.00
Mgp	1.83	0.00	0.05
Itga8	1.83	0.00	0.02
Anxa1	1.83	0.00	0.00
Pdzk1ip1	1.82	0.00	0.04
Ccna2	1.82	0.00	0.00
Snhg1	1.82	0.00	0.04
Col1a1	1.81	0.00	0.02

H2-Eb1	1.8	0.00	0.00
Spc25	1.79	0.00	0.01
Klrd1	1.79	0.00	0.04
Cdt1	1.79	0.00	0.01
Armcx4	1.78	0.00	0.01
Map4k4	1.77	0.00	0.01
Abcb1a	1.77	0.00	0.05
Ect2	1.77	0.00	0.02
Csf2rb2	1.76	0.00	0.03
Itih5	1.76	0.00	0.01
Col6a2	1.75	0.00	0.01
Ms4a4b	1.75	0.00	0.04
Steap2	1.74	0.00	0.00
Nid1	1.74	0.00	0.01
Rnaseh2b	1.74	0.00	0.01
Icam1	1.74	0.00	0.04
Col4a2	1.74	0.00	0.01
Ctla2a	1.74	0.00	0.01
Mad2l1	1.73	0.00	0.01
Pecam1	1.73	0.00	0.02
H2-Ab1	1.73	0.00	0.03
Cyp3a44	1.73	0.00	0.05
Aim1	1.72	0.00	0.03
Csrp1	1.72	0.00	0.01
Glipr1	1.71	0.00	0.01
Plcg2	1.7	0.00	0.01
Cd52	1.7	0.00	0.02
Sh3bgrl3	1.7	0.00	0.01
Bicc1	1.7	0.00	0.02
Postn	1.7	0.00	0.01
Gdf10	1.7	0.00	0.00
Tmtc2	1.7	0.00	0.05
Psat1	1.69	0.00	0.01
Arl2bp	1.69	0.00	0.04
Acot9	1.69	0.00	0.05
Npdc1	1.69	0.00	0.03
Cmtm7	1.68	0.00	0.03
Cybb	1.68	0.00	0.04
Tmem164	1.67	0.00	0.01
Rdh9	1.67	0.00	0.00
Trim24	1.67	0.00	0.03
Sparc	1.67	0.00	0.00
Bax	1.66	0.00	0.00
Sirpa	1.66	0.00	0.03
Gm32031	1.66	0.00	0.00
Fmo4	1.65	0.00	0.02
Col4a5	1.65	0.00	0.02
Itpripl2	1.64	0.00	0.00
Tmem178	1.64	0.00	0.03
Hpse	1.64	0.00	0.02
Ppic	1.64	0.00	0.03

Laptm5	1.64	0.00	0.02
Myof	1.63	0.00	0.04
Gja1	1.63	0.00	0.01
Rab3d	1.62	0.00	0.02
St3gal5	1.62	0.00	0.02
Col4a1	1.62	0.00	0.00
Fam84b	1.62	0.00	0.01
Cdca3	1.62	0.00	0.04
H2-Aa	1.62	0.00	0.03
Cers6	1.61	0.00	0.04
Ptgr1	1.61	0.00	0.04
Plekho1	1.61	0.00	0.03
Fam46a	1.6	0.00	0.03
Zfp53	1.6	0.00	0.03
Chtf8	1.6	0.00	0.02
Mfge8	1.6	0.00	0.03
Pam	1.6	0.00	0.01
Cd9	1.6	0.00	0.04
Rhoc	1.59	0.00	0.00
Adcy7	1.59	0.00	0.00
Soat1	1.59	0.00	0.01
Cd74	1.59	0.00	0.03
Slc6a8	1.58	0.00	0.02
Isyna1	1.58	0.00	0.03
Cxcl16	1.57	0.00	0.04
Ppap2c	1.57	0.00	0.02
Arhgap11a	1.57	0.00	0.03
Cygb	1.57	0.00	0.04
Mapkapk3	1.56	0.00	0.03
Setd7	1.56	0.00	0.01
Ctss	1.56	0.00	0.01
Tubb6	1.55	0.00	0.02
Phlda3	1.55	0.00	0.03
Lxn	1.55	0.00	0.02
Ptprcap	1.55	0.00	0.02
Tagln2	1.54	0.00	0.02
Pou2af1	1.53	0.00	0.02
Fam102b	1.52	0.00	0.01
Mndal	1.52	0.00	0.01
Mxra8	1.52	0.00	0.02
Ptpre	1.52	0.00	0.03
Nhlrc2	1.52	0.00	0.05
Wbp5	1.52	0.00	0.01
Iqgap1	1.51	0.00	0.04
Igsf8	1.51	0.00	0.04
Tbc1d10b	1.51	0.00	0.02
Slamf7	1.5	0.00	0.05
Down-regulated			
Hsd3b5	-14.54	0.00	0.01
Fitm1	-11.68	0.00	0.00
Susd4	-11.17	0.00	0.00

Lect1	-6.72	0.00	0.00
Cyp7b1	-5.62	0.00	0.00
Olig1	-5	0.00	0.00
Serpina4-ps1	-4.27	0.00	0.02
Serpine2	-3.82	0.00	0.00
Adh6-ps1	-3.76	0.00	0.00
Tenm3	-3.72	0.00	0.00
Serpina12	-3.56	0.00	0.04
Lhpp	-3.49	0.00	0.01
Nxpe2	-3.46	0.00	0.00
Avpr1a	-3.25	0.00	0.01
Oat	-3.11	0.00	0.00
Sucnr1	-2.81	0.00	0.00
Cela1	-2.7	0.00	0.00
1500017E21Rik	-2.56	0.00	0.01
Slc1a2	-2.49	0.00	0.00
Cyp2u1	-2.42	0.00	0.00
Cyp2c37	-2.38	0.00	0.00
Rarres1	-2.37	0.00	0.00
Npr2	-2.34	0.00	0.00
Cml5	-2.28	0.00	0.01
Tex12	-2.26	0.00	0.01
Clstn3	-2.23	0.00	0.00
Wdr89	-2.18	0.00	0.01
Slc22a7	-2.17	0.00	0.05
Cyp4a12a	-2.14	0.00	0.04
Pnldc1	-2.14	0.00	0.01
Dct	-2.12	0.00	0.02
Nat1	-2.12	0.00	0.01
Tmem19	-2.09	0.00	0.00
Dpy19l3	-2.04	0.00	0.00
Fgf1	-2.04	0.00	0.00
Slco1a1	-2	0.00	0.04
Gna14	-1.98	0.00	0.00
Acad12	-1.97	0.00	0.00
Cyp2c54	-1.96	0.00	0.02
Slc17a3	-1.92	0.00	0.01
Pmm1	-1.92	0.00	0.00
Mogat1	-1.89	0.00	0.01
Cd163	-1.84	0.00	0.04
5033404E19Rik	-1.83	0.00	0.01
Glul	-1.83	0.00	0.04
Hdhd3	-1.82	0.00	0.02
Plbd1	-1.82	0.00	0.02
Eme2	-1.8	0.00	0.03
Tspyl4	-1.77	0.00	0.02
Rbm20	-1.76	0.00	0.04
Tsc22d1	-1.74	0.00	0.01
Gabrr1	-1.74	0.00	0.02
Pdilt	-1.74	0.00	0.00
Cyp2j6	-1.74	0.00	0.02
Tuba4a	-1.74	0.00	0.01

Gmppb	-1.74	0.00	0.04
Rmdn2	-1.72	0.00	0.00
Pfkfb1	-1.71	0.00	0.04
Hrc	-1.7	0.00	0.01
Zbtb21	-1.7	0.00	0.01
Zmat1	-1.67	0.00	0.03
Cav1	-1.66	0.00	0.02
Bmp4	-1.66	0.00	0.02
Slc22a3	-1.65	0.00	0.01
Nat8	-1.65	0.00	0.02
Capn8	-1.65	0.00	0.01
Inhba	-1.64	0.00	0.04
Ldhd	-1.63	0.00	0.00
Aatk	-1.62	0.00	0.04
Srsf3	-1.62	0.00	0.02
Adrb3	-1.61	0.00	0.04
Hes6	-1.61	0.00	0.03
2610305D13Rik	-1.6	0.00	0.05
3110070M22Rik	-1.6	0.00	0.04
Mup5	-1.6	0.00	0.02
Tada3	-1.6	0.00	0.03
Fam228a	-1.6	0.00	0.01
Ppapdc1a	-1.59	0.00	0.04
Fzd7	-1.59	0.00	0.01
Mal2	-1.59	0.00	0.02
Ufl1	-1.59	0.00	0.02
Hyal1	-1.59	0.00	0.01
Slc6a7	-1.59	0.00	0.04
Khdrbs3	-1.58	0.00	0.01
Ces1e	-1.57	0.00	0.01
Ces4a	-1.57	0.00	0.04
Them7	-1.57	0.00	0.02
Id3	-1.56	0.00	0.05
Dusp1	-1.55	0.00	0.03
Angptl6	-1.55	0.00	0.02
Trpv4	-1.54	0.00	0.03
C1qtnf4	-1.53	0.00	0.05
Mapk1ip1	-1.53	0.00	0.02
Mfsd8	-1.53	0.00	0.01
Zfhx4	-1.52	0.00	0.02
C6	-1.52	0.00	0.05
Csrp3	-1.52	0.00	0.01
Pole4	-1.52	0.00	0.01
Poc1b	-1.52	0.00	0.00
Snhg11	-1.52	0.00	0.00
1700001C02Rik	-1.52	0.00	0.01
Chic1	-1.52	0.00	0.04
Sdr42e1	-1.51	0.00	0.02
Moxd1	-1.5	0.00	0.02
Ccdc185	-1.5	0.00	0.01
Nars2	-1.5	0.00	0.01

Supplementary Table 9. IPA analysis of genes upregulated (FC > 1.5, FDR <0.05) in livers of DEN/CCl4 treated with vehicle (compared with healthy control group).

TOP CANONICAL PATHWAYS

Name	p value
Hepatic Fibrosis / Hepatic Stellate Cell Activation	2,54E-11
Atherosclerosis Signaling	1,90E-06
B Cell Development	7,23E-06
Granulocyte Adhesion and Diapedesis	1,04E-05
Dendritic Cell Maturation	1,10E-05

TOP DISEASE AND FUNCTIONS

Name	p-value
Cancer	2,88E-04 - 1,04E-29
Organismal Injury and Abnormalities	2,88E-04 - 1,04E-29
Gastrointestinal Disease	2,09E-04 - 8,99E-22
Immunological Disease	2,65E-04 - 5,10E-20
Inflammatory Response	2,52E-04 - 2,18E-18

TOP TOX FUNCTIONS

Name	p-value
Increased Levels of LDH	1,22E-03 - 1,22E-03
Increased Levels of ALT	8,43E-02 - 3,38E-02
Decreased Levels of Albumin	1,74E-01 - 7,08E-02